PHASE TRANSITIONS FROM THE SOLID STATE OF MONATOMIC ELEMENTS

Thesis by

Ronald L. Kerber

In Partial Fulfillment of the Requirements
For the Degree of
Doctor of Philosophy

California Institute of Technology

Pasadena, California

1970

(Submitted July 1, 1969)

ACKNOWLEDGMENTS

I would like to express my gratitude to my thesis advisor, Dr. Milton Plesset, for his guidance and encouragement during my studies at the Institute and throughout the preparation of this thesis. Special thanks are due to Dr. Din-Yu Hsieh for his assistance during the development of the theory of sublimation and the initial studies of the melting problem. I would also like to thank Dr. Cornelius Pings for introducing me to the study of the Percus-Yevick equation and for his help during the final stages of this research.

I have received financial support from the National Science Foundation for 1965 - 1966 and from the National Aeronautics and Space Administration for 1966 - 1969. Additional support was made available by the California Institute of Technology in the form of a Graduate Teaching Assistantship for 1967 - 1969 and by a California State Scholarship for 1968 - 1969. The research was supported in part by the Office of Naval Research. I gratefully acknowledge this support.

I would also like to thank Mrs. Barbara Hawk and Miss Cecilia Lin for their assistance in preparing the manuscript.

Finally, I would like to thank my wife and my parents for their encouragement during my graduate tenure.

ABSTRACT

The principle aims of this thesis include the development of models of sublimation and melting from first principles and the application of these models to the rare gases.

A simple physical model is constructed to represent the sublimation of monatomic elements. According to this model, the solid and gas phases are two states of a single physical system. The nature of the phase transition is clearly revealed, and the relations between the vapor pressure, the latent heat, and the transition temperature are derived. The resulting theory is applied to argon, krypton, and xenon, and good agreement with experiment is found.

For the melting transition, the solid is represented by an anharmonic model and the liquid is described by the Percus-Yevick approximation. The behavior of the liquid at high densities is studied on the isotherms $kT/\epsilon = 1.3$, 1.8, and 2.0, where k is Boltzmann's constant, T is the temperature, and ϵ is the well depth of the Lennard-Jones 12-6 pair potential. No solutions of the Percus-Yevick equation were found for $\rho\sigma^3$ above 1.3, where ρ is the particle density and σ is the radial parameter of the Lennard-Jones potential. The liquid structure is found to be very different from the solid structure near the melting line. The liquid pressures are about 50 percent low for experimental melting densities of argon. This discrepancy gives rise to melting pressures up to twice the experimental values.

TABLE OF CONTENTS

I. INTRODUCTION

Phase transitions may be characterized by the appearance of a discontinuity or a singularity in the equation of state of matter. A complete theory of a phase transition must include the isolation of the molecular interaction responsible for the transition and the incorporation of this interaction into physical laws which permit the extraction of the macroscopic properties of the transition. This linking of molecular interactions and macroscopic properties is formed by statistical mechanics.

We may justify the study of phase transitions in two ways. Firstly, understanding the phenomenon is sufficient in its own right to merit such studies. Hopefully, this understanding will verify results of previous experiments and predict behavior which may eliminate the need for future experiments. Secondly, the transition may serve as a vehicle to imply characteristics of a state which is not completely understood. This may be done by studying a transition to this state from a well defined theoretical state. A classic example is the melting of a solid to a liquid.

Reviews of the main aspects of the theory of phase transitions have been made by Brout[1] and Cohen[2]. These authors point out the importance of reviewing the various phase transitions that occur in nature. Such a review might include transitions in the following areas: ferromagnetism, antiferromagnetism, superconductivity, order-disorder, binary alloys, lattice gases, condensation, sublimation, and melting. Although the advanced theories of these transitions

may be very different, the basic phenomenon involved is often analogous. For this reason, the phase transitions of the relatively simple rare gases are ideal for the study of transition properties since their molecular structure is simple and does not add further complications.

In this thesis we will develop molecular models of sublimation and melting (or freezing) for monatomic elements and apply these models to the rare gases. In Fig. 1 we have indicated the transition lines that we will study on the phase diagram of argon.

The thesis is divided into two parts. In Part I a simple molecular model is used to represent sublimation of a solid. With this model the basic mechanism of the phase transition is easily seen. The equilibrium vapor pressure is calculated and an estimate of the latent heat of the transition is made. The model is applied to argon, krypton, and xenon and excellent agreement with experiment is found.

In Part II a model of melting is developed from fundamental principles. The molecular interaction is represented by a Lennard-Jones[3] 12-6 pair potential function. In this model the emphasis is placed on testing the Percus-Yevick[4] approximation for the liquid state model. This model of the liquid is matched with an anharmonic model for the solid. We find that the equation of state of the Percus-Yevick liquid begins to deviate from the experimental data when the particle density reaches 70 per cent of the particle density along the melting line. This gives rise to melting pressures which are higher than the experimental values. As the particle density is increased to values 20 to 30 per cent above the melting line, it is found that the

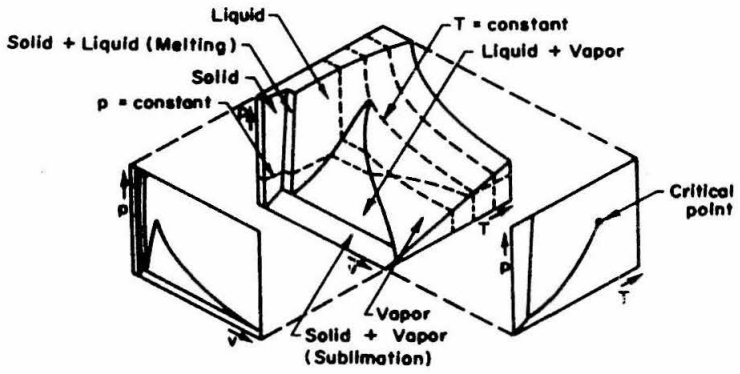

(a) Schematic Representation of the P, T, V Surface for Argon

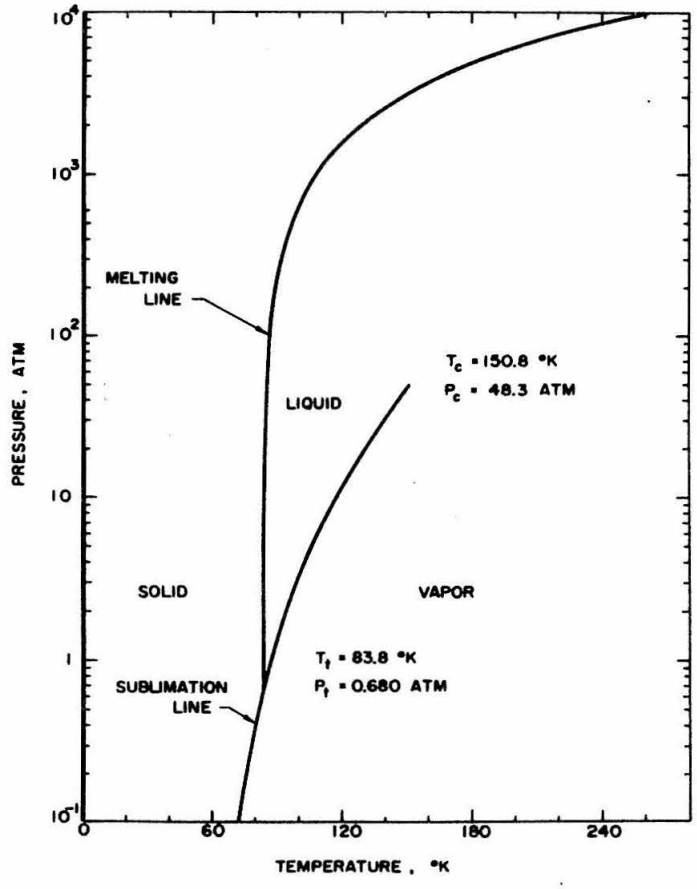

(b) P-T Phase Diagram for Argon

Fig. 1 Phase Diagrams for Argon

solution of the Percus-Yevick equation will no longer converge.

Although the agreement with experiment is poor, we may study how the properties along the melting line depend on the pair potential function and anharmonicity. It is demonstrated that the critical test of a theory of melting is not how well it predicts the slope or shape of the melting curve, but rather how well it predicts the changes of entropy and volume of the transition.

PART I

SUBLIMATION OF A MONATOMIC ELEMENT

II. FORMULATION OF A MODEL OF SUBLIMATION

A. INTRODUCTION

In the past, studies of sublimation have been focused on the determination of the vapor pressure of the solid. By noting that the two physical systems, the gas state and the solid state, are in equilibrium, a relation between the vapor pressure and the critical temperature may be calculated[5, 6].

For a monatomic solid, the vapor pressure is given by the expression[5]

$$\ell n p = - \frac{L_o}{kT} + \frac{5}{2} \ell n T - \int_o^T \frac{dT'}{kT'^2} \int_o^{T'} C_p(T'')dT'' + \ell n\left[\left(\frac{m}{2\pi}\right)^{3/2} \frac{k^{5/2}}{\hbar^3}\right] \qquad \text{(II-1)}$$

where L_o is the heat of sublimation per molecule at $0°K$, C_p is the heat capacity at constant pressure per molecule of the crystal, m is the atomic mass, k is Boltzmann's constant, and $\hbar$ is Planck's constant divided by 2π.

Empirically, the vapor pressure may be related to the temperature by a relation of the form

$$\ell n p = - \frac{1}{2} \ell n T - \frac{L_o + E_o}{kT} + \ell n\left[\frac{\omega_g^3 m^{3/2}}{(2\pi)^{3/2} k^{1/2}}\right] , \qquad \text{(II-2)}$$

where E_o is the lattice zero-point energy per molecule and ω_g is the "geometric mean frequency" of the lattice vibrational spectrum. Salter[6] has derived Eq. (II-2) from first principles assuming perfect crystal structure, quasiharmonic lattice vibrations, and a nearly

ideal vapor for $T \geqslant \theta_D/2$, where θ_D is the Debye temperature.

The calculations of the vapor pressure of solids as exemplified by Eqs. (II-1) and (II-2) do not shed much light on the nature of the phase transition. In those analyses, the solid and gaseous states are treated as if they were different physical systems rather than two phases of a single element.

It is the purpose of this Chapter to develop the theory of sublimation in a new manner by considering sublimation as a bridge between the solid and the gas states. The solid and gas phases arise as two components of a single particle system. A critical temperature, T_c, can be defined such that at temperatures less than T_c, the system behaves like a solid; and for temperatures greater than T_c, it is a gas. As the temperature increases across T_c, we find that a latent heat, L, will accompany the phase transition; and L is related to T_c. Moreover, the variation of the vapor pressure with temperature can be calculated. It is found that the vapor pressure is related to the environment of the particle in the gas state.

B. THEORY

To represent sublimation, we assume that the solid-gas system can be represented by N independent particles, each in its own cell. The potential, which characterizes the cell, is assumed to represent the aggregate interaction with all other atoms. When the energy of the particle is lower than a certain energy, E_1, we assume every particle lies in a three-dimensional harmonic potential

$$V = \frac{m}{2}\omega^2 r^2 \qquad E \leqslant E_1 \tag{II-3}$$

where ω is the Einstein frequency[7] and r is the excursion from the equilibrium position.

At E_1, the particle suddenly experiences a free particle potential

$$\begin{aligned} V &= E_1 && r < R_o \\ & && E > E_1 \end{aligned} \quad . \tag{II-4}$$
$$V = \infty \qquad r \geqslant R_o$$

Each particle is confined to a cell which is shown schematically in Fig. 2.

For energies below E_1, the particle energy states[8] are

$$\epsilon_n = \hbar\omega(n+3/2) \tag{II-5}$$

with degeneracy

$$g_n = \frac{(n+1)(n+2)}{2} \quad . \tag{II-6}$$

For simplicity, we neglect the interaction of the free particle with the harmonic potential when the energy of the particle is greater than E_1. This is justifiable since $R_o \gg \left[\frac{E_1}{m\omega^2}\right]^{\frac{1}{2}}$ for all cases under consideration.

We will find that the free particle states are essentially continuous; therefore, we can express the density of energy states (the number of energy states between ϵ and $\epsilon + d\epsilon$) in the form[9]

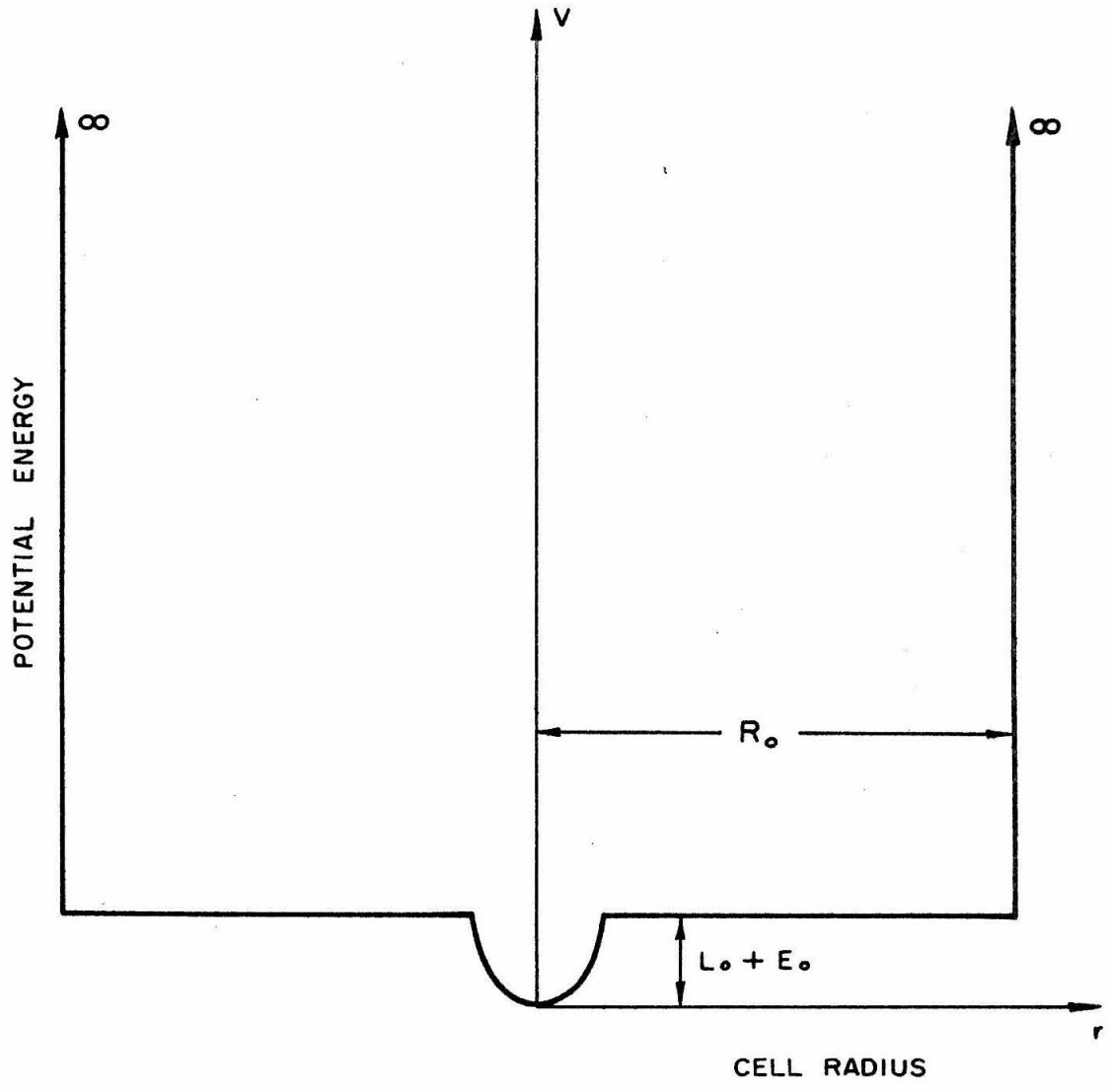

Fig. 2 - Energy Cell

$$D(\epsilon - E_1) = \frac{(2m^3)^{\frac{1}{2}}}{2\pi^2} \frac{V_c}{\hbar^3} (\epsilon - E_1)^{\frac{1}{2}} \qquad \text{(II-7)}$$

where V_c is the volume of the cell containing the free particles. This density of energy states is independent of the shape of V_c. We expect V_c to decrease with increasing pressure. The idea that dense gas particles should be considered as confined to a volume much less than the total volume of the container was proposed by Lennard-Jones and Devonshire[10].

At low temperatures, we expect the energies of most particles to be less than E_1, thus we have essentially the Einstein model[7] which is in good agreement with experiment for temperatures above $\hbar\omega/k$ for a solid. At high temperatures, we have an ideal gas.

The partition function, Z_t, for the system is

$$Z_t = Z^N \qquad \text{(II-8)}$$

where Z is the partition function for a single particle.

$$Z = \sum_{\text{all}\,\epsilon_n} \exp(-\epsilon_n/kT) g_n \quad , \qquad \text{(II-9)}$$

where ϵ_n denotes a single particle energy state.

For our model we have

$$Z = \sum_{n}^{M} \frac{(n+1)(n+2)}{2} \exp\left(-\left(n+\frac{3}{2}\right)\hbar\omega/kT\right) + \int_{E_1}^{\infty} D(\epsilon - E_1)\exp(-\epsilon/kT)d\epsilon \quad . \qquad \text{(II-10)}$$

where M is the largest integer satisfying the inequality

$$\left(M + \frac{3}{2}\right)\hbar\omega \leqslant E_1 \quad . \tag{II-11}$$

We have used the discrete energy spectrum in Eq. (II-10) because quantum effects of the harmonic oscillators are present near the triple point of rare gas solids. This has been noted by Moelwyn-Hughes[11]. If the ratio of kT and $\hbar\omega$ is large, we can use a continuous approximation for the density of states of the solid. This approximation is treated in Appendix A.

Let us denote

$$L_o = E_1 - \frac{3}{2}\hbar\omega \tag{II-12}$$

which can be interpreted as the zero-point latent heat. Also, it is convenient to define the new variables:

$$X = \exp(-\hbar\omega/kT) \quad , \tag{II-13}$$

$$I = \sum_{n=o}^{M} X^n \quad , \tag{II-14}$$

$$V_c = \alpha V_s \quad , \tag{II-15}$$

$$A = \frac{(2m^3)^{\frac{1}{2}} V_s \omega^3}{4\pi^{3/2}(\hbar\omega)^{3/2}} \quad , \tag{II-16}$$

and

$$C = kT/\hbar\omega \quad , \tag{II-17}$$

where V_s is the average atomic volume in the solid, which is essentially constant.

With the use of Eqs. (II-7) and (II-11) - (II-17), then Eq. (II-10) becomes

$$Z = X^{3/2}\left[\frac{X^2 I''}{2} + 2XI' + I + \alpha A \exp(-L_o/kT)C^{3/2}\right]. \quad \text{(II-18)}$$

where I' and I'' are respectively the first and the second derivatives of I with respect to X.

The free energy and the internal energy are given by

$$F = - kT \log Z_t \quad , \quad \text{(II-19)}$$

and

$$E = - T^2 \frac{\partial (F/T)_v}{\partial T} \quad . \quad \text{(II-20)}$$

By using Eqs. (II-8), (II-18), (II-19), and (II-20), we find the energy

$$\frac{E}{N\hbar\omega} = \frac{\frac{X^3}{2} I''' + \frac{15}{4} X^2 I'' + 6XI' + \frac{3}{2} I + \alpha A \exp(-L_o/kT)C^{3/2}\left[\frac{L_o}{\hbar\omega} + (C+1)\frac{3}{2}\right]}{\frac{X^2}{2} I'' + 2XI' + I + \alpha A \exp(-L_o/kT)C^{3/2}} \quad , \quad \text{(II-21)}$$

where I''' is the third derivative of I with respect to X. We note that

$$I = \frac{1 - X^{M+1}}{1 - X} \quad . \quad \text{(II-22)}$$

It is clear that the only undetermined parameter of the model is α, the number of volumes V_s available to the free particle. We also noted that V_c decreases with increasing pressure. Let us then take

$$\alpha = \alpha(p) \quad \text{(II-23)}$$

where $\alpha(p)$ decreases with increasing pressure.

It is instructive to examine Eq. (II-21) in detail. We note that

$$E = E(T, \omega, L_o, A\alpha(p)) \quad . \tag{II-24}$$

For low temperatures, the energy is that of a collection of harmonic oscillators and for high temperatures, we have the energy of an ideal gas. In fact, for either temperature extreme, the energy is independent of $\alpha(p)$. In the application of this model to argon, krypton, and xenon, we will demonstrate that $\alpha(p)$ is only important near the transition point, T_c, defined by

$$\left.\frac{\partial C_v}{\partial T}\right|_{T=T_c} = 0 \quad , \tag{II-25}$$

where C_v is the specific heat at constant volume. For this reason, we define the pressure of Eq. (II-23) to be the equilibrium vapor pressure. From Eqs. (II-24) and (II-25), we have

$$T_c = T_c(\omega, L_o, A\alpha(p)) \quad . \tag{II-26}$$

For a particular solid, Eq. (II-26) becomes

$$T_c = T_c(\alpha(p)) \quad . \tag{II-27}$$

Equation (II-27) yields the equilibrium vapor pressure curve, once $\alpha(p)$ is known.

For most practical applications, T_c is essentially independent of ω; therefore, Eq. (II-26) can be written more simply as

$$T_c = T_c(L_o, A\alpha(p)) \quad . \tag{II-28}$$

This is exactly true for the classical solid described in Appendix A if A is replaced by A_1.

Therefore, for solids with similar molecular structure, such as the rare gas solids, one might expect from the law of corresponding states (Ref. 12, p. 19) that for some characteristic pressure

$$T_c = T_c(L_o) \quad . \tag{II-29}$$

In Table I, we illustrate the experimental relationship of T_c and L_o for argon, krypton, and xenon at their triple point temperatures, T_t.

TABLE I

Ratio of zero-point latent heat and kT_t

Element	L_o/kT_t^*
Argon	11.08
Krypton	11.58
Xenon	11.93

*Calculated from values given by G. L. Pollack, Rev. Mod. Phys. 36, 748 (1964).

TABLE II

Physical Constants

Element	Zero-point latent heat L_o(cal/mol)[e]	Zero-point energy E_o(cal/mole)[e]	Atomic mass m(amu.)	Average atomic volume V_s(Å^3)	Triple Point P_t(mm)	Triple Point T_t(°K)
Argon	1846[a]	184.6[b]	39.948[c]	39.73[d]	516.86[a]	83.810[a]
Krypton	2666[a]	145[a]	83.80[c]	45.19[d]	548.7[a]	115.78[a]
Xenon	3828[a]	123[a]	131.30[c]	59.62[d]	612.2[a]	161.37[a]

[a]G. L. Pollack, Rev. Mod. Phys. 36, 748 (1964).

[b]Pollack gives 187 cal/mole and G.G. Chell and I. J. Zucker, J. Phys. C(Proc. Phys. Soc.), Ser. 2., 1, 35 (1968), give 182.3 cal/mole. We use 184.6 cal/mole for numerical convenience.

[c]R.C. Weast, Handbook of Chemistry and Physics (The Chemical Rubber Co., Cleveland, Ohio, 1967 - 1968) 48th ed. p. B3.

[d]Calculated from nearest neighbor distances given by Pollack.

[e]We convert these values to energy per molecule for this analysis.

C. APPLICATION TO ARGON, KRYPTON, AND XENON

1. Preliminary Calculations

To apply the theory, we need to calculate $E(T)$ given by Eq. (II-21) and its derivatives. To calculate the constants of Eq. (II-21) we need the following physical constants: the zero-point latent heat, L_o, the zero-point energy, E_o, the atomic mass, m, and the average atomic volume in the solid state, V_s. We will also need the triple point pressure, P_t, and the triple point temperature, T_t, for future reference. These constants are given in Table II.

The zero-point energy is given by

$$E_o = \frac{3}{2} \hbar\omega \quad . \tag{II-30}$$

By using the physical constants of Table II and Eqs. (II-11) and (II-16), we may calculate M and A for each element. These constants are listed in Table III.

TABLE III

Model Constants

Element	M	A
Argon	15	921.3
Krypton	27	2212
Xenon	46	4472

The energy may now be calculated from Eq. (II-21) as a function of temperature with the parameter α. The internal energies of argon, krypton, and xenon are shown graphically in Figs. 3, 4, and 5 respectively, for selected values of α. The phase transition is obvious. We have noted the critical temperature of each curve.

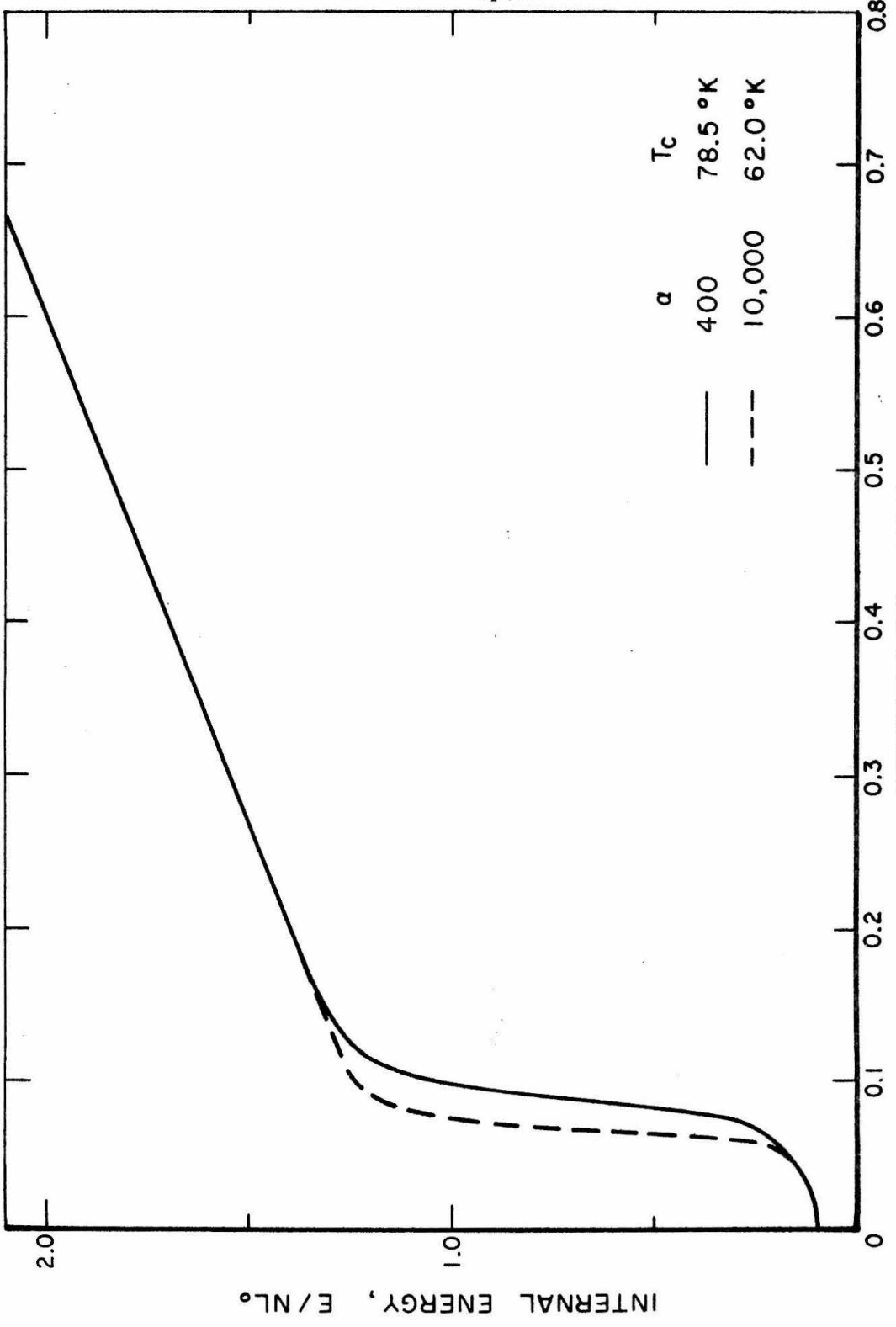

Fig. 3 - Internal Energy of Argon

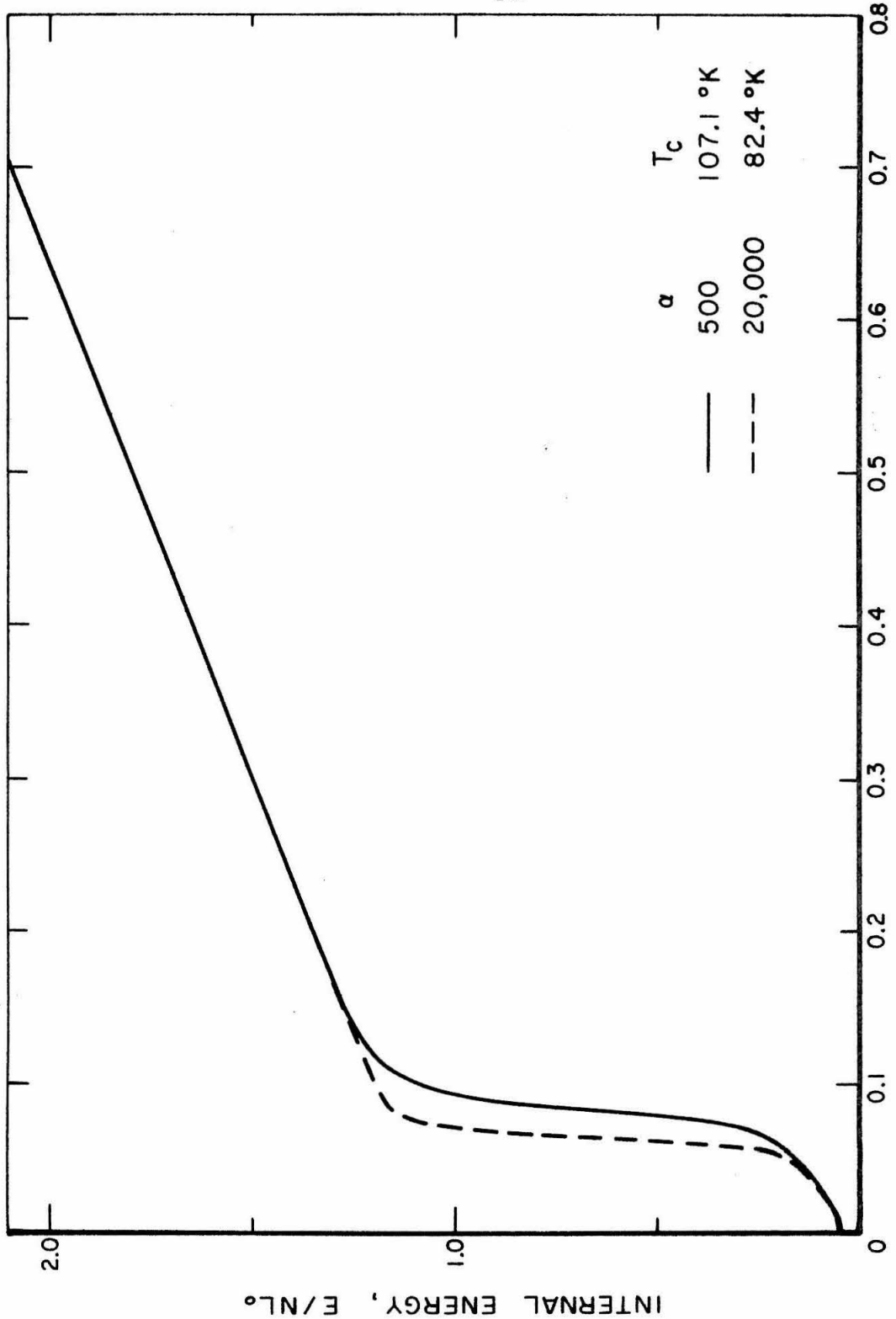

Fig. 4 - Internal Energy of Krypton

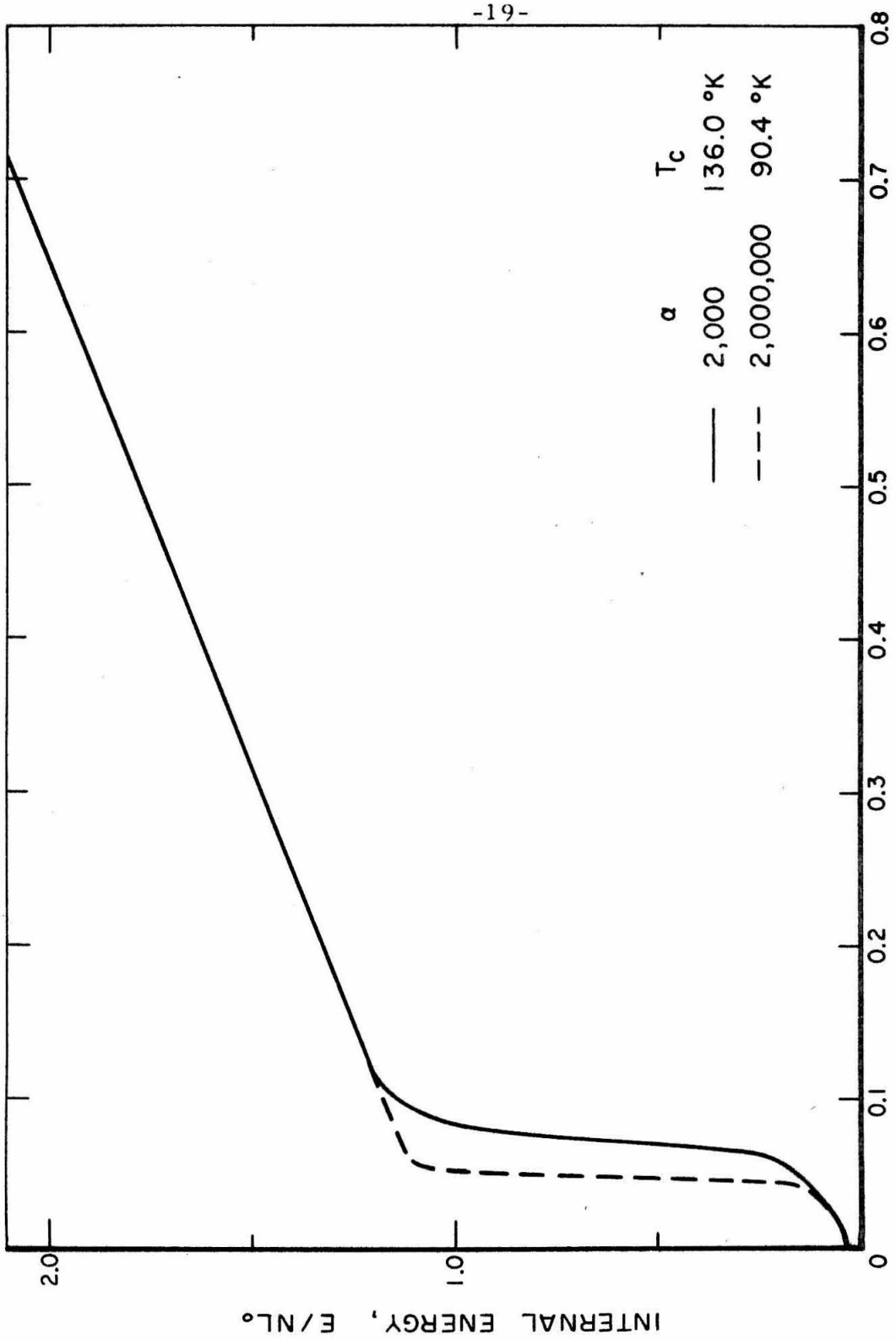

Fig. 5 - Internal Energy of Xenon

The specific heat,

$$C_v = \left(\frac{\partial E}{\partial T}\right)_v \qquad \text{(II-31)}$$

may also be calculated from Eq. (II-21) by differentiation. The shape of the specific curve is shown in Figs. 6, 7, and 8 for argon, krypton, and xenon, respectively. The critical temperature of each curve is about 75 percent of the triple point temperature. We note that krypton and xenon are behaving as nearly classical solids before the transition temperature is reached, but that argon is not.

2. Identification of the Equilibrium Vapor Pressure

To this point, we have been using α as a free parameter. As we vary α, we change the critical temperature. This is shown in Figs. 3, 4, and 5. This behavior was predicted by Eq. (II-27). As we noted in the previous section, if we know the functional form of $\alpha(p)$ we can determine the vapor pressure curve from Eq. (II-27). With the knowledge that $\alpha(p)$ is a decreasing function with pressure and that $\alpha(p)$ is proportional to the volume seen by the free particle, we assume

$$\alpha = \frac{G}{p} \qquad \text{(II-32)}$$

where G is a constant and p is the equilibrium vapor pressure. Since our model has no provision for a third phase, the liquid state, we shall adjust G to the triple point data. We list in Table IV the values of G found for the elements studied. By numerically differentiating Eq. (II-21), we may calculate the critical curve by using Eq. (II-32) in Eq. (II-25). These results are compared with

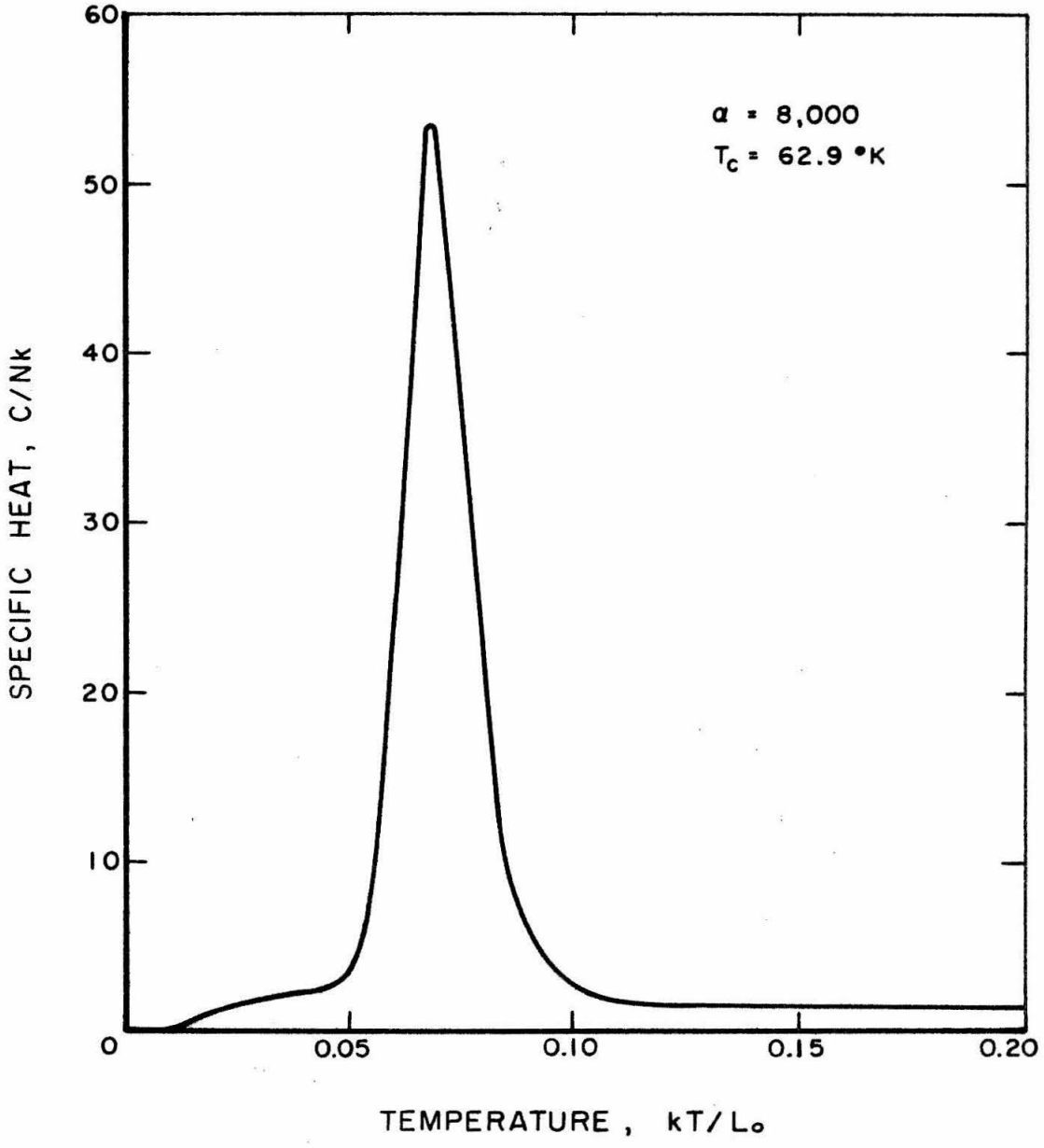

Fig. 6 - Specific Heat of Argon

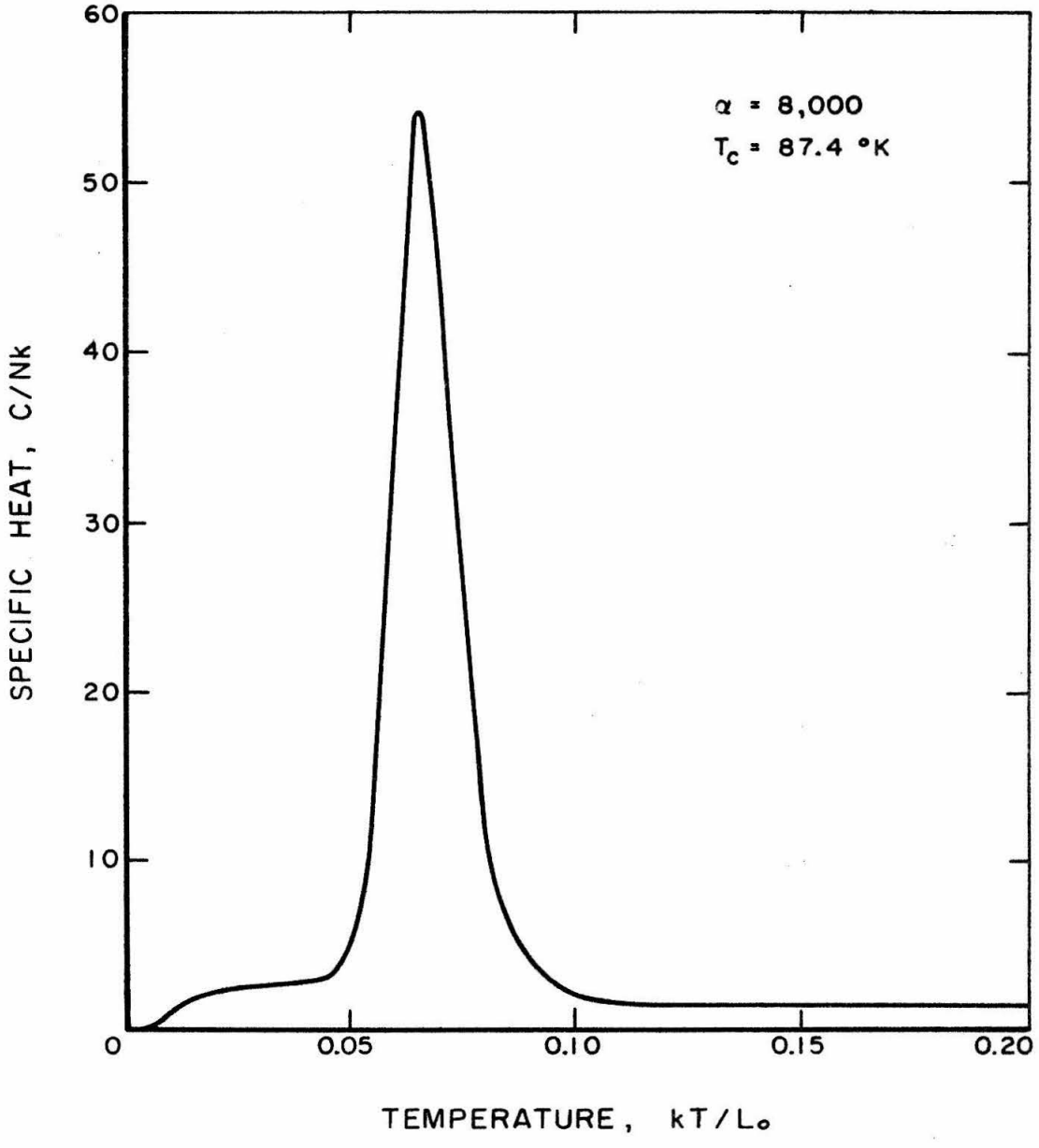

Fig. 7 - Specific Heat of Krypton

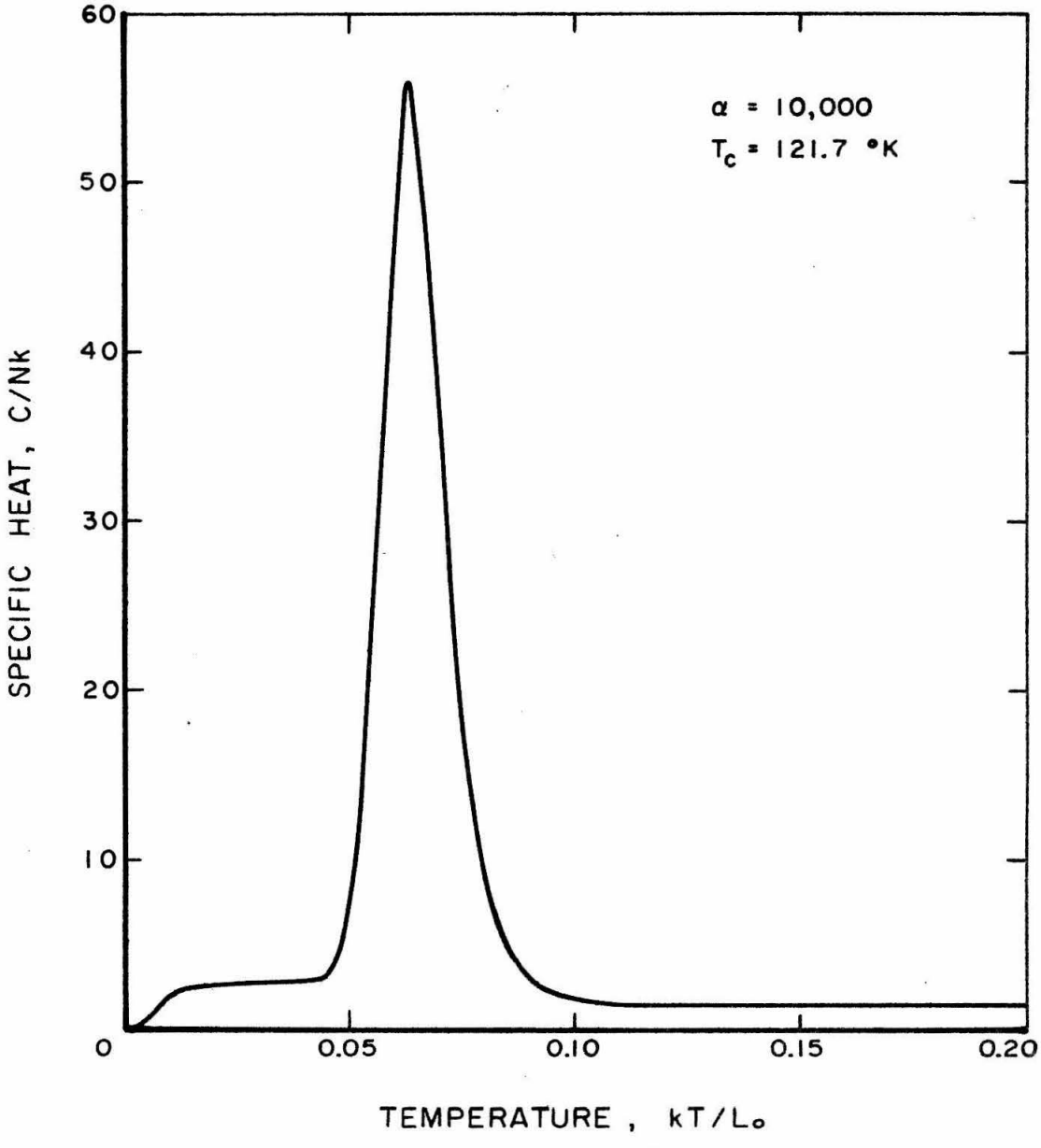

Fig. 8 - Specific Heat of Xenon

TABLE IV

Product of $\alpha p = G$

Element	$G(mm \times 10^5)$
Argon	1.00
Krypton	1.08
Xenon	1.42

experimental data in Fig. 9 obtained by Flubacher, et al[13], Freeman and Halsey[14], and Clark, et al[15] for argon. In Fig. 10 we compare the vapor pressure of krypton measured by Beaumont, et al[16], Fisher and McMillan[17], and Freeman and Halsey[14] with our theoretical curve. Finally, we compare our results with the vapor pressure of xenon measured by Freeman and Halsey[14], Podgurski and Davis[18], and Peters and Weil[19] in Fig. 11. We note that Freeman and Halsey[14] gave an experimental curve; the figures show selected points of these curves. We conclude that our assumed relation (II-32) is valid.

Although a theoretical interpretation of G has not been found, we mention that G is the same order of magnitude as $\alpha_t kT_t/V_t$, where $\alpha_t V_s$ is the volume of the free particle cell and V_t is the volume per particle of an ideal gas at the triple point. We can see from (II-32) that G would be exactly this value if the vapor could be considered an ideal gas and the aggregate interactions were negligible. We may state this interpretation more clearly by noting that $\alpha_t V_s$ and V_t are equal when these interactions are negligible.

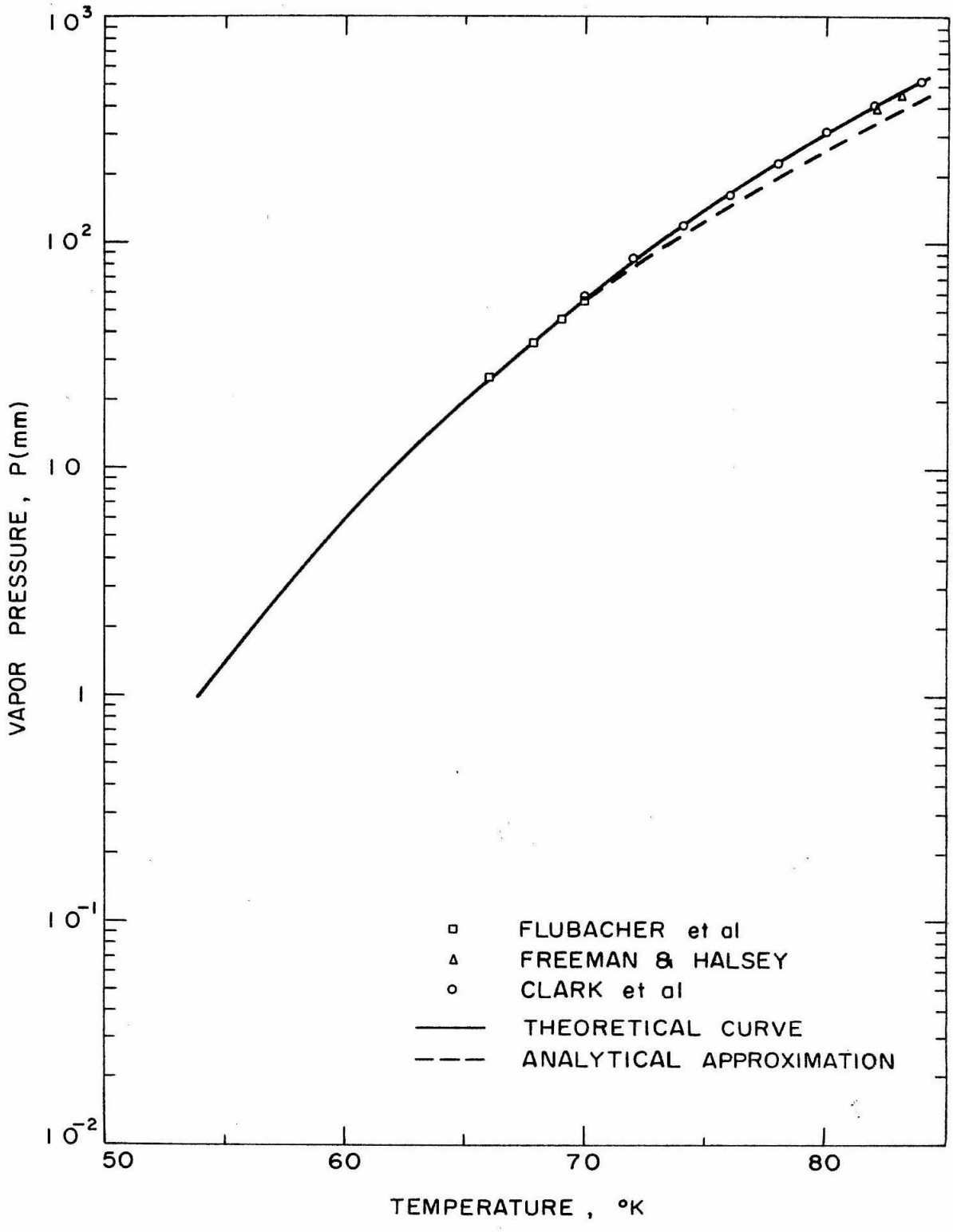

Fig. 9 - Vapor Pressure of Argon

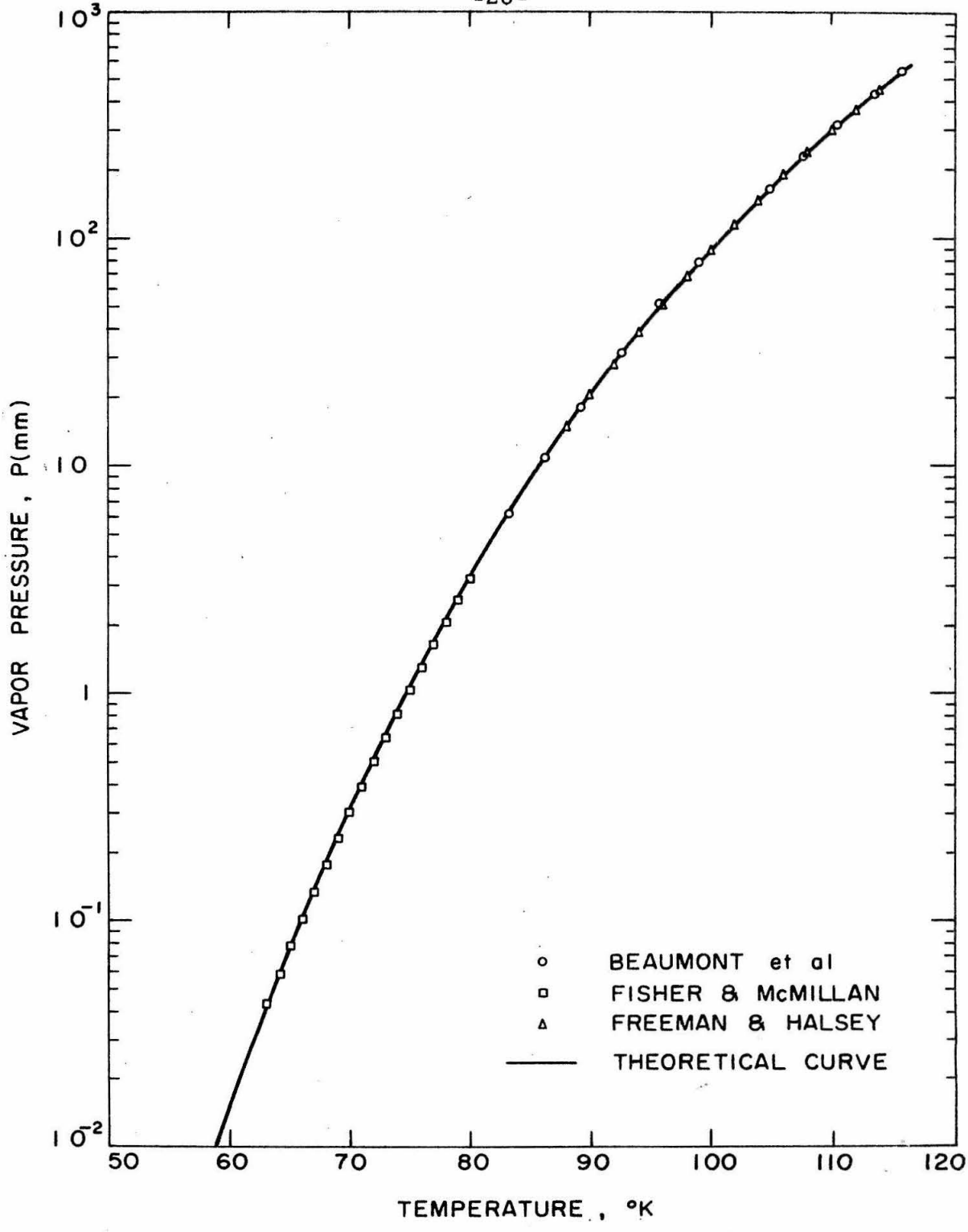

Fig. 10- Vapor Pressure of Krypton

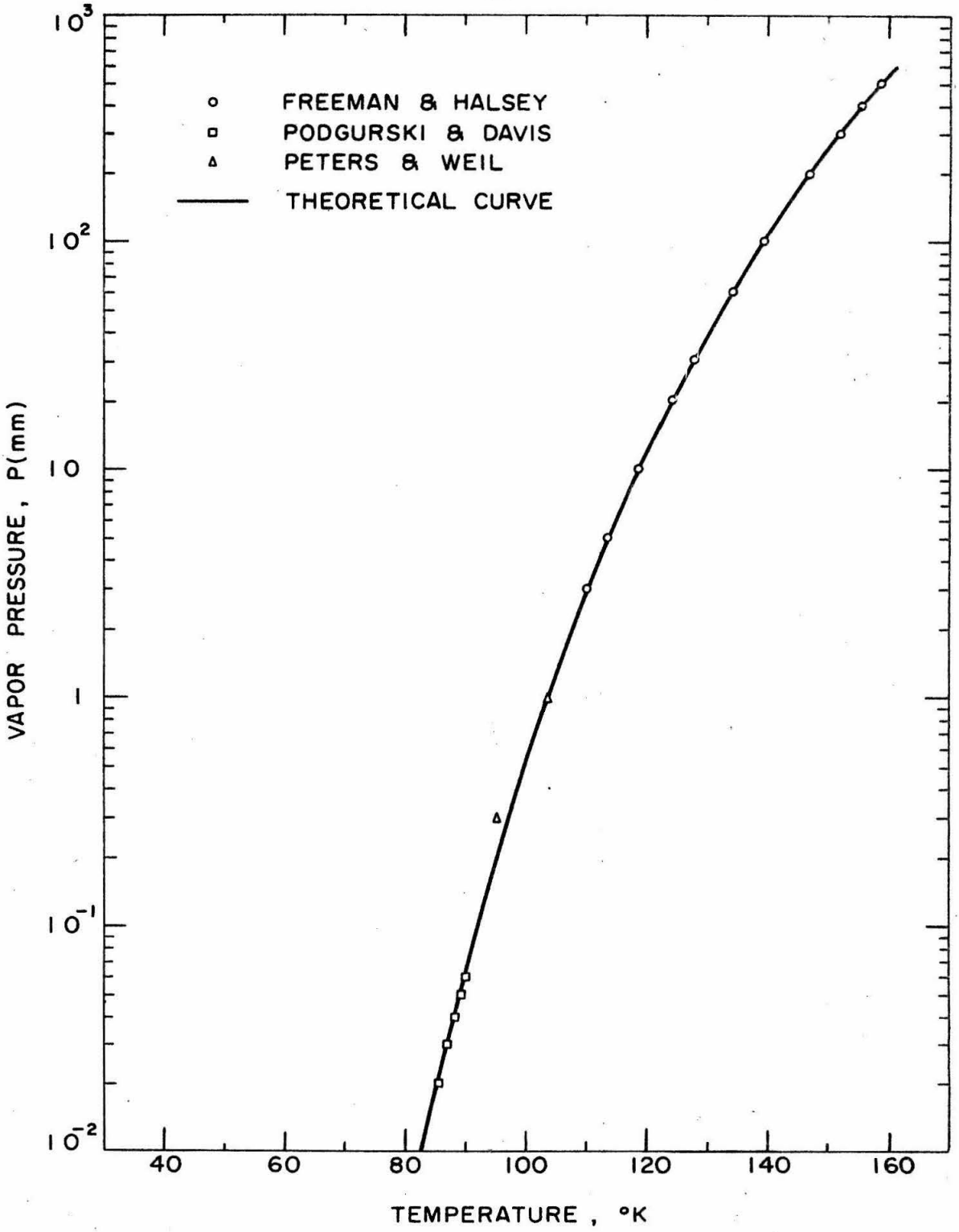

Fig. 11 - Vapor Pressure of Xenon

By taking values of α smaller than the triple point value, we begin to trace out the condensation curve of Fig. 1. We can see from Fig. 1 that the sublimation line and the condensation line join very smoothly. This is as we would expect since these transitions are physically similar as long as the liquid density is near solid densities.

Analytically setting the second derivative of E with respect to T equal to zero is very tedious. In Appendix B we calculate an approximate expression for the vapor pressure analytically. We find

$$\ell n p = -\frac{L_o}{kT} - \frac{1}{2}\ell n C + \ell n[C^2(1-e^{-1/C})^3] + \ell n\left[1+f\left(\frac{\hbar\omega}{L_o}, T\right)\right] + \ell n[GA] \quad \text{(II-33)}$$

where $f\left(\frac{\hbar\omega}{L_o}, T\right) \to 0$ as $\frac{\hbar\omega}{L_o} \to 0$. In deriving Eq. (II-33), we have assumed

$$\alpha A C^{3/2} \gg X(1-X)^{-4} M^3 \quad \text{(II-34)}$$

and

$$\frac{L_o}{\hbar\omega} \gg 1 \quad . \quad \text{(II-35)}$$

We can not neglect $f\left(\frac{\hbar\omega}{L_o}, T\right)$ in Eq. (II-33) since it is as large as 0.6. For argon, we find

$$f\left(\frac{\hbar\omega}{L_o}, T\right) = \frac{\hbar\omega}{L_o}\left[\frac{17}{2} C - \frac{65}{8} C^2 - \frac{9X}{1-X} + \frac{81}{2}\frac{XC}{1-X} - \frac{81}{2}\frac{X^2}{(1-X)^2}\right] + O\left[\frac{(\hbar\omega)^2}{L_o^2}\right]. \quad \text{(II-36)}$$

This approximate solution for the equilibrium vapor pressure

of argon is shown as the dashed line in Fig. 9. Since Eq. (II-33) is already more cumbersome than Eq. (II-2) no further approximations were attempted.

In concluding our study of the equilibrium vapor pressure, we demonstrate one of the advantages of this model. As we noted, previous studies have considered sublimation as the equilibrium of two physical systems. We can do this by considering the solid and gas phases to be in equilibrium. For the partition function of the solid, we have from Eq. (II-18),

$$Z_s = X^{3/2}\left[\frac{X^2 I''}{2} + 2XI' + I\right] \qquad \text{(II-37)}$$

and for the gas,

$$Z_g = \alpha A e^{-L_o/kT} C^{3/2} X^{3/2} \quad . \qquad \text{(II-38)}$$

By equating the chemical potentials of these separate systems and using Eq. (II-32) we find the vapor pressure is described exactly by Eq. (II-33) with $f\left(\frac{\hbar\omega}{L_o}, T\right)$ equal to zero. This leads to a large error in p. With this approach we have lost the inherent corrections due to vacancy formations of our cell model. These corrections must be handled separately as Salter demonstrates.

3. Estimate of the Latent Heat

Finally, we want to calculate the latent heat. Since the energy is a continuous function of T, the beginning and end of the transition is not precisely defined. Therefore, the latent heat is somewhat arbitrary. The latent heat per molecule may be calculated from

$$L = \Delta E + p\Delta v \quad . \tag{II-39}$$

We have found that (for $\alpha \gg 1$),

$$p\Delta v = p\alpha V_s \quad . \tag{II-40}$$

By using Eq. (II-32), we have

$$p\Delta v = G V_s \quad . \tag{II-41}$$

Figures 3, 4, and 5 indicate that ΔE is the order of L_o for all T_c. We choose to define ΔE by extending the "natural" tangents of the energy curve above and below T_c as shown in Fig. 12. We are in part assuming that the specific heat at constant pressure and C_v are nearly the same. With this definition of ΔE, we find by similar triangles

$$\frac{\Delta E}{L_o} = 1 + \frac{E_o}{L_o} - J - \left(\langle C_v \rangle - \frac{3}{2}\right)\frac{kT_c}{L_o} \quad , \tag{II-42}$$

where $Nk\langle C_v \rangle$ is the average specific heat at the point of inflection of the specific heat curve of the solid as sublimation begins and J is the intercept of this tangent line.

Therefore, as an approximate expression for the latent heat, we have

$$\frac{L}{L_o} = 1 + \frac{E_o}{L_o} - J - \left(\langle C_v \rangle - \frac{3}{2}\right)\frac{kT_c}{L_o} + \frac{GV_s}{L_o} \quad . \tag{II-43}$$

For argon, krypton, and xenon, we find $\langle C_v \rangle$ to be 2.50, 2.75, and 2.95, respectively, and J to be .046, .018, and .005, respectively. We may take $\langle C_v \rangle$ to be constant over a wide range of temperatures

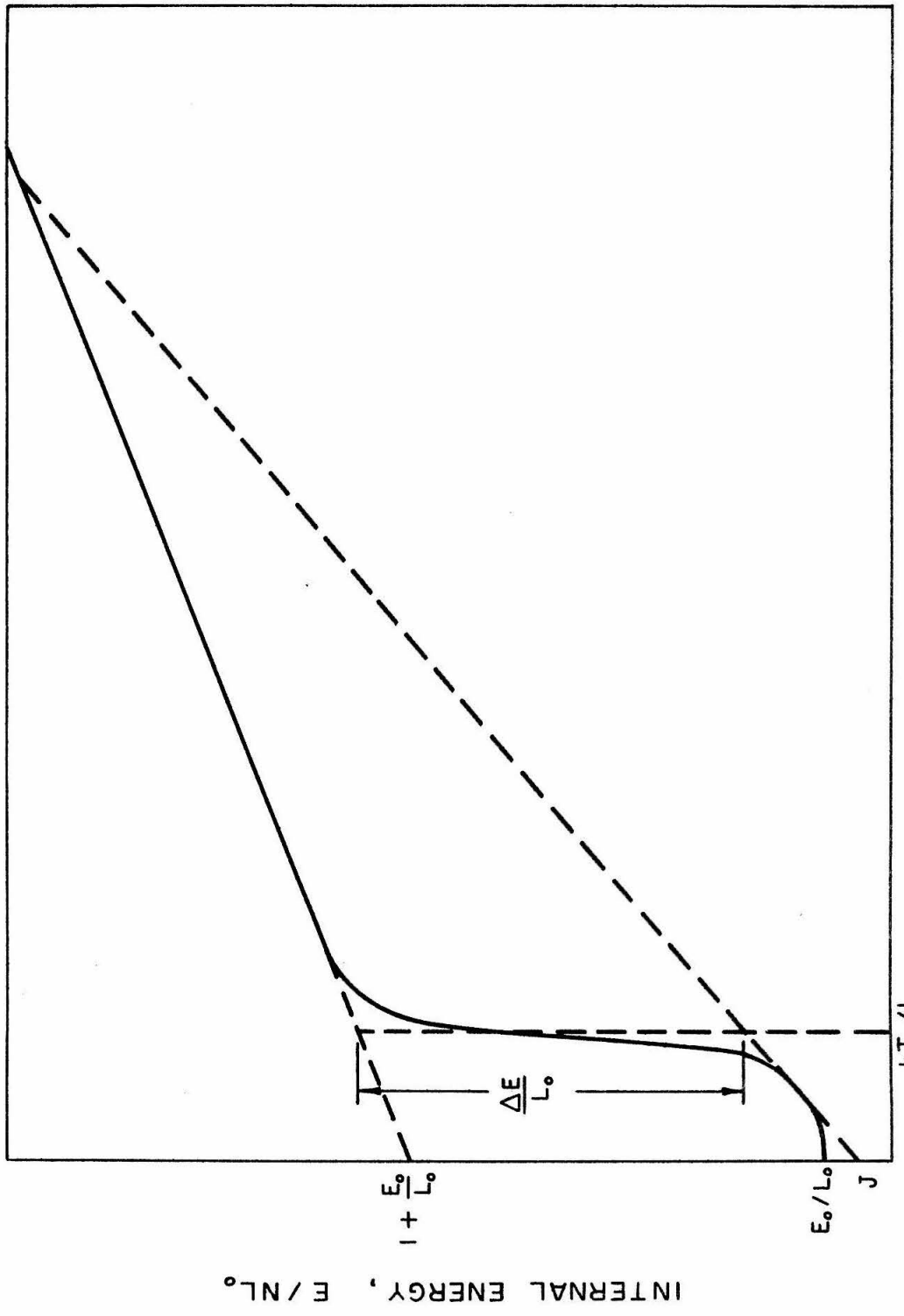

Fig. 12 - Method of defining the change of internal energy for sublimation. With this definition of ΔE, $L = \Delta E + GV_S$.

since the corrections resulting from its dependence on T_c are small and these corrections are less than the inherent uncertainty of Eq. (II-43). We note that an error in the estimate of $\langle C_v \rangle$ is compensated for when J is calculated. For a variation of $\pm .02$ in $\langle C_v \rangle$, we find L varies less than 1/2%.

With this definition of L, we compare the theoretically estimated values with the experimental data at the triple point in Table V.

TABLE V

Latent heats at the triple point

Element	Theoretical (L/L_o)	Experimental (L/L_o)*
Argon	1.01	1.01
Krypton	0.963	.967
Xenon	0.948	.901

*G. L. Pollack, Rev. Mod. Phys. 36, 748 (1964).

D. CONCLUDING REMARKS ON SUBLIMATION

1. Summary of Results

The agreement between the theoretical and experimental results as shown in Figs. 9, 10, and 11, is indeed very remarkable. At this point, it is especially noteworthy that, for each element, the only unknown parameter is G, since L_o and E_o may be obtained from theories of the solid state[20]. One point on the vapor pressure

curve, e.g. the triple point, then determines G unequivocally. In this connection, we may remark that Eq. (II-2), as derived by Salter, consists also of one parameter, ω_g, which has to be determined by experiment in practice. But the range of validity of Eq. (II-2) is somewhat less than the present theory. For example, Eq. (II-2) begins to deviate from experimental data for krypton at about 75°K; but this model is consistent with all experimental data available.

The sublimation process according to the present model does not represent a singularly sharp phase transition. Although, whether the transition is in fact a sharp transition is still not a settled question, we do not intend to raise this issue here. We only point out that the energy and specific heat curves as shown in Figs. 3, 4, 5, 6, 7, and 8 clearly reveal a phase transition across the temperature region in the neighborhood of T_c. In fact, the transition becomes sharper as T_c becomes smaller.

The mechanism of the sublimation process can also be seen from this physical model. The tendency for the system to stay at a lower energy in the harmonic potential is constantly competing with the tendency to be in the free particle cell at higher energy. The Boltzmann factor will favor the lower energy states. On the other hand, the free particle cell provides a much larger number of available states. The sudden predominance of the large density of states for the free particle cell over the Boltzmann factor across a narrow temperature range results in the sublimation transition. This competition between the Boltzmann factor and the density of states,

we believe, underlies all the phenomena of phase transition. The system will change from one phase to another when the latter has a much larger density of states even at the expense of a finite jump in energy. This jump in energy gives rise to the latent heat.

For the present physical model, sublimation is not a discontinuous process. So there is some ambiguity in defining the latent heat. We have defined L as shown in Fig. 12. The inferences of such a definition are consistent with all experimental evidence. The latent heat thus defined varies slightly with T_c. From the physical model, we can see that it tends to L_o at 0°K. For the nearly classical solids in the temperature range where this theory is valid, L decreases as T_c increases.

We have represented the solid phase by the Einstein model[7] mainly because we are primarily interested in the problem of sublimation. In the temperature range in which we have been interested, the Einstein model gives nearly as good a representation as the Debye model[21]. The use of the Einstein model yields a simple picture of a particle confined in a cell, and enables us to visualize graphically the process of sublimation. At low temperatures, we need to revise our representation of the solid state to accommodate the inadequacy of the Einstein model. Also, we may need to incorporate the anharmonic effects in our model to deal with the situation in the immediate vicinity of the triple point.

2. Suggestions for Further Research

This model of sublimation has pointed out at least two areas

of study where the ideas developed here may be used or tested.

i) Formulation of a simple model may be instructive in isolating the principles involved in any phase transition that one is studying. For example, such a model of melting may be very useful in improving our understanding of the liquid state.

ii) Experimental measurements of the specific heat, as the sublimation line is crossed, would determine how sharp the transition is. This data along with measurements of the latent heat as a function of sublimation temperature will determine to what extent our model may be used as a quantitative tool.

PART II

THE PERCUS-YEVICK LIQUID APPLIED TO THE MELTING PROBLEM

III. INTRODUCTION TO THE THEORY OF MELTING

A. REVIEW OF PREVIOUS WORK

A comprehensive review of the theory of melting is not available in the literature. Reviews of selected aspects of the theory have been made by Ubbelohde[22] (for complicated molecular structures), Cohen [2] (selected mathematical models), and Brout[1] (existence and stability of the phases). Reviews of the melting theories of the rare gases have been made by Dobbs and Jones[23], Pollack[24], and Horton[25]. In the following paragraphs we will give a brief review of the existing theories of melting.

A successful theory of melting does not exist at the present time. That is to say, there is no molecular model from which one can demonstrate from first principles a transition from the solid state to the liquid state or vice versa. This theory must predict the melting curve and the changes in volume, ΔV_m, and entropy, ΔS_m, of melting. The main difficulty found in formulating such a fundamental model of melting is the lack of a good theoretical representation of the liquid state.

In the past, the study of melting has been concentrated in two areas. The first area of research deals mainly with the establishment of the existence of the transition. Examples of work in this area includes the general study of phase transitions by Yang and Lee[26] and the studies of melting by Kirkwood and Monroe[27] and Brout[1]. The second area is concerned with correlating the physical quantities in connection with the melting process. We will confine

our interest to the latter.

Since the molecular structure of argon is relatively simple for theoretical calculations and a large reservoir of experimental data is available, it has been customary to apply melting theories to argon. In this thesis, we will follow this custom.

An essential feature of any phase transition is the existence of a critical temperature above which the transition does not exist. For the melting transition the existence of a critical temperature is not a settled question[28] - [30]. However, the general belief, based on the experimental results of Bridgman[31] and Lahr and Eversole[32], is that no critical temperature exists.

1. The Lindemann and Simon Equations

The first molecular model used to explain the melting of a solid was formulated by Lindemann[33] in 1910. He assumed that melting occurred when the thermal vibrations of the solid molecules became so large that the adjacent molecules could touch. The resulting formula is

$$\frac{m(V_m)^{3/2}\theta^2}{T_m} = \text{constant} \quad , \qquad \text{(III-1)}$$

where V_m is the volume and T_m is the temperature along the melting line. θ is a characteristic temperature (not necessarily the Debye or Einstein temperature). Although we know that such large amplitudes are not found, the success of the Lindemann equation in predicting the form of the melting line for a large number of substances is amazing. Attempts to extend and justify Eq. (III-1) have

had only limited success[34] - [38]. Other than its phenomenological nature, the major weakness of the Lindemann model is its inability to give any prediction of the change in the entropy or volume associated with melting. Therefore, we do not have any estimate of the liquid properties adjacent to the melting line.

A more useful melting equation would relate the melting pressure P_m with T_m. Salter[39] has shown that the Lindemann equation may be combined with the Grüneisen equation of state of a solid to give a melting equation in the form

$$\frac{P_m}{a} = \left(\frac{T_m}{T_t} \right)^c - 1 \qquad \text{(III-2)}$$

where a and c are constants. This equation was originally proposed by Simon and Glatzel[40] from experimental observations and it is known as the Simon melting equation. Babb[41] has listed the empirically determined values of a and c for many substances. These constants for the rare gases are given in Table VI.

TABLE VI

The Simon Constants of the Rare Gases

Element*	a(bars)	c
Argon	2114	1.593
Krypton	2376	1.617
Xenon	2610	1.589

*Neon and radon will not be considered in this thesis.

More recently, Gilvarry[37] and Babb[38] have used their quantum-mechanically corrected versions of the Lindemann formula and the Murnaghan equation of state of a solid to derive the Simon equation in a manner similar to that of Salter. (We note that all of these models approach melting from the solid side of the melting curve.)

2. Order-Disorder Theories

One of the more successful theories of melting is the order-disorder theory developed by Lennard-Jones and Devonshire[42],[43]. They assumed that the melting system is composed of two interpenetrating lattices. When the system is in the solid state essentially all molecules are on one lattice structure. After melting, the molecules are nearly randomly distributed on the two lattices (short range order may exist after melting). The formulation is based on the theories of binary alloys of Bragg and Williams[44],[45] and Bethe[46]. This model is the Ising model[47], and it has been widely studied[48],[49]. Although the interpenetrating lattice structure is not a physical reality, the qualitative agreement with experiment at low temperatures is good. In Table VII the results of this order-disorder model are compared with experiment, for selected points near the triple point of argon.

TABLE VII

Melting Properties of Argon
Derived from the Lennard-Jones and Devonshire Model*

Physical Quantity	$\Delta_m V/V$	$\Delta_m S/k$ (83.8°K)	P_m/dyne-cm (90.3°K)	$\frac{1}{V}\left(\frac{\partial V}{\partial T}\right)$/°K (Liquid)
Method of Bragg and Williams	1.35	1.70	286×10^6	0.0040
Method of Bethe	1.28	1.74	294×10^6	0.0049
Experimental	0.12	1.60	291×10^6	0.0045

* J. A. Barker, Lattice Theories of the Liquid State (Pergamon Press, Oxford, 1963), p. 41.

This apparent success of the order-disorder model is of limited value since it has a critical temperature. For argon, this critical temperature is near 130°K; however, the melting transition has been observed up to 360°K and, as we indicated earlier, there is no indication of a critical temperature. A second weakness of the order-disorder model is found when more accurate mathematical representations are used; it is found that the agreement between theory and experiment becomes poorer. This behavior indicates that many of the physical features have been hidden by the semiempirical selection of the model parameters in the less accurate representation. We conclude, as other have, that there is a fundamental difference between melting and the order-disorder transition and that further development of this model would not be beneficial.

3. Hard Sphere Models

In recent years, some promising developments in the theory of melting have been made by assuming that the major contribution to melting comes from the hard core part of the intermolecular potential. The molecular dynamics calculations by Alder and Wainwright[50] - [52] and Alder, Hoover, and Wainwright[53] of hard spheres and disks have demonstrated that a phase transition exists for this simple interaction. A typical isotherm is shown in Fig. 13.

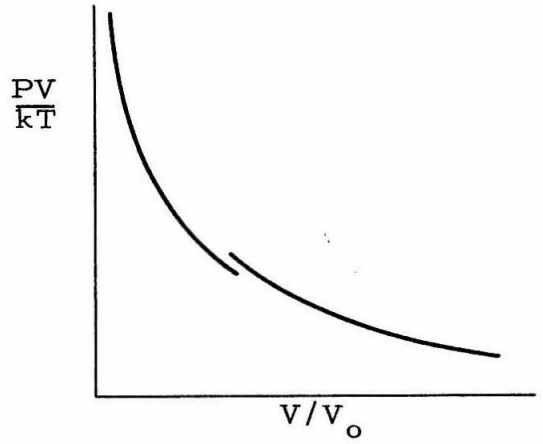

Fig. 13 Phase Transition of Hard Spheres

More recently, Longuet-Higgins and Widom[54] have approximated the melting system by hard spheres plus an average contribution resulting from attractive forces. The average attractive potential is

$$\phi_{ATT.} = -\frac{2a}{V} \quad . \tag{III-3}$$

And the resulting equation of state is

$$P = P_{H.S.} - a/V^2 \quad , \tag{III-4}$$

where $P_{H.S.}$ is the hard sphere pressure and a is a parameter.

By a suitable choice of $\underline{a}$, they found excellent agreement with experiment at the triple point. Some of their results are shown in Table VIII.

TABLE VIII

Melting Properties of Argon
Derived from the Longuet-Higgins and Widom Model

	V_ℓ / V_s^*	$\ell n(PV_\ell / kT)_t^*$	$(\Delta S/k)_t^*$	$(E_\ell / kT)_t^*$
Theory	1.19	-5.9	1.64	-8.6
Experiment	1.114	-5.88	1.69	-8.53

*The subscripts "ℓ", "s", and "t" will refer to liquid, solid, and triple point respectively throughout the remainder of the text. E is the internal energy.

The agreement between theory and experiment is impressive; however, for higher temperatures the theoretical predictions become very poor. Crawford and Daniels[55] have shown that this model may be corrected to account for this high temperature region by using (III-3) and (III-4) for the liquid and by calculating attractive potential in Eq. (III-3) from a Lennard-Jones potential for the solid. This assumption gives rise to a new parameter V_b. For molecular volumes above V_b the liquid equation of state is used and for volumes less than V_b the solid equation of state is used. The resulting model has two parameters V_b and $\underline{a}$ that are determined by semiempirical means.

Finally, the most elegant analysis of the melting problem, which uses a hard sphere model, has been made by Henderson and

Barker[56]. By using their recently developed hard sphere perturbation theory of liquids and the Lennard-Jones and Devonshire[10] cell model for the solid, they have calculated the melting curve of argon, Fig. 14. The melting pressure is obtained from the slope of the common tangent in a plot of solid and liquid free energies versus volume. The change in volume and entropy of melting have not been calculated with this model.

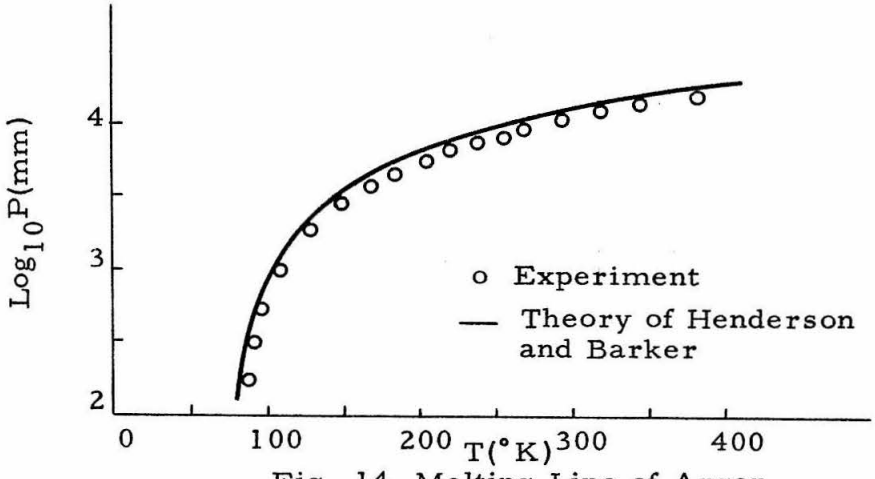

Fig. 14 Melting Line of Argon

The success of these models has lead to a general belief that hard sphere packing is the essential feature of melting.

4. Other Models

We will not attempt to list all other models; however, we would like to note two interesting approximations. Emtage[57] has assumed that the essential feature of melting is the mismatch of bits of lattice structures as the solid melts. The resulting melting curve and the changes in volume and entropy are in qualitative agreement

with experiment.

In the second model by Tsuzuki[58], the two body distribution function $4\pi^2 g(r)$ is assumed to be constant for $r_i(1-\Delta) \leqslant r \leqslant r_i(1+\Delta)$, where r_i is the location of the i^{th} shell of neighboring molecules in the solid, and Δ is a measure of the liquid irregularity. A free volume approximation is used for the entropy. With this crude model, the change in volume, the change in entropy, and the melting temperature are calculated for the case $P_m \approx 0$ (the triple point). The calculated melting temperature is 0.82 in reduced units compared to the experimental value, 0.67.

5. Summary of Existing Theories

In the preceding paragraphs, we have tried to give a complete picture of the current state of the theory of melting. We would like to point out that none of these theories predicts from first principles the melting curve, the change in volume, and the change in entropy. (The model by Henderson and Barker is most closely aligned with fundamental reasoning.) We have also indicated that many models have been developed with semiempirical parameters. It is suggested that these parameters may be concealing important physical phenomena. We believe that this review has demonstrated the need for a melting model, developed from first principles, from which a greater understanding of the melting transition may be obtained.

B. PURPOSE OF THIS STUDY

We will develop a theory of melting from the fundamental point of view. By assuming microscopic models for the solid and liquid states, the macroscopic properties are computed with statistical mechanics. The melting points are then determined in a formal way by equating the chemical potentials of the solid and liquid states. The validity of the solid and liquid models near the melting curve will be studied. The models selected were believed to be the best available at the outset of this study.

We have made only four assumptions in formulating this melting model.

1) The configurational energy of any collection of atoms is the sum of the energy of pairs of atoms.

2) This configurational energy for two atoms a distance r apart may be represented by the Lennard-Jones[3] (LJ) 12-6 potential. The LJ potential is

$$u(r) = 4\epsilon \left[\left(\frac{\sigma}{r} \right)^{12} - \left(\frac{\sigma}{r} \right)^{6} \right] \quad . \tag{III-5}$$

The pair potential is regarded as a basic physical quantity. Ideally the constants for $u(r)$ would be determined from a quantum-mechanical calculation of the force between two atoms[59]. However, in practice these constants are determined from experimental measurements of the second virial coefficient of the gas[60]. For argon, we have

$$\epsilon / k = 119.8 \ ^\circ K \tag{III-6}$$

and

$$\sigma = 3.405\,\text{Å} \quad . \tag{III-7}$$

Although Eq. (III-5) with the constants defined above is generally accepted as the "best" pair potential function for argon, considerable effort is being made at the present time to determine $u(r)$[61]. Since there is some uncertainty in $u(r)$, we will discuss the effect of slight shifts in ϵ and σ.

3) We will represent the solid by an anharmonic model developed by Henkel[62] and Guggenheim and McGlashan[63]. The anharmonic effects are calculated from a perturbation theory of a harmonic oscillator. The oscillator frequency and the perturbation energy are computed directly from lattice sums of the pair potential function, Eq. (III-5). This solid model is compared with the widely used cell model of Lennard-Jones and Devonshire[10].

4) Finally, we assume that the Percus-Yevick (PY) equation is a valid approximation for the liquid state. Recently, Watts[64],[65] has shown that the thermodynamic functions predicted by the PY approximation are in excellent agreement with experiment for moderate liquid densities. Details of this assumption will be discussed in Chapter IV.

Although the validity of the first three assumptions may be questioned, they are generally used in the study of the rare gases. There has been considerable controversy, however, concerning the merits of the PY equation. Therefore, a basic aim of this study is to test the PYequation at higher densities. We should note that once

we have assumed 1) - 4), the properties of the system are determined.

The liquid state properties will be studied along three isotherms (kT/ϵ = 1.3, 1.8, and 2.0) above the liquid-vapor critical point. These isotherms are shown schematically on the phase diagram in Fig. 15.

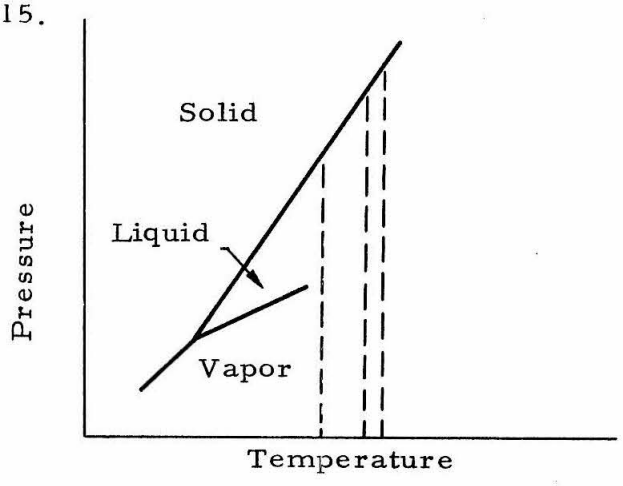

Fig. 15 Schematic Diagram of the Isotherms Studied.

Although melting may have occurred in a thermodynamic sense, the density will be increased until the solution of the PY equation does not converge.

IV. THEORY OF MELTING

A. THERMODYNAMIC CONDITIONS FOR MELTING

We may represent the equilibrium of the solid and liquid phases by equating their chemical potentials

$$\mu_s(P, T) = \mu_\ell(P, T) \quad . \tag{IV-1}$$

Once we have an equation of state for each phase and Eq. (IV-1) is satisified, we may immediately calculate the volume change and the latent heat of the transition.

For the solid, we have

$$\mu_s = F_s + PV_s \quad , \tag{IV-2}$$

where F and V are the free energy and the volume per particle respectively*. These thermodynamic quantities will be calculated in a later section.

Similarly for the liquid, we have

$$\mu_\ell = F_\ell + PV_\ell \quad . \tag{IV-3}$$

We calculate the pressure by using the relation

$$P = - \left.\frac{\partial F}{\partial V}\right)_T \quad . \tag{IV-4}$$

We differentiate Eq. (IV-3) with respect to volume. By using Eq.

---

*We will use the value per particle for all extensive quantities unless otherwise stated.

(IV-4), we find

$$\left.\frac{\partial \mu_\ell}{\partial V_\ell}\right)_T = V_\ell \left.\frac{\partial P_\ell}{\partial V_\ell}\right)_T \quad . \tag{IV-5}$$

Integration of this relation along an isotherm from state (1) to state (2) gives

$$\mu_\ell(2) - \mu_\ell(1) = \int_{1,\ T=\text{constant}}^{2} V_\ell \, dP_\ell \quad . \tag{IV-6}$$

By adding and subtracting the same quantity, we have

$$\mu_\ell(2) - \mu_\ell(1) = \int_{1,\ T=\text{constant}}^{2} \left[V_\ell - \frac{kT}{P_\ell}\right] dP_\ell + kT\,\ell n\left[\frac{P(2)}{P(1)}\right] \quad . \tag{IV-7}$$

We rewrite this in the form

$$\frac{\mu_\ell(2)}{kT} = \int_{1,\ T=\text{constant}}^{2} \left[\frac{V_\ell}{kT} - \frac{1}{P_\ell}\right] dP_\ell + \ell n\, P(2) + \frac{\mu_\ell(1)}{kT} - \ell n\, P(1) \tag{IV-8}$$

By letting $P(1) \to 0$, state (1) $\to$ ideal gas; for an ideal monatomic gas (Ref. 12, p. 15), we have

$$\frac{\mu_\ell(1)}{kT} = \ell n\, P(1) - \ell n\left[\left(\frac{m}{2\pi}\right)^{3/2} \frac{(kT)^{5/2}}{\hbar^3}\right] \quad . \tag{IV-9}$$

By using this relation in Eq. (IV-8), we have

$$\frac{\mu_\ell(2)}{kT} = \int_{o}^{P(2)} \left[1 - \frac{\rho_\ell kT}{P_\ell}\right] \frac{dP_\ell}{\rho_\ell kT} + \ell n\left[\left(\frac{2\pi}{m}\right)^{3/2} \frac{\hbar^3 P(2)}{(kT)^{5/2}}\right] \tag{IV-10}$$

where

$$\rho_\ell = 1/V_\ell \quad . \tag{IV-11}$$

Therefore, we may calculate the chemical potential at P(2) if we have an equation of state of the liquid along the isotherm for all pressures less than P(2).

B. THE LIQUID STATE

We shall not make an extensive review of the theories of liquids. For such a review the reader may consult one of the many books in the field[12], [60], [66] - [68]. We shall merely outline the steps leading to our representation of the liquid.*

For a liquid of N molecules, the Hamiltonian may be written as

$$H = \sum_{i=1}^{N} \frac{p_i^2}{2m} + U(\vec{r}_1, \ldots, \vec{r}_N) \quad , \tag{IV-12}$$

where $\vec{p}_i$ is the momentum of particle i, m is again the mass of a molecule, and $U(\vec{r}_1, \ldots, \vec{r}_N)$ is the potential energy of the N molecules located at $\vec{r}_1, \ldots, \vec{r}_N$ respectively. If we denote $\rho_N^{(n)}(\vec{r}_1, \ldots, \vec{r}_N)d\vec{r}_1 \ldots d\vec{r}_N$ as the probability of finding a molecule in $d\vec{r}_1$ at $\vec{r}_1$, another in $d\vec{r}_2$ at $\vec{r}_2$, . . . , and another in $d\vec{r}_n$ at $\vec{r}_n$, regardless of where the remaining N-n molecules are

---

*This outline is in part a paraphrase of the representations on pp. 41-44, 73, and 100-106 of Ref. 66 and on pp. 13-15, and 54-58 of Ref. 67.

located, then we may write

$$\rho_N^{(n)}(\vec{r}_1, \ldots, \vec{r}_N) = \frac{N!}{(N-n)!} \frac{\int \ldots \int_V e^{-\beta U(\vec{r}_1, \ldots \vec{r}_N)} d\vec{r}_{n+1} \ldots d\vec{r}_N}{Z_N} , \tag{IV-13}$$

where β is $1/kT$, V is the total volume (NV_ℓ), and

$$Z_N = \int_V \ldots \int e^{-\beta U(\vec{r}_1, \ldots \vec{r}_N)} d\vec{r}_1 \ldots d\vec{r}_N . \tag{IV-14}$$

The function $\rho_N^{(n)}$ is known as the generic probability density.

We introduce the fugacity,

$$z = e^{\mu/kT} . \tag{IV-15}$$

In the grand canonical ensemble, we have

$$\rho^{(n)}(\vec{r}_1, \ldots \vec{r}_n) = \frac{\sum_{N \geq n}^{\infty} z^N Z_N \rho_N^{(n)}(\vec{r}_1, \ldots \vec{r}_n)/(N! \Lambda^{3N})}{\sum_{N \geq o}^{\infty} z^N Z_N/(N! \Lambda^{3N})} , \tag{IV-16}$$

where Λ is $h(2\pi mkT)^{-\frac{1}{2}}$. Λ is called the thermal wave length of the molecule.

We now assume that U is equal to the sum of potentials, $u(|\vec{r}_i - \vec{r}_j|)$ between pairs of molecules. This is the first assumption that we discussed in the introduction. We then have

$$U(\vec{r}_1, \ldots, \vec{r}_N) = \sum_{1 \leqslant i < j \leqslant N} u(|\vec{r}_i - \vec{r}_j|) \quad . \tag{IV-17}$$

By using this assumption and Eq. (IV-16), we find upon differentiation of Eq. (IV-16) with respect to the coordinates of the molecule at $\vec{r}_1$

$$-kT\vec{\nabla}_1\rho^{(n)} = \sum_{i=2}^{n} \vec{\nabla}_1 u(|\vec{r}_1 - \vec{r}_i|)\rho^{(n)} + \int_V \vec{\nabla}_1 u(|\vec{r}_1 - \vec{r}_{n+1}|)\rho^{(n+1)} d\vec{r}_{n+1} \quad . \tag{IV-18}$$

From (IV-18), we see that we have a hierarchy of equations in which $\rho^{(n)}$ is defined in terms of $\rho^{(n+1)}$. For a thermodynamic system, we have on the order of 10^{23} equations so that an exact solution is impossible. Therefore, one of the current problems in the theory of liquids is the determination of a successful method of truncating this hierarchy of equations. We shall find that the thermodynamic properties may be determined if we know $\rho^{(2)}$. For this reason, the most efficient way to truncate (IV-18) is to make an approximation for $\rho^{(3)}$ in the equation for $n = 2$. In the following paragraphs, we shall set up the analytic formalism necessary to understand our method of truncating (IV-18).

Since the liquid is in thermal equilibrium and it is macroscopically isotropic, we may write

$$\rho^{(2)}(\vec{r}_1, \vec{r}_2) = \rho^{(2)}(|\vec{r}_1 - \vec{r}_2|) \quad . \tag{IV-19}$$

A more familiar form of the pair distribution is the radial distribution function defined as

$$g(r) = \left(\frac{V}{N}\right)^2 \rho^{(2)}(r) \quad , \tag{IV-20}$$

where

$$r = |\vec{r}_1 - \vec{r}_2| \quad . \tag{IV-21}$$

The function $g(r)$ is proportional to the probability of finding a molecule at a distance r if there is one at the origin; it is normalized to 1 for large r. The first equation of (IV-18) may be written with $g(r)$ to give

$$-kT\vec{\nabla}_1 g(r) = \vec{\nabla}_1 u(r) g(r) + \left(\frac{V}{N}\right)^2 \int_V \vec{\nabla}_1 u(|\vec{r}_1 - \vec{r}_3|)\rho^{(3)}(\vec{r}_1, \vec{r}_2, \vec{r}_3)d\vec{r}_3 \quad . \tag{IV-22}$$

The probability of a third molecule being in $d\vec{r}_3$ at $\vec{r}_3$ when two molecules are at $\vec{r}_1$ and $\vec{r}_2$ may be written as

$$P(\vec{r}_3 \,|\, \vec{r}_1, \vec{r}_2)d\vec{r}_3 = \frac{\rho^{(3)}(\vec{r}_1, \vec{r}_2, \vec{r}_3)d\vec{r}_3}{\rho^{(2)}(|\vec{r}_1 - \vec{r}_2|)} \quad ; \tag{IV-23}$$

and we find that Eq. (IV-22) may be expressed in the form

$$\nabla_1 \left\{ \ell n\, g(r) + \frac{u(r)}{kT} \right\} = -\frac{1}{kT} \int_V \nabla_1 u(|\vec{r}_1 - \vec{r}_3|) P(\vec{r}_3 | \vec{r}_1, \vec{r}_2) d\vec{r}_3 \quad . \tag{IV-24}$$

By rewritting this equation, we have

$$\frac{\partial}{\partial r}\left\{ \ell n\, g(r) + \frac{u(r)}{kT} \right\} = -\frac{1}{kT} \int_V \frac{\partial u(|\vec{r}_1 - \vec{r}_3|)}{\partial |\vec{r}_1 - \vec{r}_3|} \frac{\vec{r} \cdot (\vec{r}_1 - \vec{r}_3)}{r|\vec{r}_1 - \vec{r}_3|} P(\vec{r}_3 | \vec{r}_1, \vec{r}_2) d\vec{r}_3 \quad . \tag{IV-25}$$

This equation may be written in the form

$$g(r) = \exp\left(- \frac{u(r)+W(r)}{kT} \right) \quad , \qquad \text{(IV-26)}$$

where

$$W(r) = \int_r^\infty dr' \int_V \frac{\partial u(|\vec{r}_1-\vec{r}_3|)}{\partial|\vec{r}_1-\vec{r}_3|} \frac{\vec{r}'\cdot(\vec{r}_1-\vec{r}_3)}{r'(|\vec{r}_1-\vec{r}_3|)} P(\vec{r}_3|\vec{r}_1', \vec{r}_2')d\vec{r}_3 \quad . \qquad \text{(IV-27)}$$

Therefore, a truncation of the heirarchy of equations, (IV-18), may be made by making an approximation of $W(r)$.

First we introduce a new function, $c(r)$, called the direct correlation function. $c(r)$ is defined by the integral equation (Ref. 67, p. 56)

$$g(r) - 1 = c(r) + \frac{N}{V} \int_V c(|\vec{r}-\vec{r}'|)\,(g(r')-1)d\vec{r}' \quad . \qquad \text{(IV-28)}$$

The advantage of introducing $c(r)$ is that it is short-ranged in comparison with $g(r)$. For large r, $c(r)$ approaches 0. By using this fact, Baxter[69] has shown that if

$$c(r) = 0 \quad , \quad \text{for} \quad r > R \quad , \qquad \text{(IV-29)}$$

and if the integral of $|g(r) - 1|$ over all space is absolutely convergent, then Eq. (IV-28) may be written as

$$\begin{aligned} g(r)-1 = c(r) &+ \frac{2\pi}{r} \frac{N}{V} \int_o^r ds \int_o^s t(g(t)-1)(t-s)(g(t-s)-1)dt \\ &+ \frac{4\pi}{r} \frac{N}{V} \int_o^R s\,c(s)\left[\int_o^s t(g(t)-1)dt - \int_o^{|r-s|} t(g(t)-1)dt\right]ds \\ &+ \frac{4\pi^2}{r} \frac{N^2}{V^2} \int_o^R s\,c(s)\left[\int_o^r dt\, W(s,t)\right]ds \quad , \end{aligned} \qquad \text{(IV-30)}$$

for $0 < r < R$, where $W(s,t)$ is defined by

$$W(s,t) = - W(t,s) \qquad \text{(IV-31)}$$

and for $s > t$,

$$W(s,t) = \int_o^s u(g(u)-1)\left[\int_{|s-t-u|}^{s-|t-u|} v(g(v)-1)dv\right]du \quad . \qquad \text{(IV-32)}$$

Of course the integral condition is satisfied for any disordered liquid. With this form of Eq. (IV-28), the range of integration has been reduced from infinity to a finite value, R, which in practice is only a few times the parameter σ. Therefore, Eq. (IV-30) is very useful for numerical calculations.

As we have stated, we are interested in truncating the series of equations, (IV-18). We also indicated that this is most efficiently done by approximating $P(\vec{r}_3|\vec{r}_1,\vec{r}_2)$, which may be interpreted as an approximation of $W(r)$ or vice versa. Recent calculations[64],[65] indicate that the most promising approximation for dense systems is the Percus-Yevick[4](PY) approximation, which may be written as

$$\frac{W(r)}{kT} = - \ell n\{g(r) - c(r)\} \quad . \qquad \text{(IV-33)}$$

This equation is found by an elegant formulation of the many body system in collective coordinates. Such a formulation lends itself to a dense system; however, it was found that the PY equation would predict the first four virial coefficients of the gas state. The implications of the PY equation have never been completely understood. The common method of illustrating this approximation is to compare the

cluster expansion for $c(r)$

$$c(r) = [o-o] + \frac{N}{V}\left[\text{ 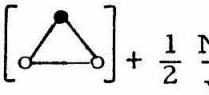 }\right] + \frac{1}{2}\frac{N^2}{V^2}\left[2\,\text{  } + 4\,\text{  } + \text{  } + \text{  }\right] + \ldots$$

(IV-34)

with the expansion consistent with the PY equation

$$c(r) = [o-o] + \frac{N}{V}\left[\text{ 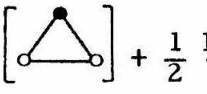 }\right] + \frac{1}{2}\frac{N^2}{V^2}\left[2\,\text{  } + 4\,\text{  }\right] + \ldots \quad , \text{(IV-35)}$$

where

$$o-o = f_{12} = e^{-u(|\vec{r}_1 - \vec{r}_2|)/kT} - 1 \quad ,$$

and

$$\text{ 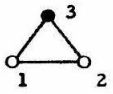 } = \int_V f_{12} f_{31} f_{23} d\vec{r}_3 \quad , \text{ etc.}$$

The PY approximation has neglected two classes of cluster integrals for the higher orders of the density expansion; it is believed that these integrals must essentially cancel each other.

Surprisingly, this equation has had little application at the high densities for which it was derived[70]. Therefore, an excellent test of this equation can be made for the densities along the melting line.

By combining Eq. (IV-26) and Eq. (IV-33), we have the PY equation

$$c(r) = g(r)\ (1 - e^{u(r)/kT}) \quad . \qquad \text{(IV-36)}$$

This equation may be used with Eq. (IV-28) or Eq. (IV-30) to form an integral equation for either $g(r)$ or $c(r)$. The resulting equation may then be solved by numerical means[64],[65],[70] - [78].

We have outlined a procedure for calculating g(r) and c(r) from u(r). In order to determine μ_ℓ from Eq. (IV-10), we must compute an equation of state. We may use the compressibility equation

$$\frac{1}{kT}\left.\frac{dP_\ell}{d\rho_\ell}\right|_T = 1 - 4\pi\rho_\ell \int_o^\infty c(r)r^2dr \qquad \text{(IV-37)}$$

and then integrate over the density to compute the pressure. For an alternate method of calculating the pressure, we could use the virial equation

$$\frac{P_\ell}{kT} = \rho_\ell - \frac{2\pi\rho_\ell^2}{3kT}\int_o^\infty r^3 \frac{du(r)}{dr} g(r)dr \quad . \qquad \text{(IV-38)}$$

We will use Eq. (IV-37) since the rapid variation of du/dr and g(r) near $r = \sigma$ is very significant in determining how accurately the pressure may be calculated from Eq. (IV-38) with approximate expressions of g(r) and u(r). For the energy of the liquid, we have

$$E_\ell = \frac{3}{2} kT + 2\pi\rho_\ell \int_o^\infty u(r)g(r)r^2dr \quad . \qquad \text{(IV-39)}$$

We have introduced these equations without proof. Again we refer the reader to Rice and Gray[66] for a more detailed analysis.

C. THE SOLID STATE

As we have indicated in the introduction, we shall develop the theory of melting from first principles. We assume that the two-body interaction energy, Eq. (III-5), is a fundamental property of the molecules. It is known that the conditions of mechanical stability

require the crystals of the rare gases to be in a face-centered cubic or a hexagonal close packed lattice structure[79], [80]. Although the zero point energy of these two structures differ by only 0.01%, the rare gases are known to be in the face-centered cubic form for temperatures as low as 4.2°K[24]. We assume that the solid is in this form for our calculations.

We will base our model of the solid on the analysis of Guggenheim and McGlashan[63]. This model was introduced by Henkel[62]. We may expand the 12-6 potential energy about an equilibrium position of the lattice in the form

$$\phi(r) = -\epsilon + 36\epsilon\left(\frac{r-r_o}{r_o}\right)^2 - 252\epsilon\left(\frac{r-r_o}{r_o}\right)^3 + 1113\epsilon\left(\frac{r-r_o}{r_o}\right)^4 \quad , \text{(IV-40)}$$

where

$$\left.\frac{du(r)}{dr}\right|_{r_o} = 0 \qquad \text{(IV-41)}$$

and

$$r_o = (2)^{1/6}\sigma \quad . \qquad \text{(IV-42)}$$

Equation (IV-40) is the assumed interactions for nearest neighbor pairs. For interactions of higher order neighbors, we use

$$\phi(r) = -2\epsilon\left(\frac{r_o}{r}\right)^6 \qquad \text{(IV-43)}$$

which is the "tail" of the 12-6 potential energy.

If R is the distance between nearest neighbors, then the static lattice energy per molecule of the crystal is

$$U_o = 6\epsilon\left[-1 + 36\Delta^2 - 252\Delta^3 + 1113\Delta^4 - \frac{(C_6 - 12)}{6}(1+\Delta)^{-6}\right] \qquad \text{(IV-44)}$$

where

$$\Delta = (R - r_o)/r_o \qquad \text{(IV-45)}$$

C_n is the crystal potential constant for a potential energy of the form r^{-n} of the face-centered cubic lattice[81].

For a small displacement of a molecule about a lattice site, with components x_1, x_2, and x_3 along the principal axes of the lattice, the increase in energy is

$$\Delta E = \frac{12\rho^2\epsilon}{(1+\Delta)r_o^2}\left[12(1+3\Delta) - 252\,\Delta(1+2\Delta) + 2226\,\Delta^2\left(1 + \frac{5}{3}\,\Delta\right)\right.$$

$$\left. - \frac{5}{6}(C_8 - 12)(1+\Delta)^{-7}\right] + \frac{12\rho^4\epsilon}{(1+\Delta)r_o^4}\left[-\frac{252}{5} + \frac{1113}{5}(1+5\Delta)\right.$$

$$\left. - \frac{7}{3}(C_{10} - 12)(1+\Delta)^{-9}\right] + O(\rho^6) \quad , \qquad \text{(IV-46)}$$

where

$$\rho = (x_1^2 + x_2^2 + x_3^2)^{\frac{1}{2}} \quad . \qquad \text{(IV-47)}$$

In Eq. (IV-46) the harmonic terms are exact, but the anharmonic terms were averaged over angles according to

$$\left\langle x_i^4 \right\rangle = \rho^4/5 \qquad \text{(IV-48)}$$

and for $i \neq j$

$$\left\langle x_i^2 x_j^2 \right\rangle = \rho^4/15 \quad . \qquad \text{(IV-49)}$$

To this approximation ρ^4 may be replaced by (5/3) $(x_1^4+x_2^4+x_3^4)$. This formulation of the solid leads to a perturbation solution of the Einstein harmonic oscillator by separation of variables. For this model, the energy states are

$$E_{n_1 n_2 n_3} = (n_1+n_2+n_3+3/2)\hbar(\omega_1+\omega_2)+(n_1^2+n_2^2+n_3^2)\hbar\omega_2 \quad , \qquad \text{(IV-50)}$$

with $n_i = 0, 1, 2, \ldots$ $(i = 1, 2, 3)$ and where

$$\omega_1^2 = \frac{24\epsilon}{mr_o^2(1+\Delta)}\left[12(1+3\Delta)-252\ \Delta\ (1+2\Delta)+2226\ \Delta^2\left(1+\frac{5\Delta}{3}\right)\right.$$
$$\left. - \frac{5}{6}\ (C_8-12)(1+\Delta)^{-7}\right] \quad , \qquad \text{(IV-51)}$$

and

$$\omega_2 = -\frac{6\hbar\epsilon}{m^2 r_o^4\ \omega_1^2(1+\Delta)}\ [252-1113(1+5\Delta)+\frac{35}{3}(C_{10}-12)(1+\Delta)^{-9}] \quad . \qquad \text{(IV-52)}$$

For the perturbation solution, we have assumed

$$\omega_1 \gg \omega_2 \quad . \qquad \text{(IV-53)}$$

ω_2 is zero in the harmonic approximation.

For a canonical ensemble, the partition function is

$$Z = \sum_{\text{all } \epsilon_n} e^{-\epsilon_n/kT}\ g_n \quad , \qquad \text{(IV-54)}$$

where ϵ_n is a single particle energy state which has degeneracy g_n. By using Eq. (IV-50) in Eq. (IV-54), we find

$$Z = \left[\frac{1}{2}\ \mathrm{cosech}\left(\frac{\hbar\omega_1}{2kT}\left(1+\frac{\omega_2}{\omega_1}\right)\right)\left(1-\frac{\hbar\omega_2}{kT}\left[\frac{e^{\hbar\omega_1/kT}+1}{(e^{\hbar\omega_1/kT}-1)^2}\right]\right)\right]^3 \qquad \text{(IV-55)}$$

or

$$\ln Z = -3\ln\left(2\sinh\left(\frac{\hbar\omega_1}{2kT}\right)\right) - \frac{3}{2}\ \frac{\hbar\omega_2}{kT}\ \coth^2\left(\frac{\hbar\omega_1}{2kT}\right) + O\left(\left(\frac{\hbar\omega_2}{kT}\right)^2\right) . \qquad \text{(IV-56)}$$

For the free energy per molecule, we have

$$F_s = U_o - kT \ln Z \quad . \qquad \text{(IV-57)}$$

We differentiate the free energy with respect to temperature, Eq. (II-20), and find the internal energy

$$E_s = U_o + \frac{3}{2}\hbar\omega_1 \coth\left(\frac{\hbar\omega_1}{2kT}\right)\left[1-\frac{\hbar\omega_2}{kT}\left(\mathrm{cosech}^2\left(\frac{\hbar\omega_1}{2kT}\right) - \frac{kT}{\hbar\omega_1}\ \coth\left(\frac{\hbar\omega_1}{2kT}\right)\right)\right] .$$

(IV-58)

By differentiating the free energy with respect to volume, Eq. (IV-4), we see that the pressure may be written as

$$PV_s = -2\epsilon\left[72\Delta(1+\Delta) - 756\Delta^2(1+\Delta) + 4452\Delta^3(1+\Delta) + (C_6-12)(1+\Delta)^{-6}\right]$$

$$- \frac{24\hbar\epsilon}{\omega_1 m r_o^2(1+\Delta)}\ \coth\left(\frac{\hbar\omega_1}{2kT}\right)\left[1-\frac{\hbar\omega_2}{kT}\ \mathrm{cosech}^2\left(\frac{\hbar\omega_1}{2kT}\right) + \left(\frac{d\omega_2}{dR}\Big/\frac{d\omega_1}{dR}\right)\coth\left(\frac{\hbar\omega_1}{2kT}\right)\right]$$

$$\times\left[6-63(1+4\Delta+2\Delta^2)+1113\Delta\left(1+3\Delta+\frac{5}{3}\ \Delta^2\right) + \frac{5}{3}\ (C_8-12)(1+\Delta)^{-7}\right] .$$

(IV-59)

We are now prepared to calculate the chemical potential of the solid,

μ_s. We have

$$\mu_s = F_s + PV_s \quad , \tag{IV-60}$$

where F_s and PV_s are given by Eqs. (IV-57) and (IV-59), respectively. Finally, the entropy may be defined by

$$S_s = (E_s - F_s)/T \quad . \tag{IV-61}$$

The Lennard-Jones and Devonshire (LJD) cell model has been used to represent the solid along the melting line[10]. In Appendix C, we have shown how the thermodynamic properties are calculated for this model. In our analysis, we shall compare the behavior of the Henkel, Guggenheim, and McGlashan (HGM) model with the LJD model near the melting line.

V. APPLICATION OF THE PROPOSED MELTING MODEL TO ARGON

In the first part of this chapter, we shall compare the liquid and solid models with experimental observations for argon. Although we apply the theory directly to argon, we introduce non-dimensional variables which would permit generalization to krypton and xenon. We define the variables

$$P^* = P\sigma^3/\epsilon, \tag{V-1}$$

$$V^* = V/\sigma^3 \quad , \tag{V-2}$$

$$E^* = E/\epsilon \quad , \tag{V-3}$$

$$T^* = kT/\epsilon \quad , \tag{V-4}$$

and

$$\rho^* = 1/V^* \quad . \tag{V-5}$$

We also use

$$r^* = r/\sigma \quad . \tag{V-6}$$

With the proper choice of ϵ and σ for argon, krypton, and xenon, the non-dimensional melting lines of these elements are essentially identical (Ref. 12, p. 21). This behavior is known as the principle of corresponding states. Therefore, it is easy to extend our study of argon to krypton and xenon. For argon, we shall use the constants given in Eqs. (III-6) and (III-7).

We shall be especially interested in the behavior of our models along the melting line of argon for temperatures between 155°K and 240°K. The lower limit, 155°K, was selected since it was slightly above the liquid-vapor critical temperature, 150.8°K. We did not want to complicate our problem by attempting to integrate over the

liquid-vapor equilibrium curve. The number of calculations for the liquid model was limited by the computing costs. Therefore, the upper limit, 240°K, was chosen so that the melting temperatures studied were not so far apart that meaningful comparisons could not be made.

The last part of this chapter is devoted to the calculation of the melting properties. We shall also study the effects of the approximations that we have made.

A. APPLICATION OF THE PERCUS-YEVICK LIQUID MODEL

As we noted in the previous chapter, by substituting Eq. (IV-36) into Eq. (IV-30), we have an integral equation for $g(r)$ or $c(r)$. Formally, the truncation of $c(r)$, Eq. (IV-29), is the same as assuming that $u(r) = 0$ for $r \geq R$. This potential energy function is shown in Fig. 16.

For the numerical solution of our integral equation, the range R is divided into N segments of width $\delta = R/N$. The integral equation is approximated for this discrete mesh by the trapezoidal rule. By introducing a new variable $p(r_i)$ where $r_i = i\delta$, we may write Eq. (IV-36) as

$$c(r_i) = [e^{-u(r_i)/kT} - 1]p(r_i)$$

and

$$g(r_i) = e^{-u(r_i)/kT} p(r_i) \quad . \tag{V-7}$$

By inserting these relations in the discrete form of Eq. (IV-30), we obtain a system of N nonlinear simultaneous equations for the $p(r_i)$'s. These equations may be solved by a modified Newton-Raphson

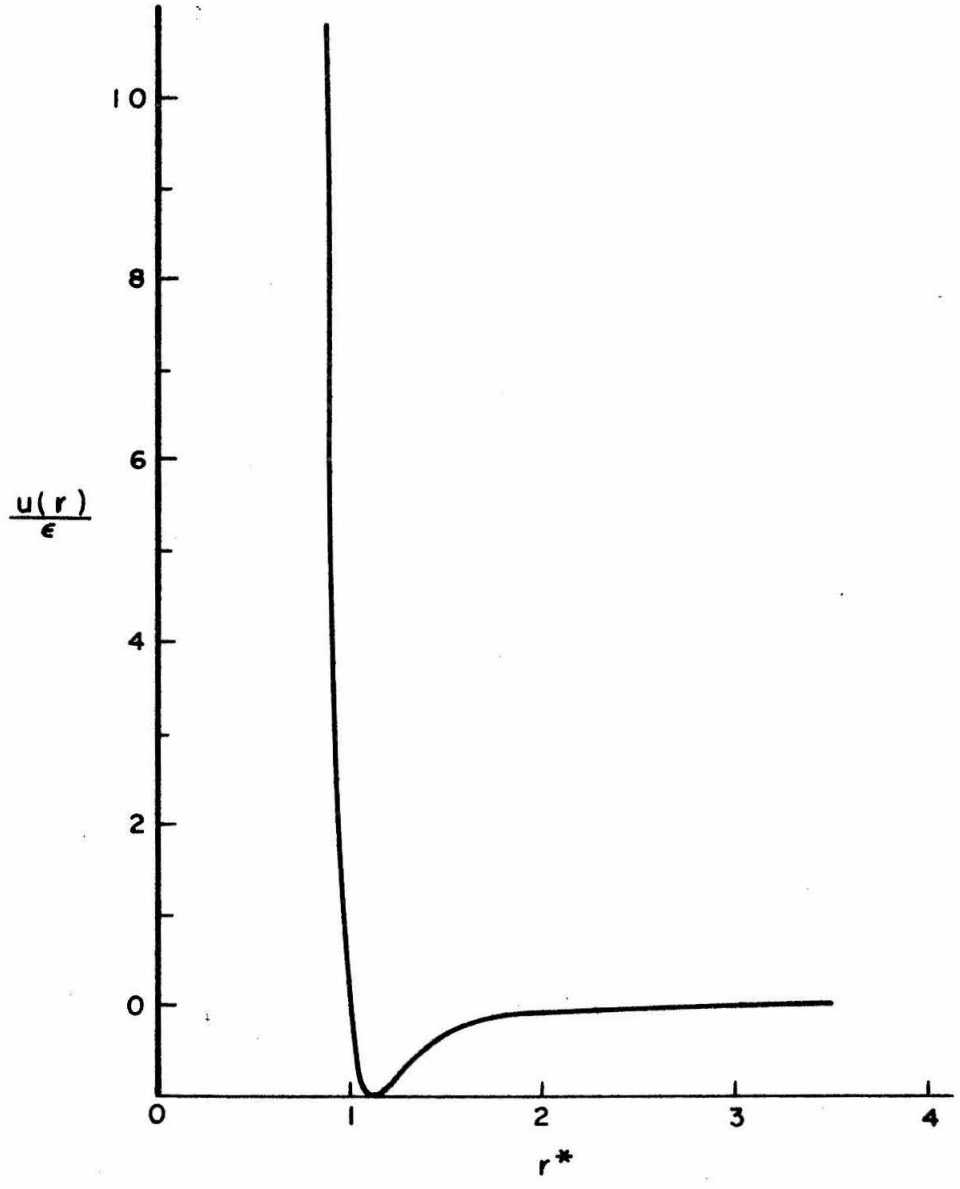

Fig. 16 Truncated Lennard-Jones Pair Potential

procedure[82]. For this Newton-Raphson method, we are required to make an initial guess of the solution. For low densities, estimates can be made from crude empirical data. For higher densities, we extrapolate from the lower density solutions to obtain our initial guess. This Newton-Raphson method was suggested by Watts[64]. In Appendix D, the numerical method is discussed in detail.

This scheme was chosen since only a few iterations were needed to converge to the solution. For the other numerical techniques, studies have indicated that a very large number of iterations was required[73].

One has no way of showing that any of these methods gives the physically unique solution. We justify our solution by comparing with experiment at low densities since we know that the PY equation is valid in this region. For the higher densities, we can only say that the qualitative features are consistent with experimental observations.

1. Comparison of the Theoretical Thermodynamic Properties with Experiment and Known Solutions

For the majority of our calculations, we have used $\delta^* = 0.1$ and $R^* = 3.5$. In the previous calculations by Watts[65], the values $\delta^* = 0.05$ and $R^* = 3.5$ were used and excellent agreement with experiment was found for $\rho_\ell^* \leq 0.6$. It was also shown that the PY equation would predict a phase change near the experimental critical point $T_c^* = 1.26$, $\rho_c^* = 0.316$. Watts found that the solution exhibited a slight dependence on R^*. In the present study, the value of R^* was varied from 3.5 to 4.0 and then to 5.0. The resulting

solutions for $g(r)$ and $c(r)$ did not change. We have no explanation for this difference in behavior.

To be certain, a mesh spacing of 0.05 is more desirable than our spacing of 0.1. However, we would like to point out that for $R^* = 3.5$ and $\delta^* = 0.1$ we have 35 simultaneous equations to solve. For $R^* = 3.5$ and $\delta^* = 0.05$, we have 70 such equations to solve. This increase in the number of equations by a factor of two gives rise to about a twelve-fold increase in the computing time.

Along with his 70-point mesh, Watts has calculated the pressure from the relation[83]

$$\frac{P_\ell}{\rho_\ell kT} = 1 + 2\pi\rho_\ell \int_o^\infty r^2 c(r) \left[\frac{c(r)}{1 - e^{u(r)/kT}} - 2 \right] dr$$

$$+ \frac{1}{2\pi^2 \rho_\ell} \int_o^\infty k^2 [\log(1 - \rho\bar{c}(k)) + \rho\bar{c}(k)] dk \quad , \qquad (V-8)$$

where

$$\bar{c}(k) = \frac{4\pi}{k} \int_o^\infty r\, c(r) \sin(kr) dr \quad . \qquad (V-9)$$

In Table IX, these results are compared with the values obtained in this study where the pressure was calculated by integrating Eq. (IV-37) over the density. The integral in Eq. (IV-37) and the integral over the resulting values for $dP^*/d\rho^*)_T$ were computed by Simpson's rule. We have also listed in Table IX the experimental values as a reference[84].

TABLE IX

COMPARISON OF THEORETICAL CALCULATIONS AND EXPERIMENTAL VALUES OF P^*_ℓ / T^*

	$T^* = 1.3$			$T^* = 2.0$		
ρ^*_ℓ	Pres. Calc. 35-pt.	Watts 70-pt.	Exptl.	Pres. Calc. 35-pt.	Watts 70-pt.	Exptl.
0.1	0.072	0.071	0.070	0.090	0.090	0.089
0.2	0.098	0.098	0.097	0.168	0.169	0.167
0.3	0.105	0.105	0.106	0.251	0.254	0.250
0.4	0.118	0.118	0.115	0.363	0.369	0.362
0.5	0.167	0.172	0.153	0.540	0.552	0.546
0.6	0.312	0.326	0.311	0.843	0.862	0.881

From our definition of the chemical potential, Eq. (IV-10), the effect of the structure of the liquid enters μ_ℓ through the pressure equation of state. For densities up to $\rho^*_\ell = 0.6$, the data reported in Table IX would indicate that our 35-point mesh is adequate.

The configurational contribution to the energy of the liquid is defined by†

$$E^*_c = E^* - 3T^*/2 \quad . \tag{V-10}$$

We have calculated E^* from Eq. (IV-39). In Table X, we compare the 35-point and 70-point mesh calculations and the experimental values of $E^{*(84)}_c$.

---

† We shall drop the subscript "ℓ" for the remainder of this section.

TABLE X

COMPARISON OF THEORETICAL CALCULATIONS AND EXPERIMENTAL VALUES OF E_c^*

ρ^*	$T^* = 1.3$			$T^* = 2.0$		
	Pres. Calc. 35-pt.	Watts 70-pt.	Exptl.	Pres. Calc. 35-pt.	Watts 70-pt.	Exptl.
0.1	-0.66	-0.78	-0.83	-0.64	-0.65	-0.66
0.2	-1.39	-1.53	-1.58	-1.25	-1.27	-1.29
0.3	-2.01	-2.18	-2.23	-1.83	-1.87	-1.88
0.4	-2.54	-2.73	-2.79	-2.43	-2.46	-2.46
0.5	-3.09	-3.32	-3.34	-3.00	-3.04	-3.03
0.6	-3.67	-3.94	-3.93	-3.57	-3.61	-3.59

From this table, we see that the present calculations of E_c^* are in better agreement with the 70-point calculations and experiment at the higher temperature. By comparing Tables IX and X, we find that our predictions of the pressure are better than those for the energy.

As a final example, we compare in Table XI a 35-point and a 70-point solution for $dP^*/d\rho^*)_T$ and E_c^* for a low temperature, high density state. This state ($T^* = 0.977$, $\rho^* = 0.7144$) is in the "true" liquid region of the P-T phase diagram. We also list the solutions of a higher temperature and lower density state in the table.

TABLE XI

STATE	MESH SIZE	$dP^*/d\rho^*)_T$	E_c^*
$T^* = 0.977,\ \rho^* = 0.7144$	35[+]	3.46[+]	-4.51[+]
	70[+]	3.67[+]	-4.81[+]
$T^* = 1.361,\ \rho^* = 0.314$	35	0.235	-2.13
	70	0.245	-2.19

[+]Calculated with the author's computer analysis by Smelser[85].

The difference in the values of the "true" liquid state should give a very good indication of the maximum discrepancy that we would find. In a later section, we shall demonstrate that even a discrepancy this large would not warrant the extra cost of a 70-point solution for the melting problem.

We would like to compare the theoretically calculated pressure with the experimental data along an isotherm at high densities. However, experimental measurements of P, V, T data have not been made for high densities in the temperature range of interest. We shall choose the isotherm $T^* = 1.3$ and make an estimate of the experimental behavior. For the lower densities, we have the values given by Levelt[84]. And along the melting line, we may use the P, V, T data and compressibility data given by Lahr and Eversole[32]. Since $(dP/d\rho)T$ of the liquid is a maximum at the melting line and since P must increase with ρ, we know that the actual isotherm must lie somewhere in the shaded region of Fig. 17. Experimental uncertainty and the recent P, V, T measurements of Crawford and

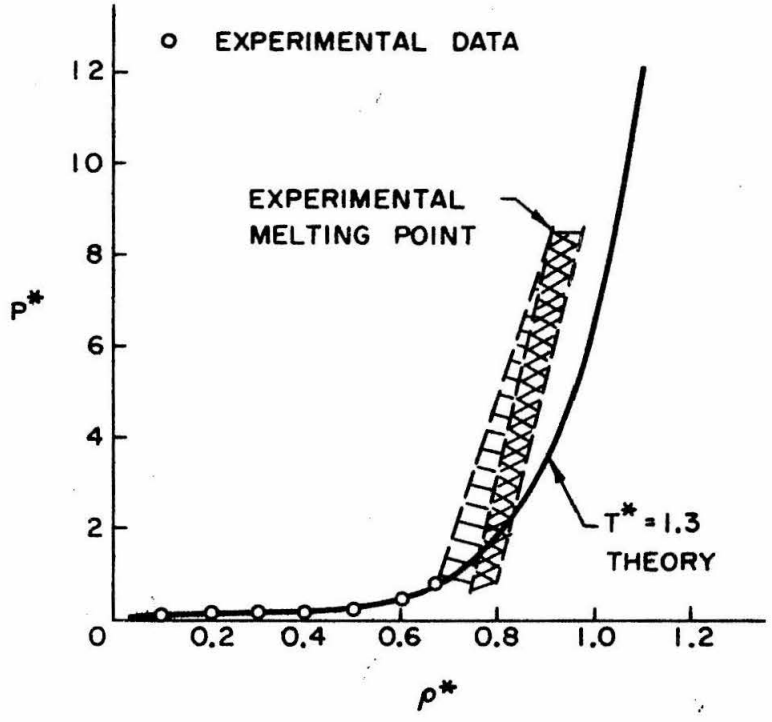

Fig. 17 Comparison of the Theoretical Isotherm and the Experimental Estimate for High Densities.

Daniels[55] along the melting line indicate that the curve could also lie in the cross-hatched region of the figure. We compare these experimental estimates with the PY pressure curve in the figure. From this figure, we can see that the PY equation of state begins to deviate measurably from experiment for densities above $\rho^* = 0.8$. For completeness, we have shown the isotherms for $T^* = 1.8$ and 2.0 in Figs. 18 and 19 respectively. The melting point data[32] are given as a reference.

Finally, we show the behavior of the energy as a function of density for $T^* = 1.3$ in Fig. 20. The minimum corresponds to the configuration where essentially all molecules lie in the minimum of the potential energy well of their nearest neighbors. We find that the energy on the isotherms $T^* = 1.8$ and 2.0 behaves in a similar manner.

2. Structural Features

To illustrate the increase in the structure of the liquid as the density (or pressure) is increased, a sequence of solutions of $g(r)$ obtained from our 35-point mesh calculations is shown in Fig. 21 for the isotherm $T^* = 1.3$. From this figure we can see that for $\rho^* \gtrsim 1.0$ the rapid variation in $g(r)$ near $r^* = 1.0$ can be followed only in a crude way by our numerical solution. However, we know from Fig. 17 that melting occurs experimentally for ρ^* between 0.90 and 0.97; therefore, these high density solutions correspond to a metastable liquid. The behavior of $c(r)$ for increasing density is shown in Fig. 22. Since $c(r)$ is a much more smoothly varying function

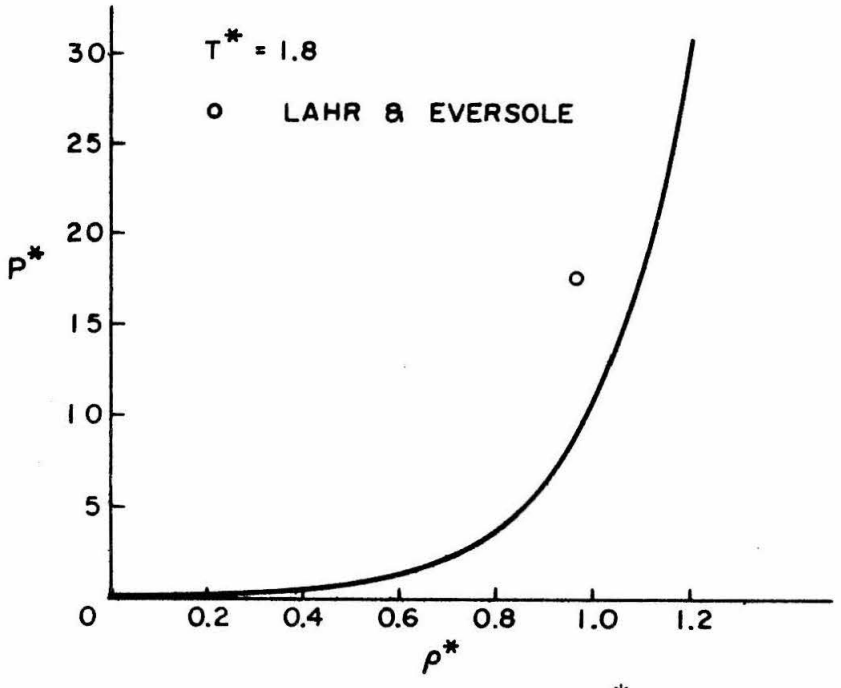

Fig. 18 Isotherm for T^* = 1.8.

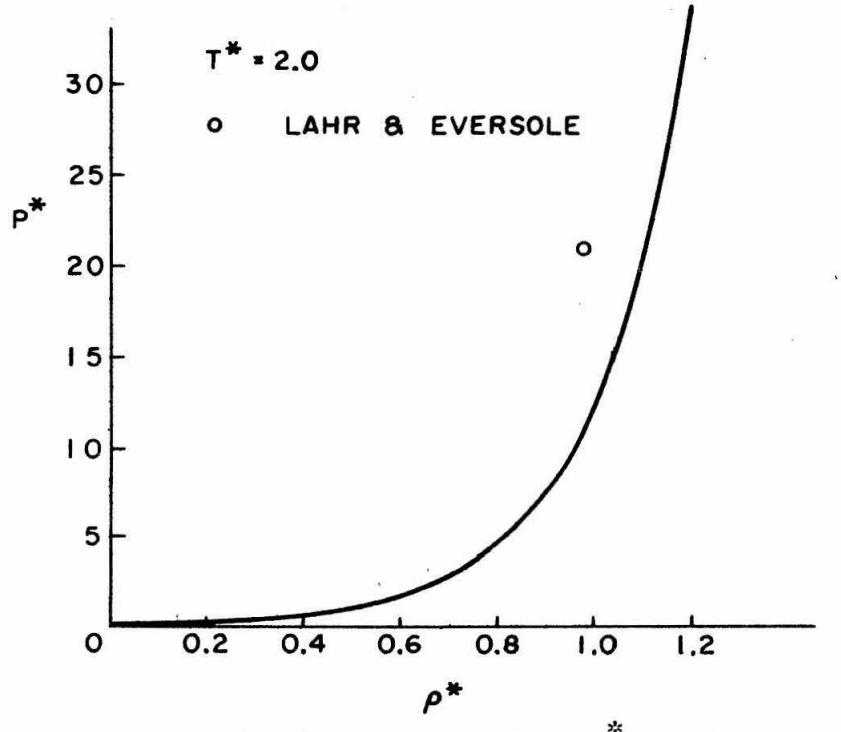

Fig. 19 Isotherm for T^* = 2.0.

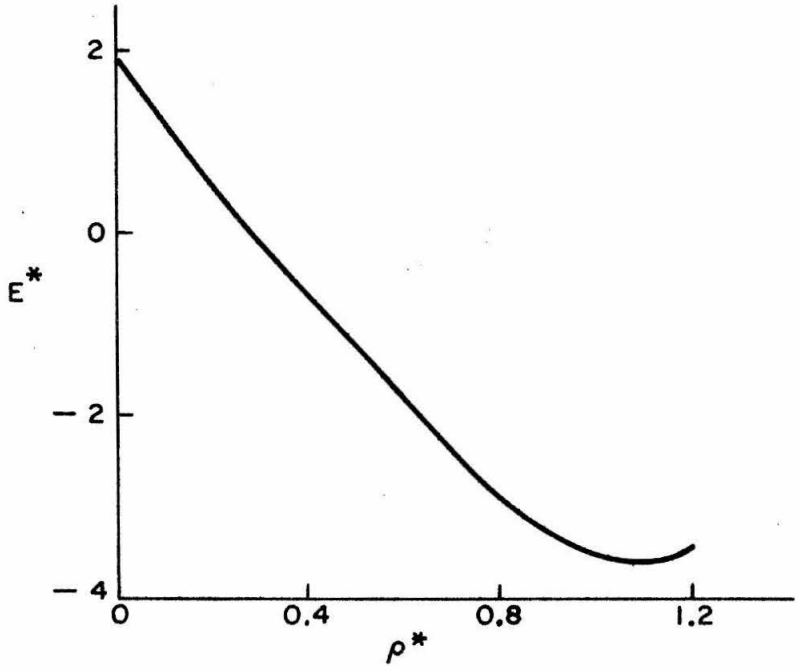

Fig. 20 Internal Energy as a Function of Density for $T^* = 1.3$.

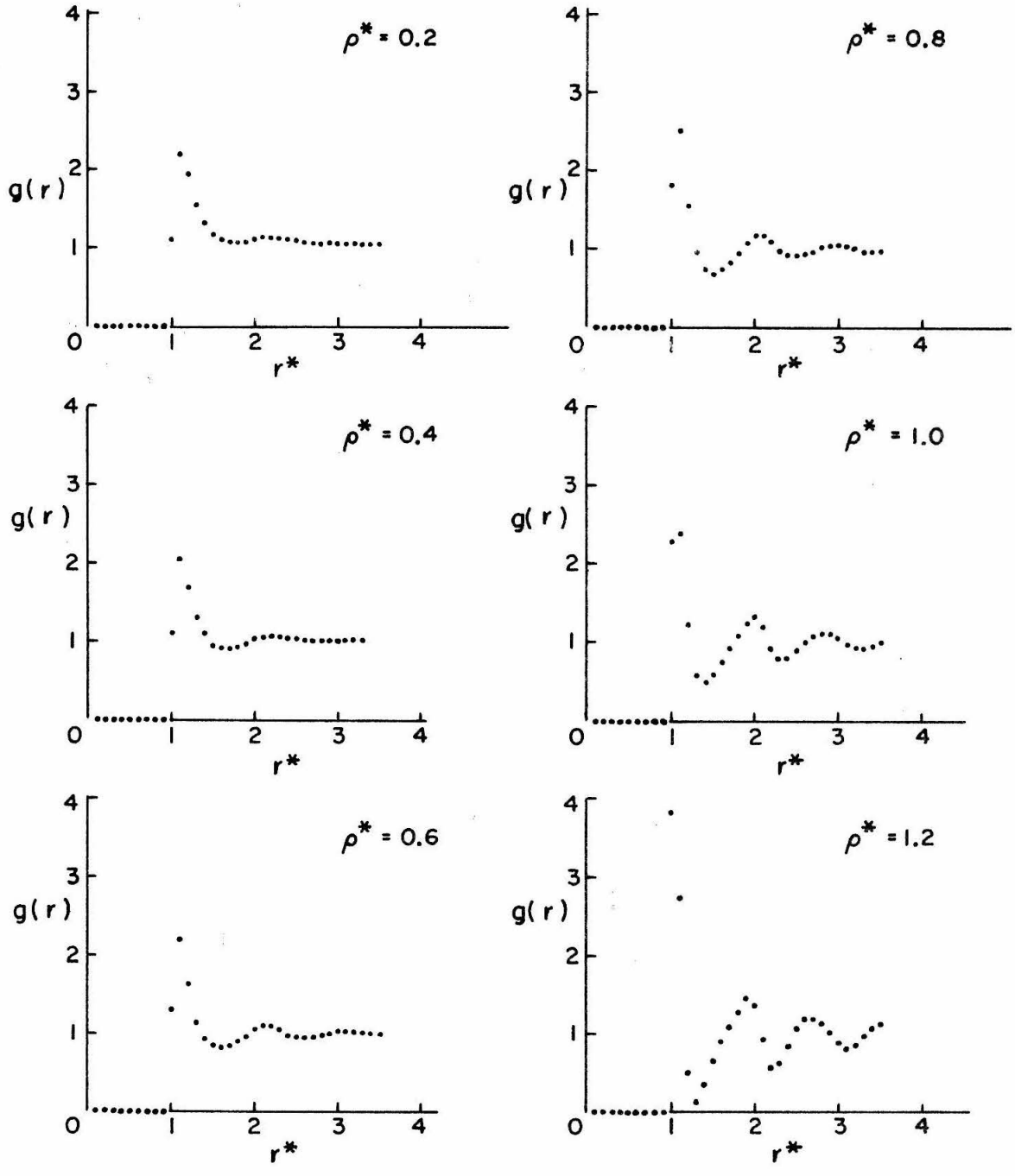

Fig. 21 Variation of the Pair Distribution Function, g(r), with Density for $T^* = 1.3$.

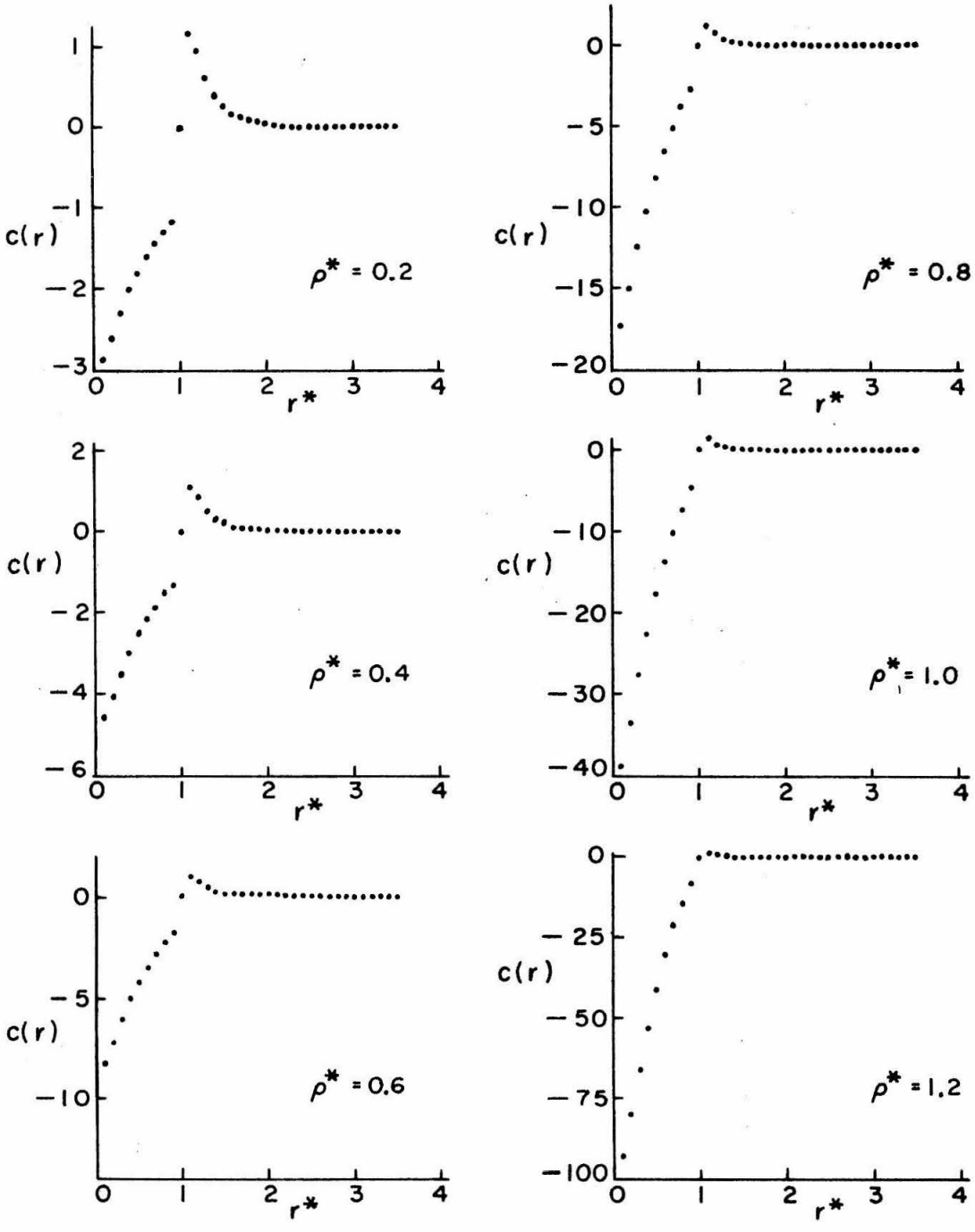

Fig. 22 Variation of the Direct Correlation Function, c(r), with Density for $T^* = 1.3$.

than g(r), we might expect the numerical evaluation of the compressibility equation (IV-37) to agree better with experiment than the numerical calculation of the energy equation (IV-39). This fact was demonstrated in Tables IX and X.

Experimental values of g(r) and c(r) have been measured by Smelser[61] for thermodynamic states in the "true" liquid region. In Figs. 23, 24, 25, and 26, we show the experimental values of g(r) and c(r) for two thermodynamic states along with those calculated with the author's computer analysis by Smelser[85]. The experimental lines are surrounded by an error band representing a 50% confidence in the experimental value. A detailed explanation of this band is given by Smelser (Ref. 61, pp. 43-44). We feel that these states give a very severe test for our solution. We note that the poorest agreement is near the first peak of g(r).

If we define r_1, r_2, and r_3 as the location of the first, second, and third peak of g(r), then it is instructive to examine the values r_2/r_1 and r_3/r_1 for the high density solutions of the PY equation. We know that these ratios are independent of density for the solid; therefore, we expect these ratios to be essentially density independent for the liquid. These ratios are shown in Table XII. For a face-centered cubic solid, we find $r_2/r_1 = 1.414$ and $r_3/r_1 = 1.732$ and for a hexagonal close packed solid, we find $r_2/r_1 = 1.414$ and $r_3/r_1 = 1.633$. Our results indicate that the structure of the liquid is not approaching the structure of the solid as we increase the density.

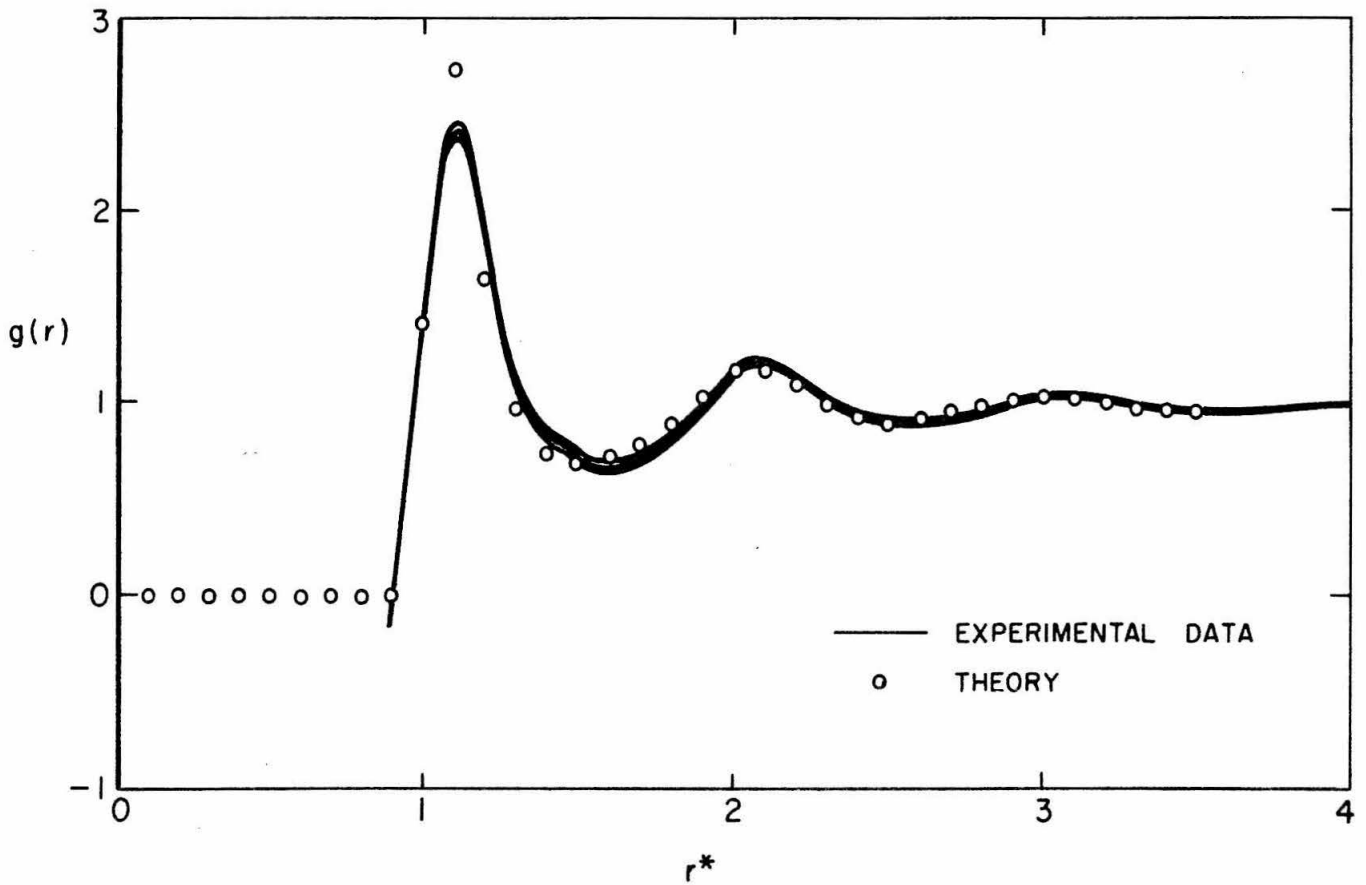

Fig. 23 Comparison of the Experimental and Theoretical Values of g(r) for $T^* = 1.153$ and $\rho^* = 0.585$.

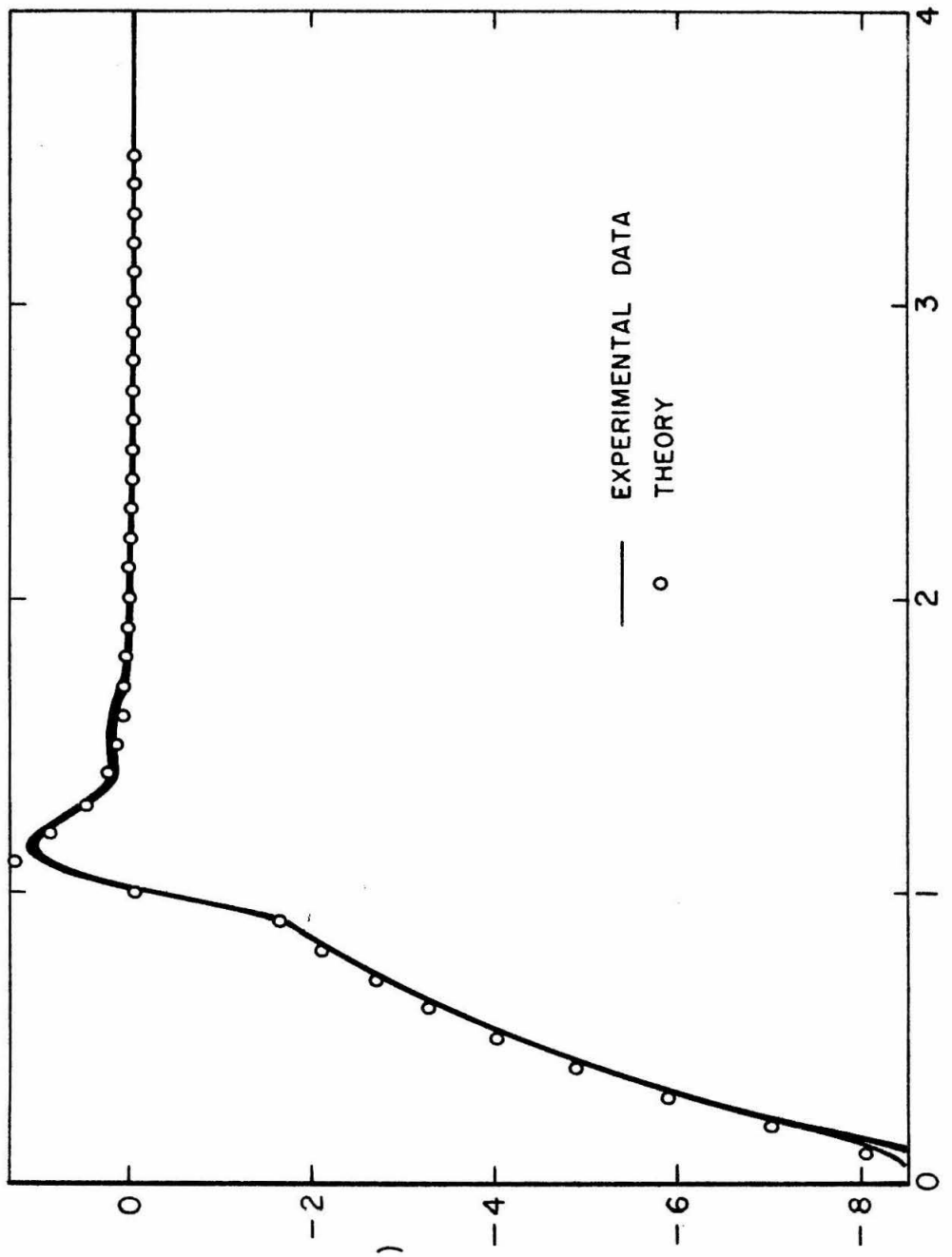

Fig. 24 Comparison of the Experimental and Theoretical Values of c(r) for $T^* = 1.153$ and $\rho^* = 0.585$.

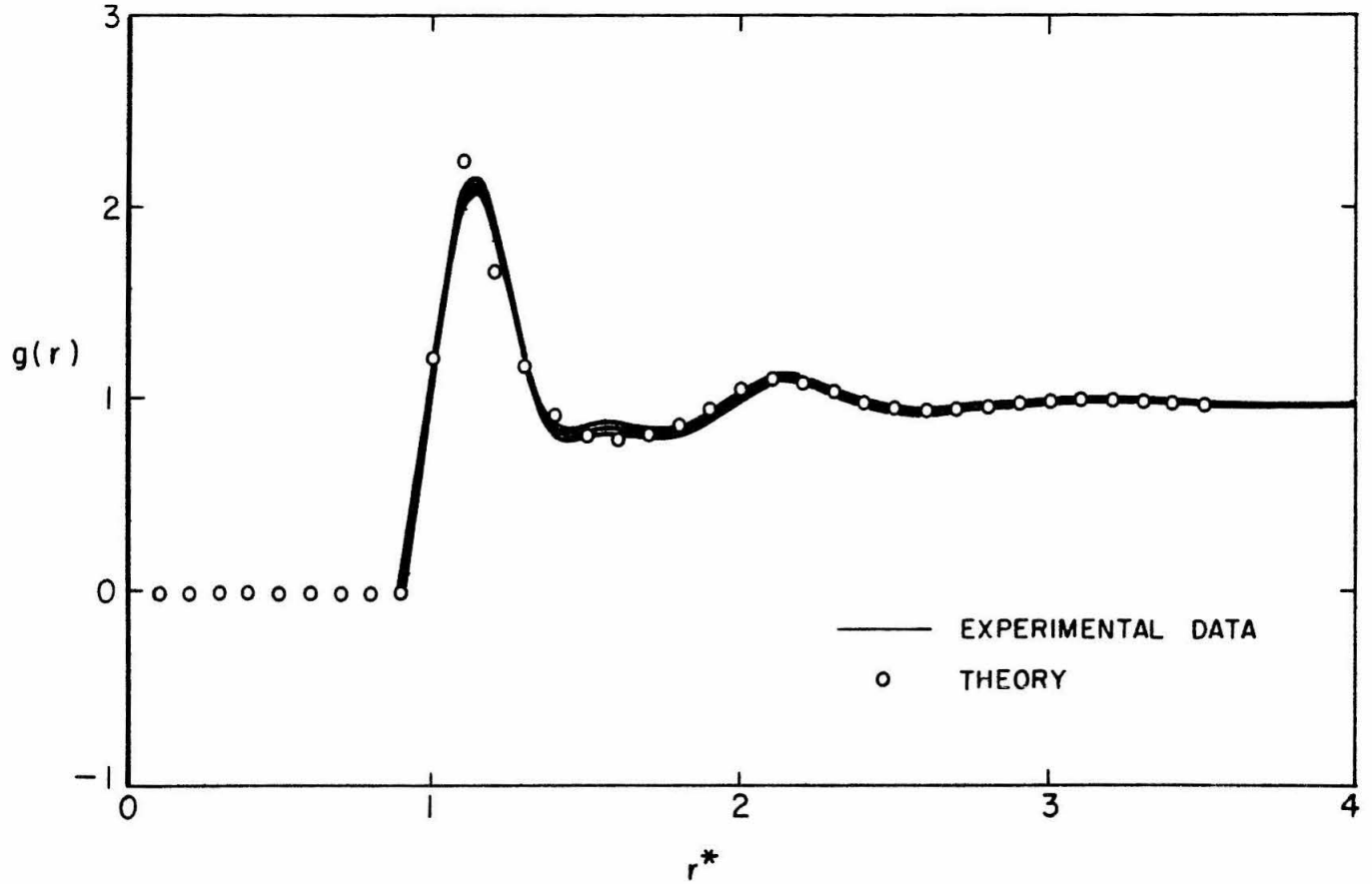

Fig. 25 Comparison of the Experimental and Theoretical Values of g(r) for $T^* = 0.903$ and $\rho^* = 0.751$.

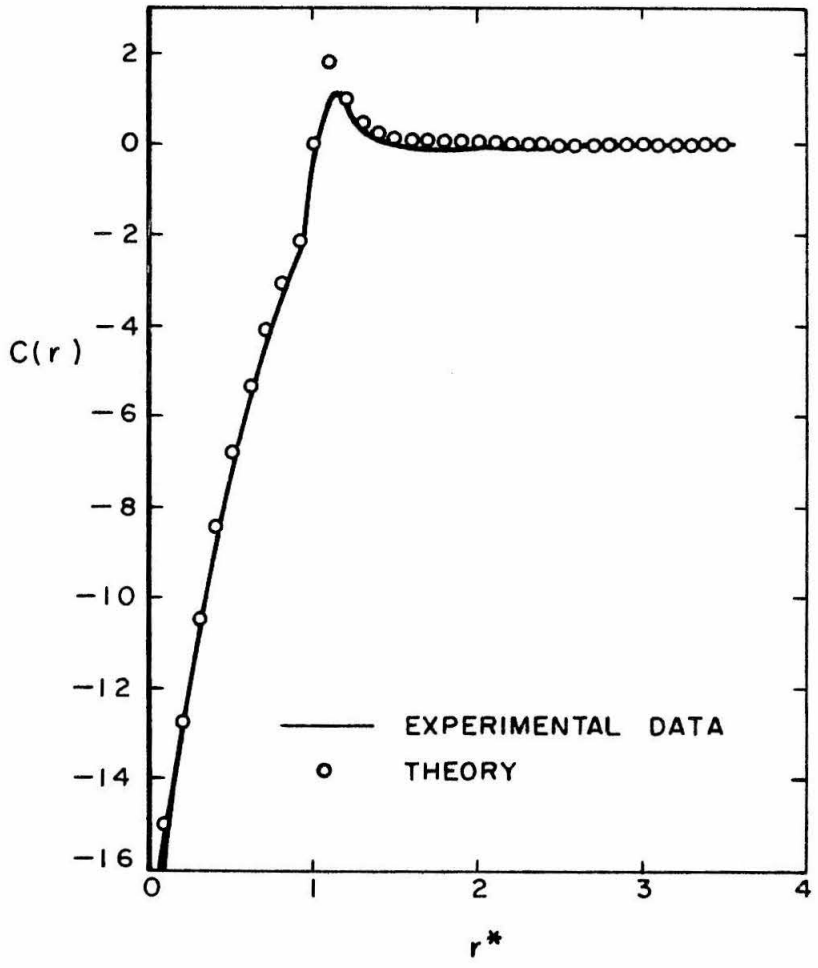

Fig. 26 Comparison of the Experimental and Theoretical Values of $c(r)$ for $T^* = 0.903$ and $\rho^* = 0.751$.

TABLE XII

COMPARISON OF PEAK LOCATIONS

OF g(r) AT HIGH DENSITY

	$T^* = 1.3$		$T^* = 1.8$		$T^* = 2.0$	
ρ^*	r_2/r_1	r_3/r_1	r_2/r_1	r_3/r_1	r_2/r_1	r_3/r_1
0.9	1.85	2.69	1.90	2.74	1.89	2.74
1.0	1.89	2.68	1.88	2.73	1.88	2.73
1.1	1.89	2.67	1.89	2.67	1.89	2.67
1.2	1.90	2.65	1.90	2.66	1.90	2.66

The density was increased in increments of 0.1 until a solution of the PY equation could no longer be found. For the isotherms $T^* = 1.3$, 1.8, and 2.0, no solution could be obtained for $\rho^* = 1.3$. As before, the first guess was made by extrapolation from the lower density solutions. Since a poor guess might be responsible for failure of the solution to converge, every effort was made to try new guesses that were suggested by the first iteration of the computer analysis to eliminate this possibility. For each case, the solution diverged. Although we can not make any positive statements about this divergence, our solutions would suggest that the behavior of c(r) near $r = 0$ is an important factor. Since c(o) is not defined by Eq. (IV-30), we may estimate it from the linear extrapolation.

$$c(o) = 2c(r^* = .1) - c(r^* = .2) \quad . \qquad (V\text{-}11)$$

We have shown the variation of c(o) with density in Fig. 27 for the isotherms $T^* = 1.3$ and 2.0.

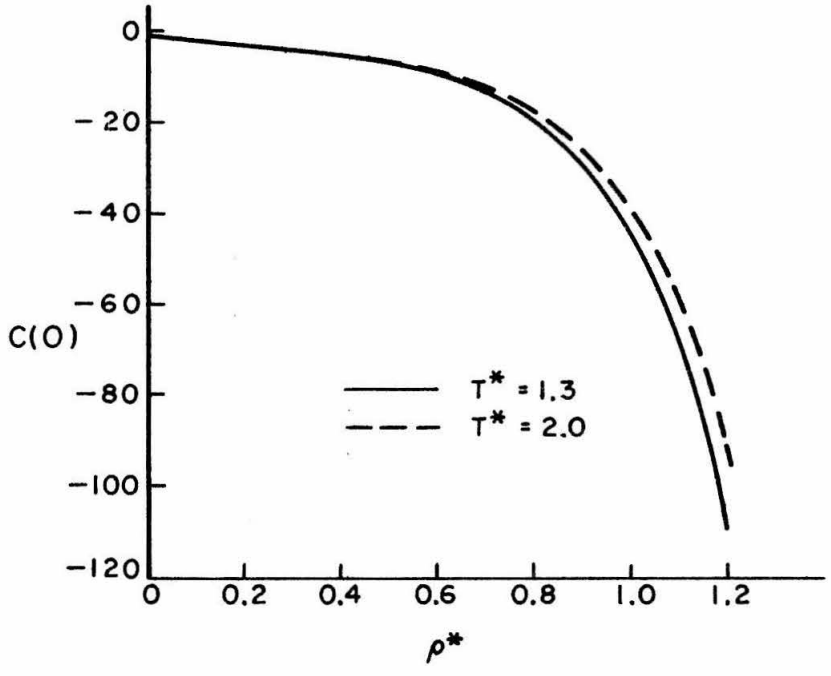

Fig. 27 Variation of c(o) with Density.

B. APPLICATION OF THE PROPOSED SOLID MODEL

An analysis of the solid state model is limited by the experimental data available. The solid models have been studied for temperatures below the triple point by several authors[62],[63],[68],[86]-[90]. However, for T = 155°K to 240°K, no studies of molecular models have been made. For these temperatures, measurements have been made of the P, V, T data along the melting line[32], [55]. We have computed the equation of state (IV-59) of the solid model (HGM) and its harmonic approximation (HAR). The resulting isotherms and discrete points on the isotherms of the LJD solid (Appendix C) are plotted in Figs. 28, 29, and 30 for $T^* = 1.3$, 1.8, and 2.0 respectively. In Fig. 28 we have shown the experimental P, V, T data corresponding to the melting point. In Figs. 29 and 30, the data of Lahr and Eversole[32] is shown with an extrapolated value obtained from the data of Crawford and Daniels[55]. We note that the major difference in these models occurs for pressures less than the experimental melting pressure. In this low pressure range, the solid is metastable. Although there is a significant difference in the experimental data, it is clear that all of the solid models predict experimental behavior in the solid region better than the PY liquid does in the liquid region.

The critical function of the solid in our melting theory is the chemical potential, μ_s, defined in Eq. (IV-60). The chemical potentials for the models under consideration are shown in Fig. 31 for the isotherm $T^* = 1.3$. The chemical potential curve of the liquid crosses μ_s as we have indicated schematically with the large

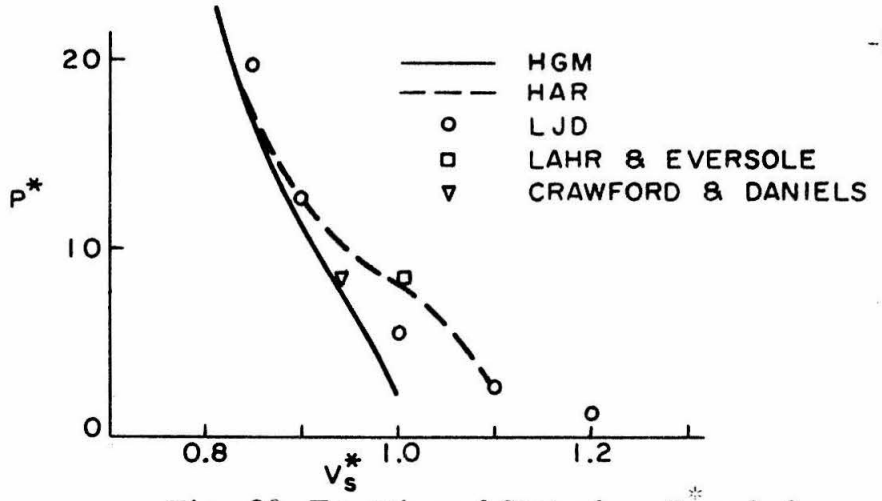

Fig. 28 Equation of State for $T^* = 1.3$.

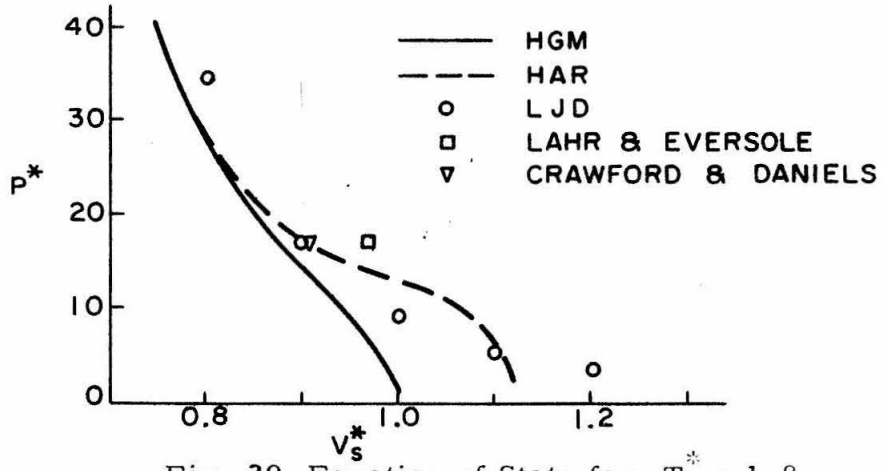

Fig. 29 Equation of State for $T^* = 1.8$.

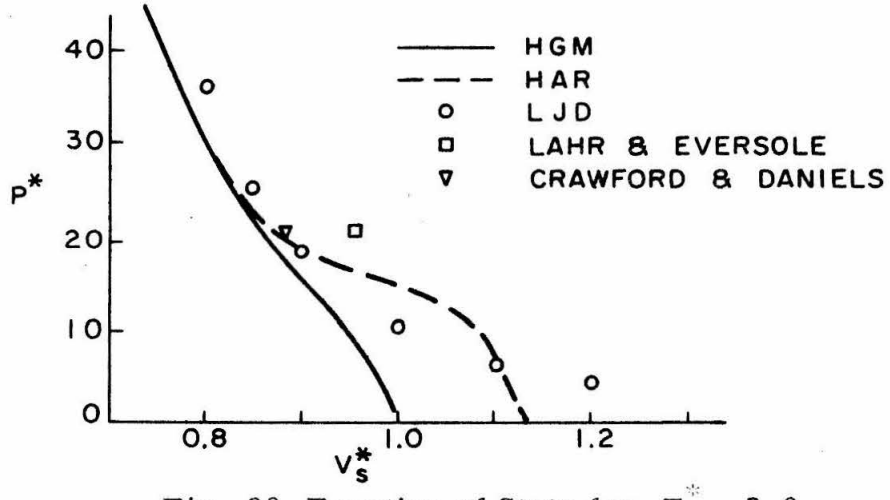

Fig. 30 Equation of State for $T^* = 2.0$.

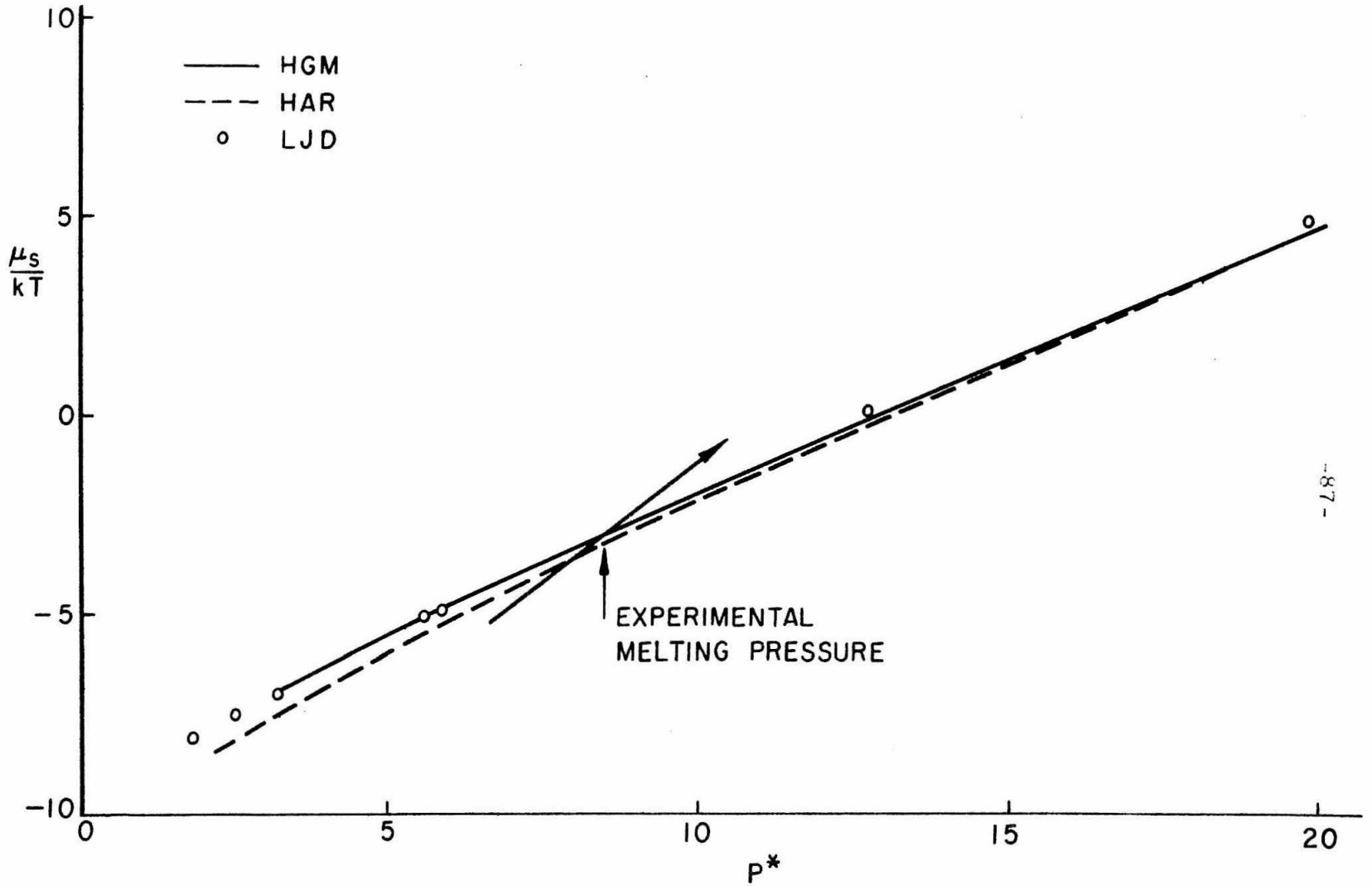

Fig. 31 Chemical Potentials of the Solid Models for $T^* = 1.3$.

arrow. Therefore, if our liquid model were a good representation of the physical state, we would find that the harmonic model (HAR) would melt at a lower pressure than the HGM or LJD models. We also see that the melting pressure would be nearly the same for the HGM and LJD models.

The behavior of the energy (IV-58) and the entropy (IV-61) of the solid must be understood so that we can interpret the discontinuity of the thermodynamic properties at the melting point. These functions along the isotherm $T^* = 1.3$ are shown in Figs. 32 and 33. We note that these curves are quite different for the three models studied. In the next section, we shall see how this difference affects the melting properties.

Finally, we are interested in the role anharmonic effects play in the melting model. In Fig. 34, we have shown the ratio of ω_2 / ω_1 as a function of reduced volume. The value of V_s^* corresponding to the experimental melting pressure for this isotherm has also been noted in the figure. We find that the condition (IV-53) is valid for the states in the stable solid regime.

Again in this section, we have concentrated our study on the isotherm $T^* = 1.3$; the thermodynamic properties on the isotherms $T^* = 1.8$ and 2.0 behave in a similar manner.

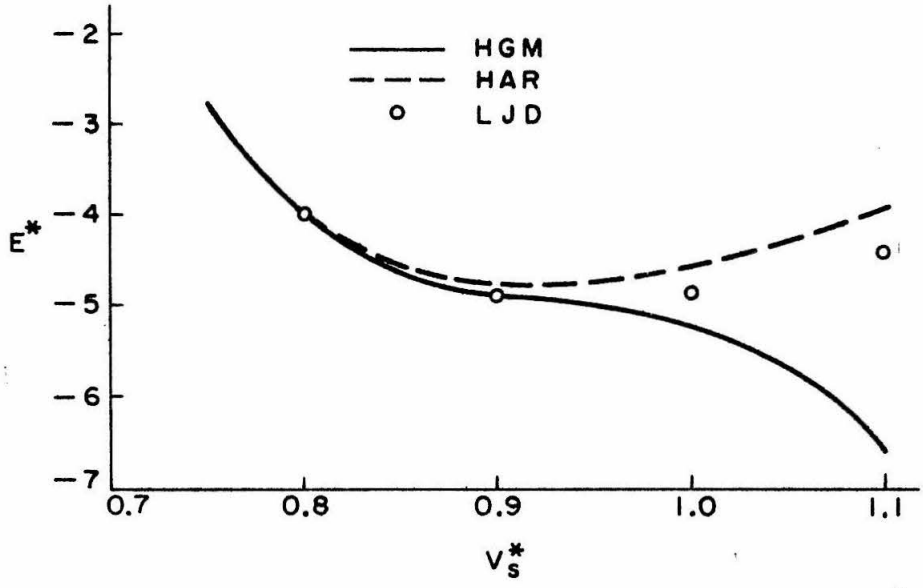

Fig. 32 Internal Energy of the Solid Models for $T^* = 1.3$.

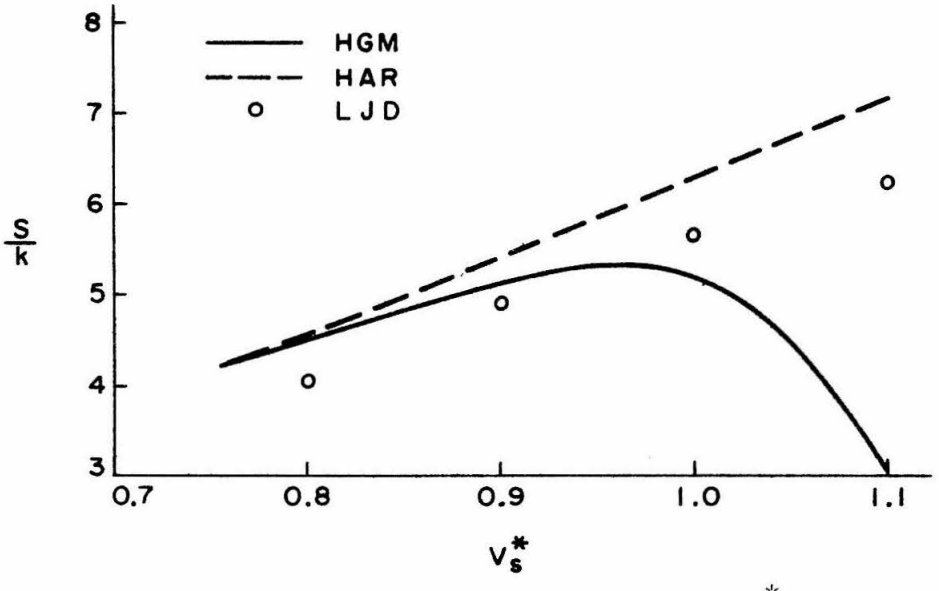

Fig. 33 Entropy of the Solid Models for $T^* = 1.3$.

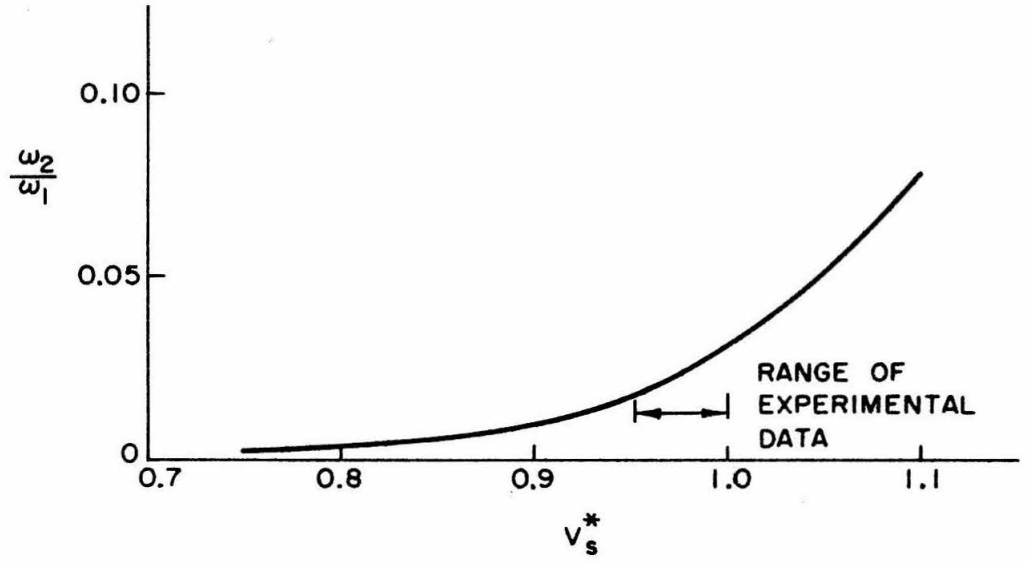

Fig. 34 Ratio of the Anharmonic Correction to the Harmonic Frequency for $T^* = 1.3$.

C. DETERMINATION OF THE THERMODYNAMIC MELTING PROPERTIES

1. Application of the Melting Model

In the preceding chapters and sections of Part II, we have tried to present the physical models in a manner that would permit better understanding of the melting properties which we are now prepared to calculate.

The equilibrium condition (IV-1),

$$\mu_s = \mu_\ell \qquad \text{(V-12)}$$

may be satisfied by increasing the pressure of the liquid state along an isotherm until μ_ℓ crosses μ_s as shown schematically in Fig. 28. Literally, this procedure corresponds to freezing rather than melting. We have made the computations indicated by Eqs. (IV-10) and (IV-60), where the equation of state of the liquid was determined by integrating Eq. (IV-37) by Simpson's rule. The discrete density mesh for this integration was $\delta\rho^* = 0.1$[+]. The integration in Eq. (IV-10) was then made by Simpson's rule for a discrete mesh of $\delta P^* = 0.120889$ ($\delta P = 50$ atm.). To minimize the error in μ_ℓ, the value of ρ^* was found by interpolation of the equation of state. We can see from Fig. 17 that this is much more accurate than finding a value of P^* by interpolation from a given ρ^*. As an example, we have shown the

---

[+] For the case $T^* = 1.3$, the final step was $\delta\rho^* = 0.001$ leading to the density $\rho^* = 1.201$.

chemical potential curves for the isotherm $T^* = 2.0$ in Fig. 35.

The melting pressures determined in this manner are compared with the experimental data in Fig. 36. We shall show that these high melting pressures are a direct result of the failure of the PY equation to predict the equation of state of the liquid which introduces μ_ℓ through the integral in Eq. (IV-10). By translating a line drawn through the calculated melting points to the experimental data, we notice that the slope of the two curves is essentially the same (dashed line Fig. 36).

Once Eq. (V-12) is satisfied, the values of V_s^* and V_ℓ^* at the melting points are readily available from our tabulations of the isotherms of the equations of state (IV-59) and the integral of Eq. (IV-37). The entropy of the liquid was obtained from

$$S_\ell/k = (E_\ell^* - F_\ell^*)/T^* \quad , \tag{V-13}$$

where

$$F_\ell^* = \mu_\ell^* - PV_\ell^* \quad . \tag{V-14}$$

Similarly for the solid, we have[+]

$$S_s/k = (E_s^* - F_s^*)/T^* \quad , \tag{V-15}$$

We denote the discontinuities of volume, energy, and entropy by

$$\Delta V^* = V_\ell^* - V_s^* \quad , \tag{V-16}$$

[+]The expressions for S_s are given implicitly in Eq. (IV-61) and in Appendix C.

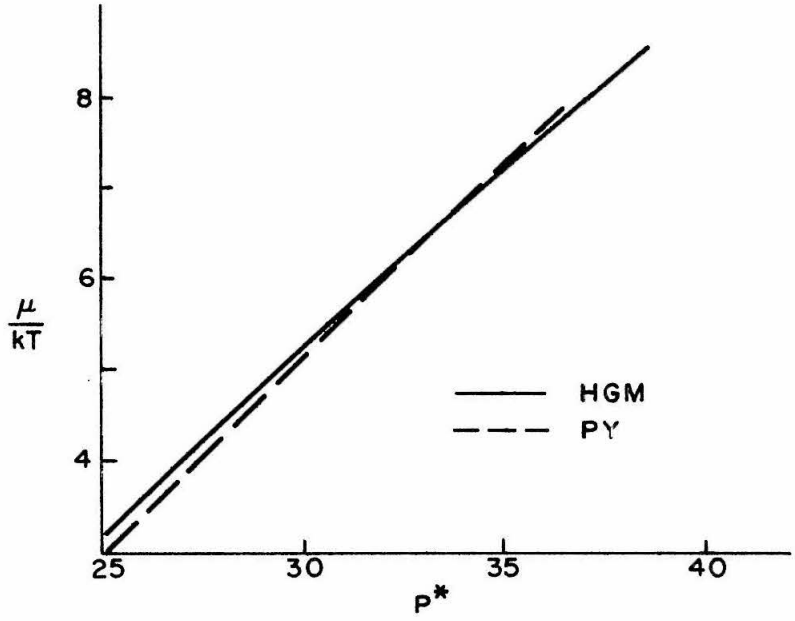

Fig. 35 Determination of the Equilibrium Pressure by Equating the Chemical Potentials for $T^* = 2.0$.

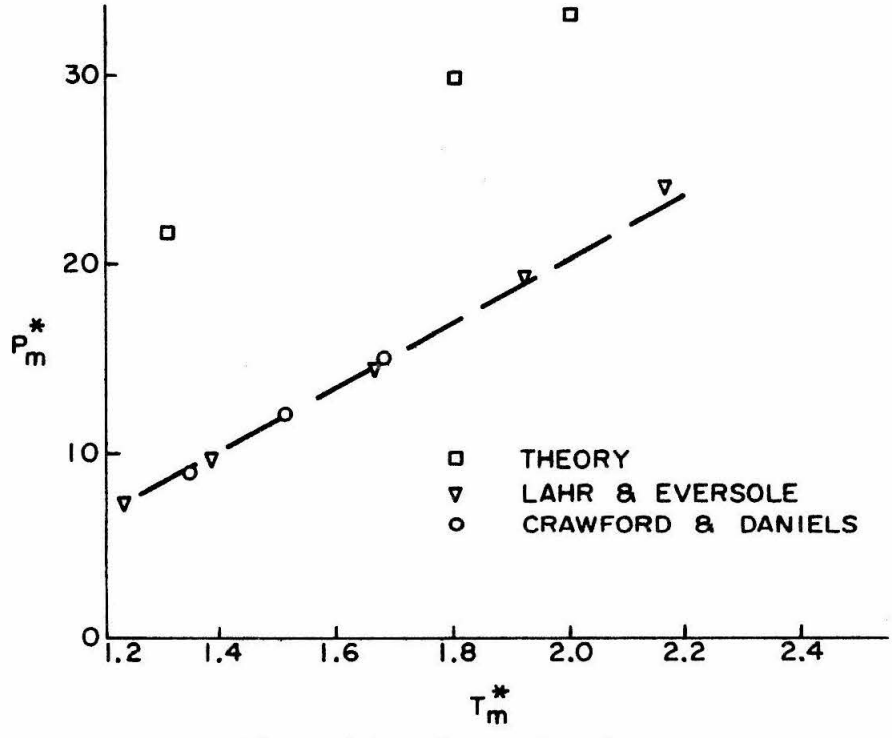

Fig. 36 Melting Curve for Argon

$$\Delta E^* = E_\ell^* - E_s \quad , \tag{V-17}$$

and

$$\Delta S = S_\ell - S_s \quad . \tag{V-18}$$

These quantities have been tabulated in Table XIII.

The low values of V_s^* and V_ℓ^* at the melting points are a direct result of the high melting pressures. The theoretical melting pressure of the isotherm $T^* = 1.3$ is so high that no meaningful conclusions can be drawn about the other melting properties.

By manipulating the Eqs. (V-13) - (V-18), we find

$$\Delta S/k = (\Delta E^* + P^* \Delta V^*)/T^* \quad . \tag{V-19}$$

For the isotherms $T^* = 1.8$ and 2.0, the change in energy is very low; however, the relatively good agreement of the change in entropy is due to the high value of $P^* \Delta V^*$.

We believe that it is more useful to study the behavior of the solid and liquid models near the melting line than it is to try to find implications from the volume and entropy changes of these high melting pressures.

2. Discussion of the Effects of the Approximations

From the outset, one of our goals has been to test the PY equation at high densities; we shall examine the effects of this approximation first. Since we expect the discrepency in the equation of state to be responsible for our high melting pressures, we would like a rough estimate of the error in μ_ℓ resulting from the error in

TABLE XIII

MELTING PROPERTIES OF THE HGM SOLID MELTING TO THE PY LIQUID

Isotherm	P_m(atm.)	V_s^*	V_ℓ^*	$\Delta V/V_s$	ΔE^*	$\Delta S/k$	$\Delta S/k\Delta V^*$
$T^* = 1.3$							
Theory	9000	0.816	0.833	0.021	0.77	0.95	55.9
Exptl.[a]	3500	1.009	1.096	0.086	1.08	1.41	16.2
Exptl.[b]	3500	0.952	1.026	0.078		1.22	16.5
$T^* = 1.8$							
Theory	12400	0.790	0.837	0.059	0.06	0.82	17.4
Exptl.[a]	7100	0.972	1.035	0.065	1.06	1.18	18.7
$T^* = 2.0$							
Theory	13800	0.781	0.836	0.070	-0.19	0.81	14.7
Exptl.[a]	8700	0.955	1.016	0.064	1.07	1.14	18.7

[a] P. H. Lahr and W. G. Eversole, J. Chem. Eng. Data 7, 42 (1962).

[b] R. K. Crawford and W. B. Daniels, Phys. Rev. Letters 21, 367 (1968). (This data was obtained by interpolation; therefore maniuplation of these numbers is not always good to three significant figures.)

the PY isotherm. The chemical potential of the liquid given by Eq. (IV-10) may be written in the form

$$\frac{\mu_\ell}{kT} = \int_0^{P^*(2)} \left[1 - \frac{\rho_\ell^* T^*}{P_\ell^*}\right] \frac{dP_\ell^*}{\rho_\ell^* T^*} + \ell n \left[\left(\frac{2\pi}{m}\right)^{3/2} \frac{\hbar^3 P(2)}{(kT)^{5/2}}\right] \quad . \qquad (V\text{-}20)$$

We recall that for a given P^* we found the value of ρ^* along each isotherm by interpolation[+]. Let us assume that the actual density of the liquid is

$$\rho_{ac}^* = \rho_{PY}^* (1+a) \qquad (V\text{-}21)$$

where ρ_{PY} is the density determined from the PY equation for a given pressure and $\underline{a}$ is a small correction factor. We also assume that $\underline{a} = 0$ for $\rho_{ac} < \rho_b$ or equivalently $P_{ac} < P_b$. By using Eq. (V-21) in Eq. (V-20), we find that at melting

$$\frac{\mu_\ell ac}{kT} - \frac{\mu_\ell^\circ}{kT} \simeq - \frac{a}{(1+a)T^*} \int_{P_b^*}^{P_m^*} \frac{dP^*}{\rho^*} \qquad (V\text{-}22)$$

where μ_ℓ° is the value calculated from the 35-point PY equation of state. For $T^* = 1.3$, we can see from Fig. 17 that the PY isotherm agrees with experiment for $\rho^* \leqslant 0.8$ or $P^* \leqslant 2.0$. For a first order approximation in $\underline{a}$, ρ^* may be removed from the integral of Eq. (V-22) and we have

$$\frac{\mu_\ell ac}{kT} \simeq \frac{\mu_\ell^\circ}{kT} - \frac{a}{\rho^* T^*} (P_m^* - P_b^*) \quad . \qquad (V\text{-}23)$$

[+]Initially we calculate P^* as the dependent variable from the independent variables T^* and ρ^*. Once we have this relation we may then use $\rho^*(T^*, P^*)$ with greater accuracy.

Again from Fig. 17, we see that for $T^* = 1.3$ we may take $\underline{a}$ to be about -0.05, ρ^* to be about 0.9, and $P_m^* - P_b^*$ to be about 6.0. Therefore, our rough estimate of μ_ℓ is

$$\frac{\mu_\ell ac}{kT} \simeq \frac{\mu_\ell^\circ}{kT} + 0.26 \quad . \tag{V-24}$$

This correction to μ_ℓ corresponds to a melting pressure of about 3500 atm. for the HGM solid. Thus in a rough manner we have accounted for the error in our model by correcting only the liquid model. Similar improvement is found for the isotherms $T^* = 1.8$ and 2.0.

To evaluate the effect of our 35-point mesh, we may use the same analysis as above by defining ρ_{ac}^* in this case to be the value found for the 70-point mesh. Again we may take $P_m^* - P_b^*$ to be 6. From Table XI, we see that $(dP^*/d\rho^*)_{T^*}$, and therefore P^*, is about 6 percent larger for the 70-point mesh. For ρ^* between 0.8 and 1.0, $(dP^*/d\rho^*)_{T^*}$ varies from 12.6 to 41. Therefore, we have

$$\delta\rho^* = \frac{\delta P^*}{(dP^*/d\rho^*)_{T^*}} \tag{V-25}$$

where δP^* is the change in P^* due to the 70-point mesh. The maximum value of $\delta\rho^*$ is about 0.005. We may restate this estimate by saying that the pressure found from the 35-point mesh may occur for a density which is about 0.005 less for the 70-point mesh values. Thus we estimate $\underline{a}$ from

$$\rho_{ac}^* \simeq \rho_{PY}^* - 0.005 \tag{V-26}$$

or with the use of Eq. (V-21), we have

$$\rho^*_{PY} - 0.005 = \rho^*_{PY}(1+a) \quad . \tag{V-27}$$

By solving for a, we have

$$a \approx - 0.005/\rho^*_{PY} \quad . \tag{V-28}$$

For $\rho^*_{PY} \approx 0.9$, we have

$$a \approx - 0.006 \quad . \tag{V-29}$$

This gives an estimated correction for the finer 70-point mesh to be roughly

$$+ 0.006 \frac{\left(P^*_m - P^*_b\right)}{\rho^* T^*} \tag{V-30}$$

and we recall that the actual correction was about

$$+ 0.05 \frac{\left(P^*_m - P^*_b\right)}{\rho^* T^*} \tag{V-31}$$

which is nearly an order of magnitude larger. We see no advantage in making the expensive 70-point calculations and we conclude that the PY equation is not accurate enough at these high densities to predict the thermodynamic properties.

For the solid models, we shall merely state some of the more obvious properties. We may deduce the behavior of these models for melting by assuming that we have a good representation of the liquid state. That is to say, μ_ℓ, P_ℓ, and ρ_ℓ are in good agreement with experiment along the isotherms. As we have stated the harmonic model melts at a lower pressure than the HGM model and with a larger volume. We see from Figs. 32 and 33 that the other effects

of anharmonicity are to increase the changes in entropy and energy. More qualitative statements can not be made since the experimental data of the solid state is limited. Recent studies by Chell and Zucker[91] imply that three-body forces are important for the solid. Their corrections for the three-body forces were the same order of magnitude as the anharmonic corrections and in the opposite direction. Since our liquid model has no provision for these forces, it would be inconsistent for us to include them in the solid model.

Finally, we would like to examine the shift in the melting points due to slight changes in ϵ or σ. For the LJD solid and any liquid model for which μ_ℓ is calculated from Eq. (V-20), it is easy to show that the non-dimensional melting line is independent of changes in ϵ or σ. However, for the HGM model the dimensionless De Boer parameter

$$\Lambda = \hbar/(\sigma(m\epsilon)^{\frac{1}{2}}) \qquad (V-32)$$

can not be removed from the equilibrium condition (V-12) analytically. This parameter was varied about ±6 percent and the resulting changes in μ_s for the HGM model and for the LJD model were essentially the same. Thus, the major result of a shift of ϵ or σ appears in the non-dimensional experimental data. One can easily show from Eqs. (V-1) and (V-4) that an increase in ϵ will decrease P^*_m(exptl.) and T^*_m(exptl.) while leaving the slope of the experimental curve unchanged. An increase in σ will correspond to an increase in P^*_m(exptl.) and an increase in the slope of the experimental melting

curve in the non-dimensional plane. However, we note that any shift in ϵ or σ would reduce the agreement with experiment found at low densities in Tables IX and X.

VI. CONCLUSIONS

A. SUMMARY OF RESULTS OF THE MELTING MODEL

The melting problem was posed with four fundamental assumptions. The melting properties were then calculated from first principles. From the beginning, the critical assumption was believed to be the Percus-Yevick representation of the liquid state. Therefore, one of the aims of this study was to test the PY equation at high densities. The liquid pressures computed from this liquid model were about 50 percent low at the experimental melting densities. These low pressures led to errors in the chemical potential of the liquid, which in turn gave rise to high melting pressures and poor estimates of the discontinuities in volume and entropy of melting. It was found that even this poor representation of the liquid would give nearly the correct value of the slope of the melting curve in the P-T plane.

By comparing the solution of the PY equation with experimental curves for $g(r)$ and $c(r)$ in the "true" liquid region, we found quantitative agreement with experiment at all points except near $r = \sigma$, which is near the bowl of the pair potential well. These calculations indicate that our solution of the PY equation is an efficient way to estimate the structure of the liquid even at high densities. Our solution of the PY equation was suggested by Watts for a finer mesh. We note that our study of melting was made for temperatures above the critical temperature. We expect the predictions of the PY equation to be even poorer in the "true" liquid region.

The density was increased until a solution of the PY equation could no longer be found. Since no effort was made to pinpoint the critical density, if one truly exists, we are cautious in drawing conclusions from this numerical instability. The liquid in the region of this divergence is metastable. The pressures corresponding to these densities would be roughly an order of magnitude larger than the experimental melting pressures. The divergence appeared to arise from the large negative values of $c(r)$ near $r = 0$.

The structure of the solid and the structure of the PY liquid are very different near the melting line. Therefore, we question the validity of the melting model proposed by Tsuzuki[58], which assumed that these structures were similar.

The ability of the PY equation to predict structure but not the thermodynamic properties at high densities is not surprising since the rapid variation in $u(r)$ and $g(r)$ near $r = \sigma$ is a critical factor in the calculation of the energy and the pressure. Thus the PY equation must give complete compatibility between $g(r)$ and $u(r)$ if the thermodynamic properties are to be correct.

Although the numerical solutions could be improved by increasing the mesh size, we have demonstrated that the change in the thermodynamic properties would be insignificant when compared with the discrepancy with experiment.

The properties of solid model of Henkel, Guggenheim, and McGlashan were compared with the cell model of Lennard-Jones and Devonshire. Insufficient experimental data are available for the solid

state; therefore, we could not determine which model is superior. We have demonstrated that these solid models would melt thermodynamically at nearly the same pressure.

B. SUGGESTIONS FOR FURTHER RESEARCH ON THE THEORY OF MELTING

1. Experimental

Additional measurements of the solid and liquid volumes along the melting line are needed so that the large differences in the present data can be reduced. The rough approximations of the P, V, T data that we were forced to make in Fig. 17 emphasize the need for measurements of selected P, V, T states on isotherms up to melting pressures in the liquid state.

2. Theoretical

With the failure of the PY equation to predict the equation of state at high density or the melting properties, we conclude that other approximations such as the perturbation liquid model of Barker and Henderson[92] are the more promising at the present time. Therefore, their initial study of melting should be repeated in more detail with the calculation of the changes in volume and entropy of melting included.

A study of the possibility of incorporating the structural properties of the PY liquid found in our study into a model similar to that suggested by Tsuzuki[58] may be useful. The need for an additional assumption regarding the form of the free volume might be

eliminated by our greater knowledge of the liquid state.

Finally, an estimate of the effect of three-body forces on the melting transition would be valuable. If the contribution of these forces is significant further studies of the two-body problem may be less fruitful.

C. IMPLICATIONS FOR THE STUDY OF OTHER PHASE TRANSITIONS

In this thesis, we have used two fundamentally different techniques to study a first order phase transition. For the sublimation model, we have modeled the transition itself. In this way, one gains more insight into the mechanisms responsible for the transition. Although we have not attempted to apply a model analogous to this one to other phase transitions, we believe that the simple ideas developed here may be helpful in other studies. Normally, this type of model will require theoretically well-defined physical states on either side of the transition.

Since no simple representation of the liquid exists, we modeled the two phases of the melting transition. The transition was then represented by a thermodynamic equilibrium condition. (Salter[6] has used this approach for sublimation.) Since the properties of the transition are determined from the small differences in the thermodynamic variables at equilibrium, this model requires a high degree of compatibility between the representations of the two phases. Therefore, with this model we expect that we will have difficulty in matching the calculated discontinuities of the transition with those

found by experiment. Thus we believe that this method may be used most effectively to make a concentrated study of one phase of the system as we have done for melting.

APPENDIX A
QUASI-CLASSICAL MODEL FOR SUBLIMATION

For the quasi-classical solid, $kT \gg \hbar\omega$, one may consider the energy states as a continuous spectrum. That is (II-5) and (II-6) become

$$\epsilon_n \simeq n\hbar\omega \tag{A-1}$$

and

$$g_n \simeq \frac{n^2}{2} \quad . \tag{A-2}$$

Therefore, the number of energy states between ϵ and $\epsilon + d\epsilon$ is

$$dn = \frac{n^2}{2\hbar\omega}\, d\epsilon \quad . \tag{A-3}$$

For the density of states in this approximation, we have

$$D(\epsilon) = \frac{\epsilon^2}{2(\hbar\omega)^3} \quad . \tag{A-4}$$

The partition function becomes

$$Z = \int_o^{E_1} \frac{\epsilon^2}{2(\hbar\omega)^3} \exp(-\epsilon/kT)d\epsilon + \int_{E_1}^{\infty} \frac{(2m^3)^{\frac{1}{2}}}{2\pi^2} \frac{aV_s}{\hbar^3} (\epsilon - E_1)^{\frac{1}{2}} \exp(-\epsilon/kT)d\epsilon. \tag{A-5}$$

By using (II-8), (II-19), and (II-20), we find

$$\frac{E}{E_1 N} = \frac{6\gamma^3 - e^{-\gamma-1}\left[1+3\gamma+6\gamma^2+6\gamma^3 - A_1 a\gamma^{\frac{1}{2}}\left(\frac{3}{2}\gamma+1\right)\right]}{2\gamma^2 - e^{-\gamma-1}\left[1+2\gamma+2\gamma^2 - A_1 a\gamma^{\frac{1}{2}}\right]} , \tag{A-6}$$

where

$$\gamma = \frac{kT}{E_1} \quad . \tag{A-7}$$

and

$$A_1 = \frac{(2m^3)^{\frac{1}{2}} V_s \omega^3}{2\pi^{3/2} (E_1)^{3/2}} \quad . \tag{A-8}$$

From Eq. (II-16) we have,

$$A_1 = 2\left(\frac{\hbar\omega}{E_1}\right)^{3/2} A \quad . \tag{A-9}$$

The energy relation (II-21) is compared with the quasi-classical energy for argon in Fig. 37. The critical temperature of the classical model is slightly higher than the critical temperature for the Einstein model.

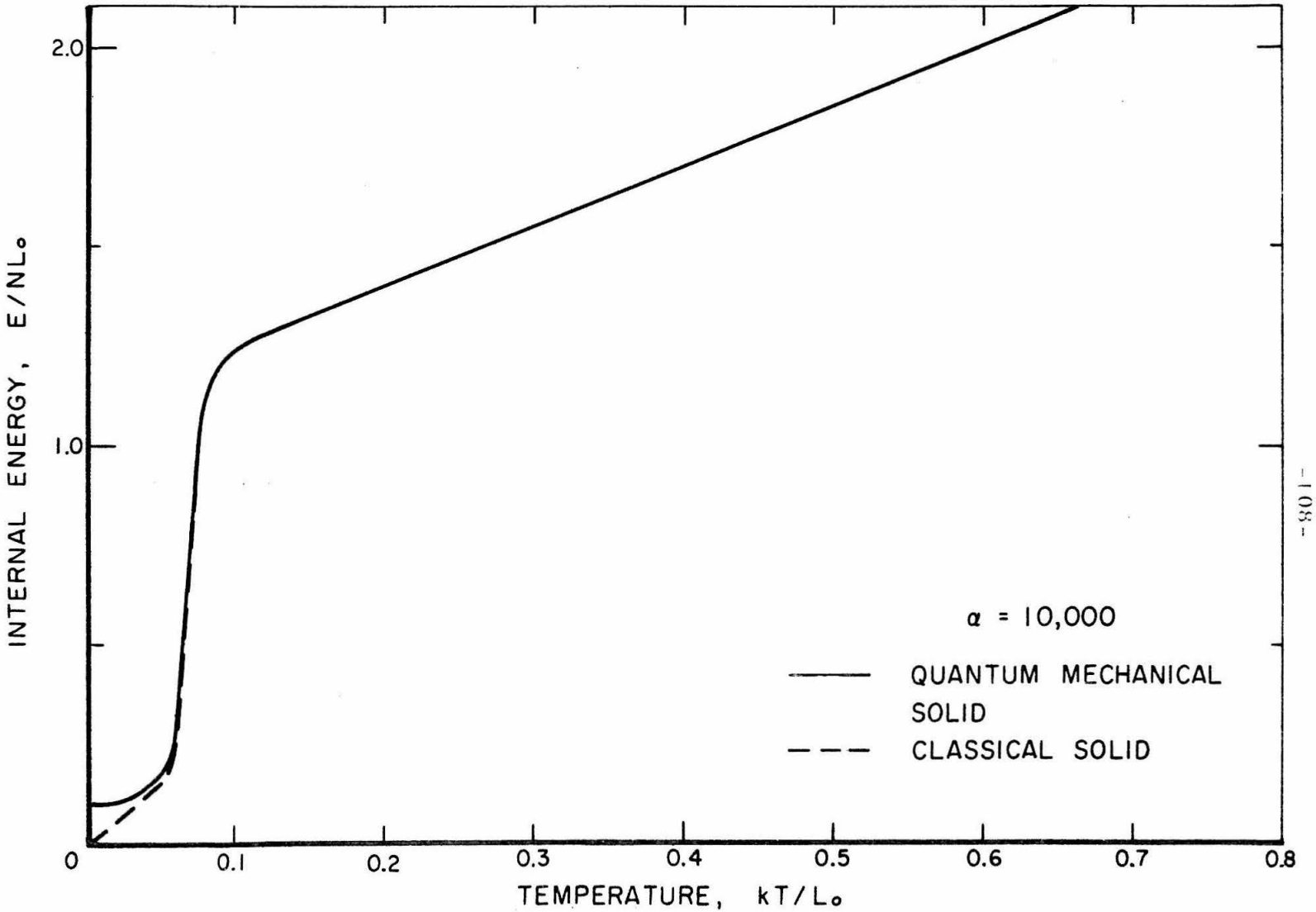

Fig. 37 - Comparison of Quantum and Classical Solid Models of Argon

APPENDIX B
ANALYTIC DETERMINATION OF THE VAPOR PRESSURE CURVE

By using (II-22), the energy in Eq. (II-21) can be written in the form

$$\frac{E}{N\hbar\omega} = \frac{Q}{W} \tag{B-1}$$

where

$$Q = \left[X^{M+4}\left(\frac{M^3}{2} + \frac{9}{4}M^2 + \frac{13}{4}M + \frac{3}{2}\right) + X^{M+3}\left(-\frac{3}{2}M^3 - \frac{33}{4}M^2 - \frac{51}{4}M - 6\right) + X^{M+2}\left(\frac{3}{2}M^3 + \frac{39}{4}M^2 + \frac{75}{4}M + 9\right) + X^{M+1}\left(-\frac{M^3}{2} - \frac{15}{4}M^2 - \frac{37}{4}M - \frac{15}{2}\right) + \frac{3}{2}(X+1)\right](1-X)^{-4} + aAe^{-L_o/kT}C^{3/2}\left(\frac{L_o}{\hbar\omega} + \frac{3}{2}(C+1)\right). \tag{B-2}$$

and

$$W = \left[X^{M+3}\left(-\frac{M^2}{2} - \frac{3M}{2} - 1\right) + X^{M+2}(M^2+4M+3) + X^{M+1}\left(-\frac{M^2}{2} - \frac{5}{2}M - 3\right) + 1\right](1-X)^{-3} + aAe^{-L_o/kT}C^{3/2}. \tag{B-3}$$

Near the transition region that we have studied, we find that C varies from 1.05 to 1.35, 1.23 to 2.38, and 1.95 to 3.91 for argon, krypton, and xenon respectively. In the region where

$$aAC^{3/2} \gg X(1-X)^{-4}M^3 , \tag{B-4}$$

we may approximate the energy equation by

$$\frac{E}{N\hbar\omega} \approx \frac{\frac{3}{2}(1+X)(1-X)^{-4}+aAe^{-L_o/kT}C^{3/2}\left[\frac{L_o}{\hbar\omega}+\frac{3}{2}(C+1)\right]}{(1-X)^{-3}+aAe^{-L_o/kT}C^{3/2}} \quad . \tag{B-5}$$

Condition (B-4) is true for argon over the entire temperature range of interest; however, it is only valid for krypton and xenon at temperatures well below the triple point.

Setting the second derivative of Eq. (B-5) to zero, we find the critical curve in the form

$$a^3A^3e^{-3L_o/kT}B_1+a^2A^2e^{-2L_o/kT}B_2+aAe^{-L_o/kT}B_3+B_4=0 \quad , \tag{B-6}$$

where

$$\begin{aligned}
B_1 = &-\frac{9}{8}(1-X)^{13}C^{7/2}+C^{5/2}\left[-\frac{3}{4}(1-X)^{13}\left(\frac{11L_o}{\hbar\omega}+\frac{15}{2}\right)\right. \\
&\left.+\frac{3}{8}(1-X)^{12}(-49+115X)\right]+C^{3/2}\left[-\frac{1}{2}\frac{L_o}{\hbar\omega}(1-X)^{13}\left(\frac{13L_o}{\hbar\omega}+15\right)\right. \\
&+\frac{3}{2}(1-X)^{12}\left(\frac{5L_o}{\hbar\omega}+7X\left(\frac{3L_o}{\hbar\omega}+1\right)\right) \\
&\left.-6X(1-X)^{11}(5+8X)\right]+C^{1/2}\left[-\frac{L_o^2}{(\hbar\omega)^2}(1-X)^{13}\left(\frac{L_o}{\hbar\omega}+\frac{3}{2}\right)\right. \\
&+\frac{3}{2}(1-X)^{12}\left(\frac{L_o^2}{(\hbar\omega)^2}+X\left(\frac{5L_o^2}{(\hbar\omega)^2}+\frac{2L_o}{\hbar\omega}-2\right)\right) \\
&\left.+6X(1-X)^{11}-\left(\frac{2L_o}{\hbar\omega}(1+2X)+1\right)+30X^2(1-X)^{10}(1+X)\right] \quad ,
\end{aligned} \tag{B-7}$$

$$B_2 = \frac{9}{2}(1-X)^{10}C^2+C\left[-3(1-X)^{10}\left(\frac{L_o}{\hbar\omega}+\frac{3}{2}\right)+\frac{9}{2}(1-X)^9(1+X)\right]$$
$$-\frac{2L_o}{\hbar\omega}(1-X)^{10}\left(\frac{2L_o}{\hbar\omega}+3\right)+(1-X)^9\left(\frac{6L_o}{\hbar\omega}+X\left(\frac{18L_o}{\hbar\omega}-\frac{3}{2}\right)\right)$$
$$-\frac{3}{2}X(1-X)^8(29+25X)+C^{-1}\left[-3X(1-X)^9\left(\frac{3L_o}{\hbar\omega}+2\right)\right.$$
$$\left.+3(1-X)^8\left(-\frac{3L_o}{\hbar\omega}+5+3X\left(-\frac{L_o}{\hbar\omega}+2\right)\right)+24X^2(1-X)^7(2+X)\right] \quad ,(B-8)$$

$$B_3 = \frac{45}{8}(1-X)^7C^{1/2}+C^{-1/2}\left[\frac{3}{4}(1-X)^7\left(\frac{7L_o}{\hbar\omega}+\frac{3}{2}\right)\right.$$
$$\left.-\frac{9}{8}(1-X)^6(1+13X)\right]+C^{-3/2}\left[\frac{1}{2}\frac{L_o}{\hbar\omega}(1-X)^7\left(\frac{5L_o}{\hbar\omega}+3\right)\right.$$
$$\left.-\frac{3}{2}(1-X)^6\left(\frac{L_o}{\hbar\omega}+X\left(\frac{9L_o}{\hbar\omega}+8\right)\right)+\frac{3}{2}X(1-X)^5(-13+7X)\right]$$
$$+C^{-5/2}\left[\frac{L_o^2}{(\hbar\omega)^2}(1-X)^7\left(\frac{L_o}{\hbar\omega}+\frac{3}{2}\right)-\frac{3}{2}(1-X)^6\left(\frac{L_o^2}{(\hbar\omega)^2}\right.\right.$$
$$\left.\left.+X\left(\frac{5L_o^2}{(\hbar\omega)^2}+\frac{8L_o}{\hbar\omega}+2\right)\right)+3X(1-X)^5\left(\frac{L_o}{\hbar\omega}+4\right.\right.$$
$$\left.\left.+X\left(\frac{5L_o}{\hbar\omega}+6\right)\right)+6X^2(1-X)^4(4-X)\right] \quad , \qquad (B-9)$$

and

$$B_4 = 3XC^{-4}(1-X^2)-6XC^{-3}(1-X)^2 \quad . \qquad (B-10)$$

We now assume that

$$\frac{L_o}{\hbar\omega} \gg 1 \quad . \qquad (B-11)$$

Actually for argon $\frac{L_o}{\hbar\omega}$ is 15 and increases to 46.6 for xenon. By

taking only the smallest order of $\hbar\omega/L_o$, the critical curve (B-6) reduces to

$$aAe^{-L_o/kT} C^{3/2}(1-X)^3\left[1+f\left(\frac{\hbar\omega}{L_o}\ ,\ T\right)\right] = 1 \qquad \text{(B-12)}$$

where $f\left(\frac{\hbar\omega}{L_o}\ ,T\right) \to 0$ as $\frac{\hbar\omega}{L_o} \to 0$.

We must limit any higher order approximation to argon; since Eq. (B-5) would not be valid for a higher order approximation in krypton and xenon.

For argon, we find

$$f\left(\frac{\hbar\omega}{L_o}\ ,T\right) = \frac{\hbar\omega}{L_o}\left[\frac{17}{2}\ C - \frac{65}{8}\ C^2 - \frac{9X}{1-X} + \frac{81}{2}\ \frac{XC}{1-X} - \frac{81}{2}\ \frac{X^2}{(1-X)^2}\right] + O\left[\left(\frac{\hbar\omega}{L_o}\right)\right]^2 . \qquad \text{(B-13)}$$

By noting that Eq. (II-32) may be written in the form

$$p = \frac{G}{a}\ , \qquad \text{(B-14)}$$

we have

$$p = GAe^{-L_o/kT} C^{3/2}(1-X)^3\left[1 + f\left(\frac{\hbar\omega}{L_o}\ ,\ T\right)\right] . \qquad \text{(B-15)}$$

After taking the logarithm of Eq. (B-15) and rearranging terms, we find

$$\ell n\, p = -\frac{L_o}{kT} - \frac{1}{2}\ \ell n\, C + \ell n[C^2(1-e^{-1/C})^3] + \ell n\left[1+f\left(\frac{\hbar\omega}{L_o}\ ,\ T\right)\right] + \ell n[GA] . \qquad \text{(B-16)}$$

We note that Eq. (B-16) has roughly the same form as Eq. (II-2) since $\ell n[C^2(1-e^{-1/C})^3]$ is nearly constant over the temperature range of argon.

APPENDIX C
THE CELL THEORY OF LENNARD-JONES AND DEVONSHIRE[+]

For the LJD theory of solids, we assume that the solid may be divided into identical cells and that each cell contains only one molecule which moves independently of all other molecules. The center of each cell is assumed to lie on one of the lattice sites of the face-centered cubic lattice. There are no vacancies in the lattice. Thus, the change in the potential energy due to the motion of the i^{th} molecule from its cell center to a position $\vec{r}_i$ relative to the cell center is of the form

$$\Delta\psi(\vec{r}_i) = \psi(\vec{r}_i) - \psi(o) \quad . \tag{C-1}$$

Since all cells are independent, the other molecules are assumed to be at their cell centers. It is also assumed that $\psi(\vec{r}_i)$ may be approximated by $\psi(|\vec{r}_i|)$. This is done by calculating a cell field and regarding the m_n neighbors in the n^{th} nearest neighbor shell to be smeared uniformly over a sphere of radius equal to the n^{th} neighbor distance a_n. With the use of a canonical ensemble, the partition function for N molecules may be written as

$$Z = \left[\frac{2\pi mkT}{h^2}\right]^{\frac{3N}{2}} \left[\int_{cell} e^{-\Delta\psi(r_i)/kT} \, d\vec{r}_i\right]^N e^{-U_o/kT} \tag{C-2}$$

where U_o is the static lattice energy.

[+] For a more detailed discussion, we refer the reader to Refs. (10) and (68).

The shape of the unit cell is in the form of a Wigner-Seitz cell; this cell is constructed by drawing perpendicular bisector planes through all nearest neighbor lattice vectors. The final approximation of the LJD theory is to deform this cell into a spherical shape of equal volume.

With the LJ pair potential, Eq. (III-5), one may calculate $\Delta\psi(r_i)$ by summing all two-body interactions, $u(a_n)$, over the entire lattice. After computing the partition function, the result of these sums appears as three factors g, g_L, and g_m in the thermodynamic variables. These factors are a function of T and V and they are tabulated in the literature [93],[94].

In the following paragraph, we list the thermodynamic variables found in this manner. The lattice energy is

$$U_o = 6\epsilon\left[1.0109\left(\frac{V_o}{V}\right)^4 - 2.4090\left(\frac{V_o}{V}\right)^2\right] \qquad \text{(C-3)}$$

where $V_o = \sigma^3$. The free energy may be written as

$$\frac{F}{kT} = \frac{U_o}{kT} + 3\ell n\left[\frac{h}{\sigma(2\pi mkT)^{\frac{1}{2}}}\right] - \ell n\left[\frac{2\pi\sqrt{2}\, g\, V}{V_o}\right] . \qquad \text{(C-4)}$$

The pressure and energy are calculated by differentiating F with respect to V and T respectively. The results are

$$\frac{PV}{kT} = 1 - \frac{12\epsilon}{kT}\left[2.4090\left(\frac{V_o}{V}\right)^2 - 2.0219\left(\frac{V_o}{V}\right)^4\right] - \frac{48\epsilon}{kT}\left[\left(\frac{V_o}{V}\right)^2 \frac{g_m}{g} - \left(\frac{V_o}{V}\right)^4 \frac{g_L}{g}\right] \qquad \text{(C-5)}$$

and

$$\frac{E}{kT} = \frac{3}{2} + \frac{U_o}{kT} + \frac{12\epsilon}{kT}\left[\left(\frac{V_o}{V}\right)^4 \frac{g_L}{g} - 2\left(\frac{V_o}{V}\right)^2 \frac{g_m}{g}\right] . \qquad \text{(C-6)}$$

And the entropy is determined from

$$S = (E - F)/T \quad . \qquad \text{(C-7)}$$

For our computations, we have used the values of g, g_L, and g_m given by Wentorf et al[93] and Díaz Peña and Lombardero[94]. Since these factors are calculated at given T and V, the thermodynamic variables of the LJ D theory appear in the text as discrete points.

APPENDIX D
METHOD OF SOLUTION OF THE PERCUS-YEVICK EQUATION

The Percus-Yevick equation may be written as, Eq. (IV-36),

$$c(r) = (1-e^{u(r)/kT})g(r) \qquad (D-1)$$

where $c(r)$ is defined by, Eq. (IV-28),

$$g(r) - 1 = c(r) + \rho \int c(|\vec{r}-\vec{r}'|)(g(r')-1)d\vec{r}' \quad . \qquad (D-2)$$

Hence, by substitution of Eq. (D-1) into Eq. (D-2), we have an integral equation for either $g(r)$ or $c(r)$. Recently, Baxter[69] has used the conditions

$$c(r) = 0 \qquad \text{when} \qquad r > R \quad , \qquad (D-3)$$

and that the integral

$$\int (g(r) - 1)d\vec{r} \qquad (D-4)$$

be absolutely convergent to rewrite Eq. (D-2) in a form such that the integrals and,hence, the functions depend only on the values of $g(r)$ and $c(r)$ for $r < R$, Eqs. (IV-30) - (IV-32). We will not rewrite these equations here; we shall proceed to write them in the discrete form necessary for numerical solution.

It is convenient to define the variables

$$H(r) = r(g(r) - 1) \qquad (D-5)$$

and

$$C(r) = r\,c(r) \quad . \qquad (D-6)$$

Then for a discrete mesh size $\delta = R/N$ we define the variables

$$r_i = i\,\delta \quad , \tag{D-7}$$

$$H_i = H(i\delta) \quad , \tag{D-8}$$

$$C_i = C(i\delta) \quad , \tag{D-9}$$

$$\mu = 2\pi\rho\delta^2 \quad , \tag{D-10}$$

and

$$\epsilon_{ik} = \frac{1}{2} \qquad \text{if} \qquad i = k \tag{D-11}$$

$$= 1 \text{ otherwise} \quad ,$$

for $1 \leqslant i \leqslant N$. We note that C_o, H_o, and C_N are zero.

By using Eqs. (D-3) and (D-4), we define a new variable

$$D_i = C_i - H_i + X1(i) + X2(i) + X3(i) \quad , \tag{D-12}$$

where

$$X1(i) = \mu \sum_{j=2}^{i} \epsilon_{ij} \sum_{k=1}^{j-1} H_k H_{j-k} \quad , \tag{D-13}$$

$$X2(i) = 2\mu \sum_{j=1}^{N} C_j \left[\sum_{k=1}^{i} \epsilon_{jk} H_k - \sum_{k=1}^{|i-j|} \epsilon_{|i-j|,k} H_k \right] \quad , \tag{D-14}$$

and

$$X3(i) = \mu^2 \sum_{j=1}^{N} C_j \sum_{k=1}^{i} \epsilon_{ik} \left[\frac{1}{2} H_j H_k + W_{jk} \right] \quad , \tag{D-15}$$

where W_{jk} is antisymmetric and for $j > k$,

$$W_{jk} = \sum_{p=1}^{j-1} H_p \sum_{q=|j-k-p|}^{j-|k-p|} \epsilon'_q H_q \quad . \tag{D-16}$$

ϵ_q' is 1/2 for the end points of the sum and 1 for all interior points.

Baxter has shown that these D_i's may be taken to be zero, thus this set of equations is the discrete form of Eqs. (IV-30) - (IV-32), where the integrals are approximated by the trapezoidal rule. Watts[64] suggested that a new variable, p_i, could be defined so that Eq. (D-1) may be written as

$$c_i = [e^{-u_i/kT} - 1]p_i \qquad \text{(D-17)}$$

and

$$g_i = e^{-u_i/kT} p_i \quad . \qquad \text{(D-18)}$$

Where c_i, g_i, and u_i are the values of c(r), g(r), and u(r) respectively at r_i. Hence, Eq. (D-12) may be considered as a non-linear set of equations for the p_i's and our solution corresponds to

$$D_i(p_k) = 0 \quad \text{for} \quad i = 1, \ldots N \quad . \qquad \text{(D-19)}$$

We have solved

$$F_i(p_k) = - D_i(p_k)/r_i = 0 \quad . \qquad \text{(D-20)}$$

For the Newton-Raphson method[82], we are required to make an initial guess of the solution to start the iteration scheme. The succeeding iterations are made by solving the matrix equation

$$\sum_{\nu=1}^{N} \Delta p_\nu^\lambda \frac{\partial F_i(\vec{p}^{\lambda})}{\partial p_\nu} + F_i(\vec{p}^{\lambda}) = 0 \qquad \text{(D-21)}$$

where $\vec{p}^{\lambda}$ is the previous set of p_k's and the new estimate for the p_k's is

$$p_k^{\lambda+1} = p_k^{\lambda} + \Delta p_k^{\lambda} \tag{D-22}$$

and where λ is the number of iterations completed.

We have calculated the derivative matrix analytically; formally we have

$$\frac{\partial D_i}{\partial p_Q} = \frac{\partial C_i}{\partial p_Q} - \frac{\partial H_i}{\partial p_Q} + \frac{\partial X1(i)}{\partial p_Q} + \frac{\partial X2(i)}{\partial p_Q} + \frac{\partial X3(i)}{\partial p_Q} \quad . \tag{D-23}$$

We shall merely write down the final expressions for these terms.

For the first two terms, we have

$$\frac{\partial C_i}{\partial p_Q} = r_i(X(i)-1)\delta iQ \tag{D-24}$$

and

$$\frac{\partial H_i}{\partial p_Q} = r_i X(i)\delta iQ \quad , \tag{D-25}$$

where

$$X(i) = e^{-u_i/kT} \tag{D-26}$$

and

$$\delta_{ij} = 1 \quad \text{if} \quad i = j$$
$$= 0 \qquad \text{otherwise} \quad .$$

For simplicity, we use the notation

$$CD_Q = \frac{\partial C_Q}{\partial p_Q} \tag{D-27}$$

and

$$HD_Q = \frac{\partial H_Q}{\partial p_Q} \quad . \tag{D-28}$$

For the third term, we have

$$\frac{\partial X1(i)}{\partial p_Q} = 2\mu \sum_{j=Q+1}^{i} \epsilon_{ij} H_{j-Q} HD_Q \qquad Q = 1,\ i-1$$

$$= 0 \qquad Q \geqslant i \tag{D-29}$$

The next term may be expressed as

$$\frac{\partial X2(i)}{\partial p_Q} = 2\mu\, CD_Q \left[\sum_{k=1}^{Q} \epsilon_{Qk} H_k - \sum_{k=1}^{|i-Q|} \epsilon_{|i-Q|,k} H_k \right]$$

$$+ 2\mu \sum_{j=Q}^{N} C_j \epsilon_{jQ} HD_Q$$

$$-2\mu HD_Q \left[\sum_{j=1}^{i-Q} C_j \epsilon_{j,i-Q} + \sum_{j=i+Q}^{N} C_j \epsilon_{j,i+Q} \right] . \tag{D-30}$$

In this expression, the term is set to zero if the upper limit of the sum is lower than the lower limit.

It is convenient to break the final term into four parts. We find

$$\left.\frac{\partial X3(i)}{\partial p_Q}\right|_1 = \mu^2\, CD_Q \left[H_Q \sum_{k=1}^{i} \frac{\epsilon_{ik}}{2} H_k + \sum_{k=1}^{i} W_{Qk} \epsilon_{ik} \right] , \tag{D-31}$$

$$\left.\frac{\partial X3(i)}{\partial p_Q}\right|_2 = \mu^2 HD_Q \sum_{j=1}^{N} \frac{\epsilon_{iQ}}{2} C_j H_j \qquad Q \leqslant i$$

$$= 0 \qquad Q > i \quad , \tag{D-32}$$

$$\left.\frac{\partial X3(i)}{\partial p_Q}\right|_3 = \mu^2 C_Q HD_Q \sum_{k=1}^{i} \frac{\epsilon_{ik}}{2} H_k \quad , \tag{D-33}$$

and

$$\left.\frac{\partial X3(i)}{\partial p_Q}\right|_4 = \mu^2 \sum_{j=1}^{N} C_j \sum_{k=1}^{i} \epsilon_{ik} \frac{\partial W_{jk}}{\partial p_Q} \quad . \tag{D-34}$$

For the derivative of W_{jk}, we find for $j > k$,

$$\frac{\partial W_{jk}}{\partial p_Q} = \left.\frac{\partial W_{jk}}{\partial p_Q}\right|_1 + \left.\frac{\partial W_{jk}}{\partial p_Q}\right|_2 \quad , \tag{D-35}$$

where

$$\left.\frac{\partial W_{jk}}{\partial p_Q}\right|_1 = HD_Q \sum_{q=|j-k-Q|}^{j-|k-Q|} \epsilon'_q H_q \qquad 1 < Q \leqslant j-1$$

$$= 0 \qquad Q > j-1 \quad , \tag{D-36}$$

$$\left.\frac{\partial W_{jk}}{\partial p_Q}\right|_2 = \sum_{p=1}^{j-1} H_p \epsilon'_Q HD_Q C^* \quad , \tag{D-37}$$

and

$$C^{*} = 1 \qquad \text{if} \qquad |j-k-p| < Q < j - |k-p|$$
$$= 0 \qquad \text{otherwise} \quad . \tag{D-38}$$

The antisymmetry condition is used for the derivative matrix for $k > j$, and of course, we have

$$\frac{\partial X3(i)}{\partial p_Q} = \left.\frac{\partial X3(i)}{\partial p_Q}\right|_1 + \left.\frac{\partial X3(i)}{\partial p_Q}\right|_2 + \left.\frac{\partial X3(i)}{\partial p_Q}\right|_3 + \left.\frac{\partial X3(i)}{\partial p_Q}\right|_4 \quad . \tag{D-39}$$

Finally, we have the derivative matrix given by

$$\frac{\partial F_i}{\partial p_Q} = \frac{(HD_Q - CD_Q)\delta_{iQ} - \frac{\partial X1(i)}{\partial p_Q} - \frac{\partial X2(i)}{\partial p_Q} - \frac{\partial X3(i)}{\partial p_Q}}{r_i} \quad . \tag{D-40}$$

As we have mentioned in the text, the initial guess for lower densities may be made from crude empirical estimates and for higher densities we extrapolate from the lower density solutions. It is found that in nearly every case the derivative matrix may assume its initial value throughout the calculation. For low to moderate density solutions, we have assumed the solution converged if

$$|F_i| \leqslant 10^{-5} \quad \text{for all } i \quad . \tag{D-41}$$

For densities above $\rho^{*} = 1.0$, the large negative values of $c(r)$ near $r = 0$ made condition (D-41) unattainable, hence, the condition was relaxed to

$$|F_i| \leqslant 7.5 \times 10^{-5} \quad \text{for all } i \quad . \tag{D-42}$$

The computer program was formulated so that the initial value of the derivative matrix was used for 10 iterations; if the solution had not converged to the desired condition, the p_k^{10}'s were used as the initial guess for a final try. This procedure was normally needed for $\rho^* > 0.8$.

As we have noted in the text, the solution diverged for $\rho^* = 1.3$ on all three isotherms. The values of the F_i's became larger than the computer could store, which is about 10^{75}, in less than 7 iterations. To try to eliminate this divergence, new guesses were attempted and the derivative matrix was changed after the first iteration. The solution still diverged. It was found that the sign of the determinant of the derivative matrix changed from iteration to iteration. (The determinant was positive for $\rho^* \leq 1.2$.) This fact indicates that the range of this determinant includes zero. We do not know if this behavior is fundamental to these equations or if it is of numerical origin.

REFERENCES

1. R. Brout, Phase Transitions (W. A. Benjamin, Inc., New York, 1965).
2. E. D. G. Cohen, Fundamental Problems in Statistical Mechanics II (North-Holland Publishing Company, Amsterdam, 1968).
3. J. E. Lennard-Jones, "The Equation of State of Gases and Critical Phenomena," Physica 4, 941 (1937).
4. J. K. Percus and G. J. Yevick, "Analysis of Classical Statistical Mechanics by Means of Collective Coordinates," Phys. Rev. 110, 1 (1958).
5. R. H. Fowler, Statistical Mechanics (Cambridge University Press, Cambridge, England, 1936), 2nd ed., p. 173.
6. L. S. Salter, "Vapour Pressure of a Monatomic Crystal," Trans. Faraday Soc. 59, 657 (1963).
7. A. Einstein, "Die Plancksche Theorie der Strahlung und die Theorie der Spezifischen Wärme," Ann. Physik 22, 180 (1907).
8. G. S. Rushbrooke, Introduction to Statistical Mechanics (Oxford University Press, London, 1949). p. 32.
9. C. Kittel, Introduction to Solid State Physics (John Wiley and Sons, Inc., New York, 1966), 3rd ed., p. 206.
10. J. E. Lennard-Jones and A. F. Devonshire, "Critical Phenomena in Gases I," Proc. Roy. Soc. (London) 163, 53 (1937).
11. E. A. Moelwyn-Hughes, "Considerations on the Harmonic Oscillator Model of Monatomic Solids," Z. Physik, Chem. (Frankfurt) 15, 270 (1958).
12. I. Z. Fisher, Statistical Theory of Liquids (University of Chicago Press, Chicago, 1964).
13. P. Flubacher, A. J. Leadbetter, and J. A. Morrison, "A Low Temperature Adiabatic Calorimeter for Condensed Substances. Thermodynamic Properties of Argon," Proc. Phys. Soc. (London) 78, 1449 (1961).
14. M. P. Freeman and G. D. Halsey, Jr., "The Solid Solution Krypton-Xenon from 90 to 120° K., The Vapor Pressures of Argon, Krypton, and Xenon," J. Phys. Chem. 60, 1119 (1956).
15. A. M. Clark, F. Din, J. Robb, A. Michels, T. Wassenaar, and Th. Zwietering, "The Vapour Pressure of Argon," Physica 17, 876 (1951).

16. R. H. Beaumont, H. Chihara, and J. A. Morrison, "Thermodynamic Properties of Krypton. Vibrational and Other Properties of Solid Argon and Solid Krypton," Proc. Phys. Soc. (London) 78, 1462 (1961).

17. B. B. Fisher and W. G. McMillan, "The Sublimation Pressure of Krypton Below 80° K," J. Phys. Chem. 62, 494 (1958).

18. H. H. Podgurski and F. N. Davis, "Thermal Transpiration at Low Pressure. The Vapor Pressure of Xenon Below 90° K.," J. Phys. Chem. 65, 1343 (1961).

19. K. Peters and K. Weil, "Schemlzpunkte und Dampfdrucke von Krypton und Xenon," Z. Physik. Chem. (Leipzig) A 148, 27 (1930).

20. N. Bernardes, "Theory of Solid Ne, A, Kr, and Xe at 0° K.," Phys. Rev. 112, 1534 (1958).

21. P. Debye, "Zur Theorie der Spezifischen Wärmen," Ann. Physik 39, 789 (1912).

22. A. R. Ubbelohde, Melting and Crystal Structure (Oxford University Press, Oxford, England, 1965).

23. E. R. Dobbs and G. O. Jones, "Theory and Properties of Solid Argon," Repts. Progr. Phys. 20, 516 (1957).

24. G. L. Pollack, "The Solid State of Rare Gases," Rev. Mod. Phys. 36, 748 (1964).

25. G. K. Horton, "Ideal Rare-Gas Crystals," Am. J. Phys. 36, 93 (1968).

26. C. N. Yang and T. D. Lee, "Statistical Theory of Equations of State and Phase Transitions I. Theory of Condensation II," Phys. Rev. 87, 404 (1952).

27. J. G. Kirkwood and E. Monroe, "Statistical Mechanics of Fusion," J. Chem. Phys. 9, 514 (1941).

28. B. J. Alder and G. Jura, "Note on the Critical Temperature of Solids," J. Chem. Phys. 20, 1491 (1952).

29. H. N. V. Temperley, "Application of the Mayer Method to the Melting Problem," Proc. Phys. Soc. (London) 74, 183 (1959).

30. C. Domb, "The Melting Curve at High Pressure," Phil. Mag. 42, 1316 (1951).

31. P. W. Bridgman, "The Melting Parameters of Nitrogen and Argon under Pressure, and the Nature of the Melting Curve," Phys. Rev. 46, 930 (1934).

32. P. H. Lahr and W. G. Eversole, "Compression Isotherms of Argon, Krypton, and Xenon Through the Freezing Zone," J. Chem. Eng. Data 7, 42 (1962).

33. F. A. Lindemann, "Über die Berechnung Molekülarer Eigenfrequenzen," Z. Physik 11, 609 (1910).

34. C. Domb, "Some Theoretical Aspects of Melting," Nuovo Cimento Supp. 9, 9 (1958).

35. J. J. Gilvarry, "The Lindemann and Grüneisen Laws," Phys. Rev. 102, 308 (1956).

36. J. J. Gilvarry, "Grüneisen's Law and the Fusion Curve at High Pressure," Phys. Rev. 102, 317 (1956).

37. J. J. Gilvarry, "Equation of the Fusion Curve," Phys. Rev. 102, 325 (1956).

38. S. E. Babb, Jr., "Values of the Simon Constants," J. Chem. Phys. 38, 2743 (1963).

39. L. Salter, "The Simon Melting Equation," Phil. Mag. 45, 369 (1954).

40. F. Simon and G. Glatzel, "Bemerkungen zur Schmelzdruck Kurve," Z. Anorg. u. Allgem. Chem, 178, 309 (1929).

41. S. E. Babb, Jr., "Parameters in the Simon Equation Relating Pressure and Melting Temperature," Rev. Mod. Phys. 35, 400 (1963).

42. J. E. Lennard-Jones and A. F. Devonshire, "Critical and Co-operative Phenomena III. A Theory of Melting and the Structure of Liquids," Proc. Roy. Soc. (London) 169, 317 (1939).

43. J. E. Lennard-Jones and A. F. Devonshire, "Critical and Co-operative Phenomena IV. A Theory of Disorder in Solids and Liquids and the Process of Melting," Proc. Roy. Soc. (London) 170, 464 (1939).

44. W. L. Bragg and E. J. Williams, "The Effect of Thermal Agitation on Atomic Arrangement in Alloys," Proc. Roy. Soc. (London) A 145, 699 (1934).

45. W. L. Bragg and E. J. Williams, "The Effect of Thermal Agitation on Atomic Arrangement in Alloys - - II," Proc. Roy. Soc. (London) A 151, 540 (1935).

46. H. A. Bethe, "Statistical Theory of Superlattices," Proc. Roy. Soc. (London) A 150, 552 (1935).

47. E. Ising, "Bertrag zur Theorie des Ferromagnetismus," Z. Physik 31, 253 (1925).

48. H. S. Green and C. A. Hurst, Order-Disorder Phenomena (Interscience Publishers, New York, 1964).

49. E. W. Elcock, Order-Disorder Phenomena (John Wiley and Sons, Inc., New York, 1956).

50. B. J. Alder and T. E. Wainwright, "Studies in Molecular Dynamics. I. General Method," J. Chem. Phys. 31, 459 (1959).

51. B. J. Alder and T. E. Wainwright, "Studies in Molecular Dynamics. II. Behavior of a Small Number of Elastic Spheres," J. Chem. Phys. 33, 1439 (1960).

52. B. J. Alder and T. E. Wainwright, "Phase Transition in Elastic Disks," Phys. Rev. 127, 359 (1962).

53. B. J. Alder, W. G. Hoover, and T. E. Wainwright, "Cooperative Motion of Hard Disks Leading to Melting," Phys. Rev. Letters 11, 241 (1963).

54. H. C. Longuet-Higgins and B. Widom, "A Rigid Sphere Model for the Melting of Argon," Mol. Phys. 8, 549 (1964).

55. R. K. Crawford and W. B. Daniels, "Melting in Argon at High Temperatures," Phys. Rev. Letters 21, 367 (1968).

56. D. Henderson and J. A. Barker, "On the Solidification of Argon," Mol. Phys. 14, 587 (1968).

57. P. R. Emtage, "A Theory of the Melting of the Rare Gas Solids," Physica 32, 1734 (1966).

58. T. Tsuzuki, "On the Theory of the Melting of Molecular Crystals," J. Phys. Soc. Japan 21, 25 (1966).

59. W. E. Bleick and J. E. Mayer, "The Mutual Repulsive Potential of Closed Shells," J. Chem. Phys. 2, 252 (1934).

60. J. O. Hirschfelder, C. F. Curtiss, and R. B. Bird, Molecular Theory of Gases and Liquids (John Wiley and Sons, Inc., New York, 1954), 2nd ed., p. 166.

61. S. C. Smelser, "An X-Ray Diffraction Study of the Structure of Argon in the Dense Liquid Region," Ph. D. thesis, Calif. Inst. of Tech. (1969).

62. J. H. Henkel, "Equation of State and the Thermal Dependence of the Elastic Coefficients of Crystalline Argon," J. Chem. Phys. 23, 681 (1955).

63. E. A. Guggenheim and M. L. McGlashan, "Interaction Between Argon Atoms," Proc. Roy. Soc. (London) A 255, 456 (1960).

64. R. O. Watts, "Percus-Yevick Equation Applied to a Lennard-Jones Fluid," J. Chem. Phys. 48, 50 (1968).

65. R. O. Watts, "Percus-Yevick Approximation for the Truncated Lennard-Jones (12,6) Potential Applied to Argon," J. Chem. Phys. 50, 984 (1969).

66. S. A. Rice and P. Gray, The Statistical Mechanics of Simple Liquids (Interscience Publishers, New York, 1965).

67. P. A. Egelstaff, An Introduction to the Liquid State (Academic Press, Inc., New York, 1967).

68. J. A. Barker, Lattice Theories of the Liquid State (Pergamon Press Ltd., Oxford, 1963).

69. R. J. Baxter, "Method of Solution of the Percus-Yevick, Hypernetted-Chain, or Similar Equations," Phys. Rev. 154, 170 (1967).

70. G. J. Throop and R. J. Bearman, "The Pair Correlation Function and Thermodynamic Properties for the Lennard-Jones 6-12 Potential and the Percus-Yevick Equation," Physica 32, 1298 (1966).

71. A. A. Broyles, "Radial Distribution Functions from the Born-Green Integral Equation," J. Chem. Phys. 33, 456 (1960).

72. A. A. Broyles, "Solutions to the Percus-Yevick Equation," J. Chem. Phys. 35, 493 (1961).

73. A. A. Broyles, S. U. Chung, and H. L. Sahlin, "Comparison of Radial Distribution Functions from Integral Equations and Monte Carlo," J. Chem. Phys. 37, 2462 (1962).

74. L. Verlet, "On the Theory of Classical Fluids III," Physica 30, 95 (1964).

75. A. A. Khan, "Radial Distribution Functions of Fluid Argon," Phys. Rev. 134, A 367 (1964).

76. A. A. Khan, "Radial Distribution Functions of Liquid Krypton," Phys. Rev. 136, A 1260 (1964).

77. A. A. Khan and A. A. Broyles, "Interatomic Potentials and X-Ray-Diffration Intensities for Liquid Xenon," J. Chem. Phys. 43, 43 (1965).

78. L. Verlet and D. Levesque, "On the Theory of Classical Fluids VI," Physica 36, 254 (1967).

79. M. Born, "On the Stability of Crystal Lattices I," Proc. Camb. Phil. Soc. 36, 160 (1940).

80. M. Born, "On the Stability of Crystal Lattices IX. Covariant Theory of Lattice Deformations and the Stability of Some Hexagonal Lattices," Proc. Camb. Phil. Soc. 38, 82 (1942).

81. J. E. Jones and A. E. Ingham, "On the Calculation of Certain Crystal Potential Constants, and on the Cubic Crystal of Least Potential Energy," Proc. Roy. Soc. (London) A 107, 636 (1925).

82. A. M. Ostrowski, Solutions of Equations and Systems of Equations (Academic Press, New York, 1966) 2nd ed., p. 186.

83. R. J. Baxter, "Pressure in the Percus-Yevick Approximation," J. Chem. Phys. 47, 4855 (1967).

84. J. M. H. Levelt, "The Reduced Equation of State, Internal Energy and Entropy of Argon and Xenon," Physica 26, 361 (1960).

85. S. C. Smelser, Private Communication, 1969.

86. E. A. Guggenheim, Applications of Statistical Mechanics (Oxford University Press, London, 1966) pp. 10 - 47.

87. C. Domb and I. J. Zucker, "Theoretical Calculations on Solid Argon," Nature, London 178, 484 (1956).

88. H. G. David and S. D. Hamann, "Lennard-Jones and Devonshire Equation of State at Low Temperatures," J. Chem. Phys. 38, 3037 (1963).

89. R. D. Reed, D. Henderson, and R. Chen, "Quantum Cell Model for Solids at Low Temperatures," J. Chem. Phys. 42, 1884 (1965).

90. W. G. Hoover and B. J. Alder, "Cell Theories for Hard Particles," J. Chem. Phys. 45, 2361 (1966).

91. G. G. Chell and I. J. Zucker, "The Effect of Long-Range Three-Body Forces on the Zero-Point Energy of the Inert Gas Solids," J. Phys. C (Proc. Phys. Soc.), Ser. 2, 1, 35 (1968).

92. J. A. Barker and D. Henderson, "Perturbation Theory and Equation of State for Fluids. II. A Successful Theory of Liquids," J. Chem. Phys. 47, 4714 (1967).

93. R. H. Wentorf, Jr., R. J. Buehler, J. O. Hirschfelder, and C. F. Curtiss, "Lennard-Jones and Devonshire Equation of State of Compressed Gases and Liquids," J. Chem. Phys. 18, 1484 (1950).

94. M. Díaz Peña and M. Lombardero, "Cell Theory Integrals of Liquid State," An. R. Soc. esp. Fis. Quim. B 58, 945 (1966).